Titre: Title:	Understanding Ozone Mechanisms to Alleviate Ceramic Membrane Fouling
Auteur: Author:	Irma Giovanna Llamosas Chu
Date:	2014
Type:	Mémoire ou thèse / Dissertation or Thesis
Référence: Citation:	Llamosas Chu, I. G. (2014). Understanding Ozone Mechanisms to Alleviate Ceramic Membrane Fouling [Master's thesis, École Polytechnique de Montréal]. PolyPublie. https://publications.polymtl.ca/1579/

URL de PolyPublie: PolyPublie URL:	https://publications.polymtl.ca/1579/
Directeurs de recherche: Advisors:	Benoit Barbeau, & Pierre Bérubé
Programme: Program:	Génie civil

UNIVERSITÉ DE MONTRÉAL

UNDERSTANDING OZONE MECHANISMS TO ALLEVIATE CERAMIC MEMBRANE FOULING

IRMA GIOVANNA LLAMOSAS CHU
DÉPARTEMENT DES GÉNIES CIVIL, GÉOLOGIQUE ET DES MINES
ÉCOLE POLYTECHNIQUE DE MONTRÉAL

MÉMOIRE PRÉSENTÉ EN VUE DE L'OBTENTION
DU DIPLÔME DE MAÎTRISE ÈS SCIENCES APPLIQUÉES
(GÉNIE CIVIL)
NOVEMBRE 2014

UNIVERSITÉ DE MONTRÉAL

ÉCOLE POLYTECHNIQUE DE MONTRÉAL

Ce mémoire intitulé:

UNDERSTANDING OZONE MECHANISMS TO ALLEVIATE CERAMIC MEMBRANE FOULING

présenté par: LLAMOSAS CHU Irma Giovanna

en vue de l'obtention du diplôme de : Maîtrise ès sciences appliquées

a été dûment accepté par le jury d'examen constitué de :

Mme PRÉVOST Michèle, Ph. D., présidente

M. BARBEAU Benoit, Ph. D., membre et directeur de recherche

M. BÉRUBÉ Pierre, Ph. D., membre et codirecteur de recherche

M. HAUSLER Robert, Ph. D., membre

DEDICATION

To my parents, Margot and Javier,

for their invaluable caring and unconditional support …

ACKNOWLEDGEMENTS

This work was supported by NSERC-Industrial Chair in Drinking Water Treatment, which is funded by the City of Montreal, John-Meunier Inc. and the City of Laval.

My appreciation also goes to:
My Director, Benoit Barbeau, for his infinite patience, good sense of humour, and precious technical advices …

The technical staff at the Chair, for their valuable advices and professional work, besides … Mireille Blais & Yves Fontaine, for their support with the set-up and water collection; Julie Philibert, for the pCBA analysis, Jacinthe Mailly, for the COD analysis, Marcellin Fotsing for the metal traces analysis.

My co-director, Pierre Bérubé, and the technical staff and post-graduate students from UBC, who supported this work with their technical advices and the SEC-analysis.

The students and interns from the Chair on Drinking Water (Félix, Hadis, Laleh, Vanessa, Kim, Evelyn, Mathieu, Stéphanie, Marie Claude, Loreto, Celso, Jasdeep, Ehsan, Mouna, Émile, Daniel, Charlène, Hélène, Mai, Cédric) and from the Waste Water Department (Jaime, Bettina, Dominic, Kunaal, Félix, Karim, Reza, Sanaz, Hadi): for their company and support, for their diversity and good-sense of humour. You greatly eased the work in the lab and my time at Poly …

To my parents Margot & Javier, my sisters Silvia & Mónica, my brothers Javier & Dante, and also to my friends, who were always by my side, whatever my decisions …

RÉSUMÉ

Les membranes céramiques représentent une perspective intéressante comme traitement de pointe dans le domaine de l'eau potable. Cependant, le coût de capital élevé et l'absence de recherche spécifique sur la performance de ces membranes diminuent leur utilisation dans ce domaine. Ainsi, sachant que le colmatage est la principale limite connue dans les procédés de filtration, cette étude à l'échelle laboratoire visait à évaluer l'impact d'un pré-traitement d'ozonation sur la réduction du colmatage des membranes céramiques UF. Les étapes de pré-ozonation et de filtration ont été réalisées en utilisant deux pH ainsi que des doses d'ozone différentes. Les valeurs de pH choisies étaient situées à la limite de la plage naturelle des eaux de surface (6,5 et 8,5) afin de garantir la praticabilité. L'eau brute de la rivière des Mille Îles à Québec-Canada a été utilisée. Le montage de filtration était composé d'une cellule de filtration frontale non agitée opérée à flux constant. Les résultats ont montré que la pré-oxydation par l'ozone réduit effectivement le degré de colmatage de la membrane en fonction de la dose appliquée (jusqu'à 60 et 85% pour les membranes 8 et 50 kDa, respectivement). L'oxydation directe de la MON a été jugée responsable de cet effet étant donné que la présence d''ozone moléculaire n'était pas indispensable pour obtenir ces résultats. Cependant, dans le cadre de cette expérience, le pH s'est montré plus efficace que le pré-traitement à l'ozone pour maintenir le colmatage à de faibles taux: 70% inférieur à pH 6,5 qu'à pH 8,5 pour les eaux non-ozonisées, ce qui est contraire à la plupart de la littérature trouvée sur le sujet (Changwon, 2013; De Angelis et Fidalgo, 2013; Karnik et al., 2005; S. Lee & Kim, 2014). Ce comportement s'explique principalement par le mode d'opération utilisé dans l'expérience, les répulsions électriques entre les molécules de MON à pH basique qui ont conduit à l'accumulation de matériau sur le côté d'alimentation de la membrane (concentration polarisation), et finalement la formation d'un gâteau. En outre, le pH de la solution d'eau a montré une influence sur la définition des mécanismes de colmatage. Avec l'échantillon d'eau à pH 6,5, qui correspond précisément au point isoélectrique des membranes (±6,5), le mécanisme de colmatage par blocage a été fréquemment détecté avant la formation d'un gâteau. Ces observations mettent en évidence le rôle important des charges électriques dans les procédés de filtration avec des membranes céramiques (Chiu, 2011; S. Lee & Kim, 2014; Szymczyk, Fievet, Reggiani, et Pagetti, 1998b).

En ce qui concerne l'ozonation, il a été confirmé que les eaux naturelles à forte teneur en MON(> 3 mg / L) déclenchent des procédés d'oxydation avancés (Acero et Von Gunten, 2001). Il a également observé que la condition de pH 6,5 a permis la décomposition de la MON de manière plus efficace que la dose d’ozone la plus élevée utilisée à pH 8,5.

ABSTRACT

Ceramic membranes are a strong prospect as an advanced treatment in the drinking water domain. But their high capital cost and the lack of specific research on their performance still discourage their application in this field. Thus, knowing that fouling is the main drawback experienced in filtration processes, this bench-scale study was aimed to assess the impact of an ozonation pre-treatment on the alleviation of the fouling of UF ceramic membranes. Pre-ozonation and filtration steps were performed under two different pH and ozone doses. Chosen pH values were at the limits of natural surface waters range (6.5 and 8.5) to keep practicability. Raw water from the Thousand Isle's river at Quebec-Canada was used for the tests. The filtration setup involved an unstirred dead-end filtration cell operated at constant flux. Results showed that pre-oxidation by ozone indeed reduced the fouling degree of the membranes according to the dose applied (up to 60 and 85% for membranes 8 and 50 kDa, respectively). Direct NOM oxidation was found responsible for this effect as the presence of molecular ozone was not essential to achieve these results. In the context of this experiment, however, pH showed to be more effective than the ozonation pre-treatment to keep fouling at low levels: 70% lower at pH 6.5 than at pH 8.5 for un-ozonated waters, which was contrary to most of the literature found on the topic (Changwon, 2013; De Angelis & Fidalgo, 2013; Karnik et al., 2005; S. Lee & Kim, 2014). This behaviour results mainly from the operation mode used in the experiment, the electrical repulsions between MON molecules at basic pH that led to the accumulation of material on the feed side of the membranes (concentration polarisation) and ulterior cake formation. In addition, solution pH showed an influence in the definition of fouling mechanisms. At solution pH 6.5, which was precisely the isoelectric point of the membranes (±6.5), the blocking fouling mode was frequently detected before the onset of a cake. These facts put in evidence the important role of electrical charges in filtration processes with ceramic membranes (Chiu, 2011; S. Lee & Kim, 2014; Szymczyk, Fievet, Reggiani, & Pagetti, 1998b).

In the ozonation side, it was confirmed that natural waters with high NOM content (>3 mg/L) trigger advanced oxidation processes (Acero & Von Gunten, 2001). It was also found that condition pH 6.5 showed higher NOM decomposition than condition pH 8.5 at the highest ozone dose used.

TABLE OF CONTENTS

LIST OF TABLES

LIST OF FIGURES

LIST OF ACRONYMS AND ABBREVIATIONS

AOP	Advanced Oxidation Process
CP	Concentration Polarization
DOC	Dissolved Organic Carbon
NOM	Natural Organic Matter
FA	Fulvic Acid
HA	Humic Acid
HMW	High Molecular Weight
HS	Humic Substance
J	Flux
J_s	Permeability
LMW	Low Molecular Weight
MF	Microfiltration
MW	Molecular Weight
NF	Nanofiltration
O_3	Ozone
•OH	Hydroxyl free radical
pCBA	para-cholorobenzoic acid
R_i	Membrane Rejection
TMP	Transmembrane Pressure
UF	Ultrafiltration
vc	Variation Coefficient

LIST OF APPENDICES

INTRODUCTION

As a result of their exceptional mechanical, chemical and thermal resistances, ceramic membranes have been sustainably expanding their application scope. Yet, despite their widespread use in industry (wastewater, pharmaceutical, chemical, metals, food, beverage, pulp and paper, etc.) (Sondhi, Bhave, & Jung, 2003), this technology is not as popular in the drinking water industry, mainly due to the high capital costs associated with their installation in comparison to the widely available polymeric membranes (Freeman & Shorney-Darby, 2011). However, significant ongoing efforts are looking at counteracting this trend as the industry works on lowering the costs of this technology and as the few large-scale ceramic applications available in the world are demonstrating superior operational performance (Freeman & Shomey-Darby, 2011). Besides their remarkable capacity in removing microscopic parasites and molecules, ceramic membranes are proving longer lifetime than polymeric membranes and very low frequency of breakdowns (Freeman & Shomey-Darby, 2011). They also offer the possibility of operating at higher pressures, and the feasibility of cleaning with harsher physical-chemical methods. As a consequence, a higher productivity and improved process stability could be achieved (Freeman & Shorney-Darby, 2011).

One important challenge of any filtration technology is fouling, which is defined as the decrease in water throughput across, in this case the membrane, caused by the deposit of material on or within its structure. For the drinking water production, the main fouling material is the natural organic matter (NOM) and numerous other factors affect fouling, including membrane characteristics and membrane operating conditions (Zularisam, Ismail, & Salim, 2006). A profuse scientific literature has addressed the fundamental understanding of the impacts of water quality, membrane characteristics and operation on fouling. However, most of the research has been directed to polymeric membranes (Howe & Clark, 2002; Kimura, Hane, Watanabe, Amy, & Ohkuma, 2004; N. Lee, Amy, Croué, & Buisson, 2004; Shao, Hou, & Song, 2011), or ceramic membranes in industrial applications. Thus, there is an urgent need to better understand fouling of ceramic membranes in the context of potable water treatment in order to further encourage their application. Fundamental studies include (Munla, 2012) who looked into the identification of reversible and irreversible fouling agents on UF ceramic membranes and (S. Lee & Kim,

2014) who compared the fouling of polymeric vs ceramic UF membranes. In addition, different strategies have been studied to control ceramic membrane fouling. These involve modification of membrane surfaces, physical-chemical cleaning, manipulation of operating parameters and feed-water pre-treatment. On the latter topic, coagulation prior to MF/UF ceramic filtration is the most discussed subject in literature (Chang, Liu, Luo, & Li, 2014; Dong, Chen, Gao, & Fan, 2007). Other pre-treatments prior to UF ceramic membranes like the use of ion-exchange resins (Kabsch-Korbutowicz & Urbanowska, 2010) or the application of ozonation and adsorption methods (Fan et al., 2014) have received less attention, evidencing the gaps and research opportunities to be overlaid in this area. Amongst the different pre-treatment strategies that have been tested so far, the use of pre-ozonation is offering the most promising results as fouling reductions up to 50% have been shown (Van Geluwe, et al., 2011; Karnik, et al., 2005; Kim, et al., 2009; Lee, et al., 2005; Geismar, et al., 2011). In addition, the use of ozone ahead of ceramic membranes is possible due to their resistance to this oxidant while it is generally not advisable for polymeric membranes as only polymeric crystalline PVDF membranes have been shown to support the contact with ozone (Hashino, et al., 2000). Recently, van Geluwe et al. (2011) have reviewed the role of ozone on alleviating fouling by NOM. The importance of the immediate ozone demand was highlighted as the direct O_3 reaction with NOM in the first seconds of ozone injection also produces oxidation conditions equivalent to an advanced oxidation process (AOP). This conclusion opens up the following research question: is it necessary to maintain ozone residual in contact with the membrane or is overcoming the immediate ozone demand (which takes place in the first 15 seconds) sufficient to achieve the goal of reducing fouling? In the case that most of the fouling reduction occurs during immediate ozone demand, it would be of interest to assess if this is mostly the result of free radicals oxidation or direct NOM oxidation by molecular ozone. The general objective of this study was to understand the fundamental role of an ozone pre-treatment in reducing the fouling of ceramic membranes used for drinking water production. More specifically, the following objectives were sought:

1. Assess the reduction of fouling gained under various ozonation regimes induced by varying the ozone dosages, the pH of ozonation and the concentration of free radicals/ scavengers. This will be achieved by: a) measuring the ozonation effect on the organic matter (COD, UVA_{254}, size) of the water sample; b) identifying the role of each ozonation regime on the

changes of the water quality; c) evaluating the pH effect over the ozonation effectiveness in reducing fouling.

Research hypothesis: Most of the fouling reduction is achieved due to the action of hydroxyl free radicals. Therefore, increasing pH of ozonation will lead to higher free radicals formation and, consequently, lower membrane fouling.

2. Compare the fouling behavior of UF ceramic membranes of two molecular weight cu-toffs (8 and 50 kDa)

   Research hypothesis: A higher fouling index due to size screening (pore blocking) is expected for the 8 kDa membrane. Electrostatic effects are expected to be more important for the 50 kDa membrane.

This work is composed of two main sections. The first one (section 3.1) deals with the ozonation process, in which three ozone doses (0.0, 0.5 and 1 mg O_3/mg C) were applied at three different pH conditions (6.5, 8.5, and 8.5+*t*-butanol) to a surface water sample. Physical-chemical and SEC analysis of the pre and post-ozonated waters were performed. The second part (section 3.2) comprehends the ultrafiltration process, where the previous samples were filtrated through 8 or 50 kDa ceramic membranes. Besides the physical-chemical and SEC analysis, the fouling mechanisms and fouling index were also investigated.

CHAPTER 1 LITERATURE REVIEW

This chapter will first review the chemistry of ozone with respect to its impact on NOM. Current knowledge on membrane fouling will be also summarized.

1.1 Ozone role in the oxidation of NOM

Ozone (O_3) is recognized as a highly reactive molecule; in fact, one of the strongest oxidants known, as shown in table 1.1:

Table 1.1: Oxidation potential for oxygen species
Extracted from (Beltrán, 2004; Gottschalk, Libra, & Saupe, 2010)

Species	Standard redox Potential
O_2	1.23 V
O_3	2.07 V
•OH	2.80 V

As a consequence, O_3 is an unstable molecule that decomposes rapidly in water containing natural organic matter (NOM) by passing through two stages: a) a first and very fast drop (first 30-120 s of contact) (M. Elovitz & Von Gunten, 1999), which exhibits a pseudo first order kinetics (38-106 µM/min has been reported by (Westerhoff, Aiken, Amy, & Debroux, 1999) at pH 7.5, which accounts for approximately 60% of O_3 decomposition. For comparison, in the absence of NOM, the O_3 decomposition is about 25% at the same pH; b) a second smooth phase where O_3 decays with first order kinetics in which by-products of the first phase and slow-reacting NOM compounds are believed to react (Von Gunten, 2003; Westerhoff, et al., 1999). The kinetics of this decomposition depends on temperature and characteristics of the water matrix (pH, alkalinity, component's type and concentration,), so that it can last from seconds to hours (Von Gunten, 2003). The decomposition products include the formation of •OH radicals (radical chain mechanism), which constitutes a unique feature of O_3 (Von Gunten, 2003). This radical chain can be divided in three phases: initiation, propagation and termination, which involve the presence of initiators, promoters or scavenger agents, which trigger, enhance or stop the radical mechanism, respectively (Gottschalk, et al., 2010).

Thus, as depicted in figure 1-1, O_3 oxidizes organic material through the action of molecular O_3, •OH radicals (radical chain reactions), or a combination of both (Von Gunten, 2003). Factors such as pH and type/concentration of organic matter determine the mode of action that will prevail.

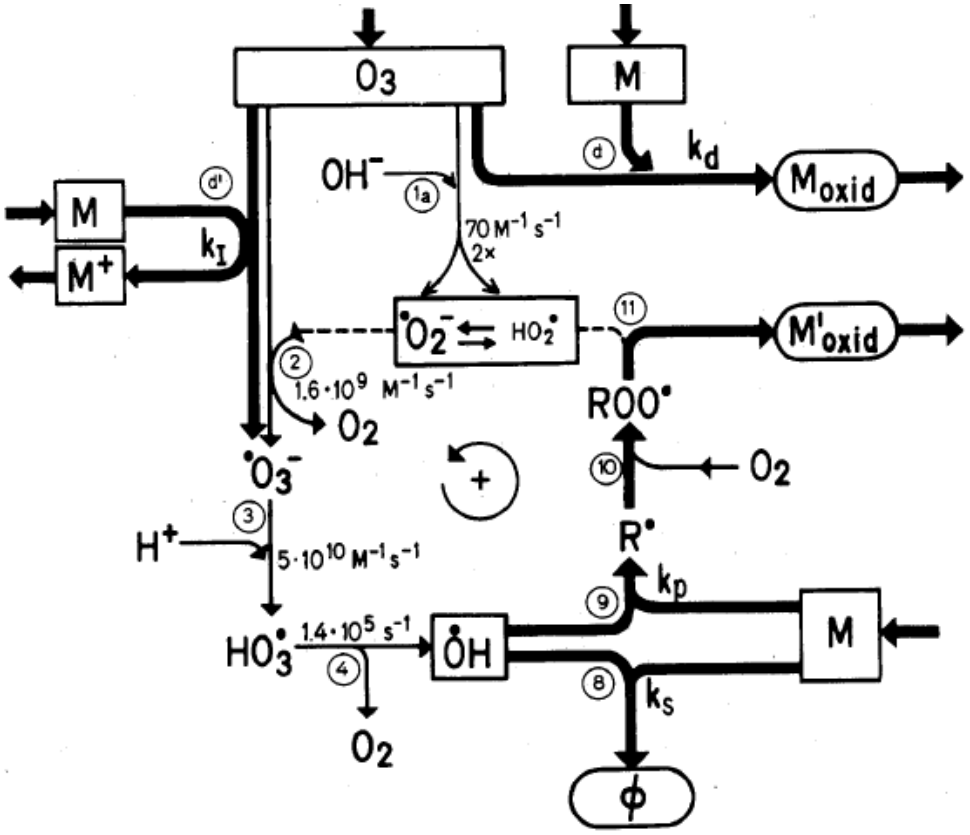

Figure 1-1: Ozone decomposition pathway in the presence of NOM
Adapted from (Staehelin & Hoigné, 1985)

1.1.1 Effect of pH

In pure water, OH^- ions trigger O_3 decomposition (autocatalysis), so that at basic pH the reaction is faster (Mizuno, 2007; Staehelin & Hoigné, 1985). In fact, Mizuno (2007) reported that the decomposition reaction can be 5 times faster with the increase of 1 unit of pH. For waters containing NOM in high concentrations (>3 mg C/L) the effect of pH is actually unknown, but a trend for higher efficiency at basic pH is recognized due to enhanced de-protonation of NOM (Buffle, Schumacher, Meylan, Jekel, & Von Gunten, 2006).

The reactions involved in the decomposition of O_3 in pure water due to pH are described below (Von Gunten, 2003):

$O_3 + OH^- \rightarrow HO_2^- + O_2$, $k = 70\ M^{-1}s^{-1}$

$O_3 + HO_2^- \rightarrow \bullet OH + \bullet O_2^- + O_2$, $k = 2.8x10^6\ M^{-1}s^{-1}$

$O_3 + \bullet O_2^- \rightarrow \bullet O_3^- + O_2$, $k = 1.6x10^9\ M^{-1}s^{-1}$

pH ≤ 8:

$\bullet O_3^- + H^+ \leftrightarrow \bullet O_3H$, where $k_f = 5\times10^{10}\ M^{-1}s^{-1}$ and $k_r = 3.3\times10^2\ s^{-1}$

$\bullet O_3H \rightarrow \bullet OH + O_2$, where $k = 1.4\times10^5\ s^{-1}$

pH ≥ 8:

$\bullet O_3^- \leftrightarrow \bullet O^- + O_2$, where $k_f = 2.1\times10^3\ s^{-1}$ and $k_r = 3.3\times10^9\ s^{-1}$

$\bullet O^- + H_2O \rightarrow \bullet OH + OH^-$, where $k_f = 10^8\ s^{-1}$

$\bullet OH + O_3 \rightarrow \bullet O_2H + O_2$, $k = 1x10^8\ M^{-1}s^{-1}$ to $2x10^9\ M^{-1}s^{-1}$

This last reaction becomes important in waters with low dissolved organic carbon (DOC) and low alkalinity, as it consumes both oxidative species: ozone and •OH radicals. This reduces the oxidation capacity of the system (Von Gunten, 2003).

1.1.2 Effect of temperature

O_3 decomposition is enhanced with increasing temperatures. Mizuno (2007) reported an increase of 2.2 times the reaction rate for a 5ºC increase in temperature while working at environmental conditions (15-30ºC).

1.1.3 Effect of alkalinity

The carbonate/bicarbonate is the most common buffering system found in natural waters. Carbonate and bicarbonate compounds are known for scavenging the •OH radicals, showing reaction rates of $4x10^8\ M^{-1}s^{-1}$ and $2x10^7\ M^{-1}s^{-1}$, respectively (Staehelin & Hoigné, 1985). As a consequence, an ozonation system tends to lose oxidation capacity if they are present in high quantities (Von Gunten, 2003). In addition, phosphate ions react slowly with •OH radicals and may act as scavengers (or sometimes as promoters) (Staehelin & Hoigné, 1985), depending on their concentration in the water matrix (Mizuno, 2007).

1.1.4 Effect of water inorganic/organic composition

O_3 reacts with inorganic and organic compounds that can accelerate or slow down O_3 decomposition. The reactions of •OH radicals with inorganic compounds are considered rather fast (rates of 10^7-10^9 $M^{-1}s^{-1}$); whereas molecular ozone reactions tend to be slower, with second order rates between 1 to 10^9 $M^{-1}s^{-1}$. These reactions involve the transfer of an oxygen atom (Von Gunten, 2003).

As for organic compounds, NOM reacts also directly with molecular O_3 or indirectly with •OH radicals:

- when NOM reacts directly with ozone it can follow two pathways: to be oxidized (O_3 + NOM → NOM_{ox}) or to form ozonide radicals (O_3 + NOM → $NOM•^+$ + $•O_3^-$). Ozonide then becomes the initiator of the radical chain (similar to the role of OH^- ions in pure water). These two reactions are observed in the presence of double bond compounds, activated aromatic rings, amines and sulfides. Direct O_3 reactions with organic saturated compounds are very low (Von Gunten, 2003). Ozone reactivity is favoured at basic pH as DOM is deprotonated and more vulnerable to an electrophilic attack (Buffle, et al., 2006);
- when NOM reacts with the •OH radicals it promotes the radical chain reactions, generating even more radicals (Acero & Von Gunten, 2001), and thus increasing the oxidative capacity of the system. It was also reported that higher pH increases •OH radical production; although Buffle, et al. (2006) indicated that a plateau could be reached. In their experiment, the team observed this plateau was reached at pH 6.7, after which an increase to pH 7.9 did not increase importantly the amounts of •OH generated.

In summary, DOC can act as initiator, promoter (formic acid, methanol), or terminator – scavenger- (alkyl groups, t-butyl alcohol) of O_3 decomposition and radical chain reactions; although it is difficult to predict NOM behaviour in a water matrix due to the heterogeneity of its composition (Staehelin & Hoigné, 1985; Von Gunten, 2003; Westerhoff, et al., 1999).

1.1.5 Molecular O_3 vs •OH radicals

Molecular O_3 is very selective, and generally follows a second order kinetics when reacting with other compounds. The rate constants are in the range of $<0.1\ M^{-1}s^{-1}$ and $7x10^9\ M^{-1}\ s^{-1}$. Because of its electrophile character, ozone attacks mainly non-protonated amine groups, double bonds, and aromatic rings; although the reactivity depends on the type of chemical functional groups associated to the unsaturated moieties (Von Gunten, 2003; Westerhoff, et al., 1999). For example, the presence of a chlorine atom will significantly reduce the moiety reactivity.

•OH radicals are non-specific for their reaction with inorganic and organic matter. However, Westerhoff, et al. (1999) reported that organic double and triple bonds react faster than single bonds. The second order reaction kinetics vary in the range of 10^8-$10^{10}\ M^{-1}s^{-1}$ for large molecules, but has a wider distribution for smaller ones (Staehelin & Hoigné, 1985; Von Gunten, 2003; Westerhoff, et al., 1999). Reaction rates increase with increasing molecular weight; although a reaction upon an active site in the core of a large molecule is slow due to diffusion patterns (Westerhoff, et al., 1999). The presence of free radicals (•OH radicals) enhances mineralization (organic matter oxidized to CO_2 and H_2O), as molecular ozone is not able to do it (Van Geluwe, Vinckier, Braeken, & Van der Bruggen, 2011). The high reactivity and non-specificity of •OH radicals grant them a very low life time, consequently very low concentrations are found with natural waters, typically $\leq 10^{-12}$ M (M. Elovitz & Von Gunten, 1999). Therefore, artificial tactics (raising pH, addition of H_2O_2, UV irradiation, etc.) need to be applied in order to increase their concentration and keep them active (Von Gunten, 2003).

Systems in which •OH radicals dominate the oxidation reactions are called advanced oxidation processes (AOP). These are aimed for the decomposition of resilient molecules such as pesticides, hormones and chlorinated solvents; although it has been reported that the process is not actually efficient due to competition reactions for •OH radicals. This regime is commonly achieved by adding H_2O_2 to the water matrix, but it can also be attained by raising the pH, irradiating with UV, etc. (Von Gunten, 2003). High concentrations of DOC in the water matrix ($\geq$ 3 mg C/L) also generate an AOP regime, as NOM acts as a promoter, rendering a yield of one •OH radical per molecule of O_3 consumed (Acero & Von Gunten, 2001), while in pure water the ratio is 3 O_3 molecules consumed per •OH radical formed (Staehelin & Hoigné, 1985).

Conversely, a system without •OH radicals can be attained by artificially adding a scavenger, for which *t*-butanol is most commonly used. When NOM is present, the addition of *t*-butanol does not prevent however the onset of the first phase of rapid O_3 decomposition, but the rate of reaction is lower than in the absence of *t*-butanol. This suggests the role of NOM as initiator and as a promoter of O_3 decomposition (Westerhoff, et al., 1999).

1.1.6 Oxidation products

The oxidation products from the ozonation of NOM are compounds of lower molecular weight than the original molecules, although they are difficult to identify and predict (Lin & Hsien, 2011). O_3 renders organic hydrophobic moieties into hydrophilic ones (carbonyl, hydroxyl, alkoxyl, amino and carboxyl groups). These by-products are resilient to further oxidation by molecular O_3, but they can be biodegraded or partially mineralized (CO_2 and H_2O) through •OH radicals (Von Gunten, 2003). In addition, ozone and •OH radicals can form undesired by-products from the oxidation of organic and inorganic compounds in water, although the only regulated one is currently bromate, which originates from the oxidation of bromide in water (M. Elovitz & Von Gunten, 1999; Von Gunten, 2003).

1.1.7 Measurement of ozone species

Molecular ozone can be evaluated through electrochemical, optical or colorimetric methods (Von Gunten, 2003). The latter one, performed with indigo colorant, is well recognized for its high sensitivity to ozone (Mizuno, 2007). •OH radicals evaluation require the use of a chemical probe, para-chlorobenzoic acid (pCBA), which reacts very fast with •OH radicals and very slow with molecular ozone (M. Elovitz & Von Gunten, 1999).

As molecular ozone and •OH radicals may co-exist in an oxidation process, the R_{ct} concept can be used to discriminate the fractions of each entity during a reaction (M. Elovitz & Von Gunten, 1999):

$$R_{ct} = \int[\bullet OH]dt / \int[O_3]dt \qquad (1)$$

where $\int[\bullet OH]dt$ represents the •OH exposure or *•OH-Ct*, and $\int[O_3]dt$ the molecular ozone exposure or *O_3-Ct*. Thus, to calculate the R_{ct} from experimental data, the following reasoning has been developed by (M. Elovitz & Von Gunten, 1999):

- As pCBA reacts relatively slow with O_3 compared to •OH radicals, its reaction rate can be neglected. Therefore, the rate of reaction is solely due to the reaction with •OH radicals expressed as:

$$\frac{-d[pCBA]}{dt} = k_{\bullet OH/pCBA}[pCBA][\bullet OH] \quad (2)$$

where $k_{\bullet OH/pCBA}$ is the second order rate constant of pCBA with •OH radicals, equivalent to 5.2 x 10^9 $M^{-1}s^{-1}$ (Acero & Von Gunten, 2001; Westerhoff, et al., 1999).

- Rearranging and integrating equation (2) gives,

$$ln\left(\frac{[pCBA]}{[pCBA]_o}\right) = -k_{\bullet OH/pCBA}\int[\bullet OH]dt \quad (3)$$

- Replacing equation (1) in (3),

$$ln\left(\frac{[pCBA]}{[pCBA]_o}\right) = -k_{\bullet OH/pCBA}R_{ct}\int[O_3]dt \quad (4)$$

where $\int[\bullet OH]dt$ represents •*OH-Ct* and $\int[O_3]dt$ represents O_3-*Ct*.
Equation 4 is a linear relation in which the slope is $-k_{\bullet OH/pCBA}R_{ct}$. As $-k_{\bullet OH/pCBA}$ is constant, the R_{ct} value can be calculated (Von Gunten, 2003).

The Rct approach is only valid for the second portion of the ozone decay where ozone residual is maintained in solution. In the case of the immediate ozone demand (taking place before approximately 15 sec), very high •OH can be generated even if no ozone residual is detected. This is especially the case when oxidizing waters with high organic content or when ozone dosage is small compared to the concentration of reactants. Under such scenario, pCBA can also be used to evaluate the •*OH-Ct* that we will define as 1st phase •*OH-Ct.* In theory, according to Eq. 4, a plot of *O_3-Ct* vs Ln(pCBA/pCBAo) should yield a straight line going through the coordinate (0,1). This is equivalent to say that at a Ct of 0, there is no oxidation of pCBA. However, the phenomenon of immediate demand often translates these curves away from the coordinate (0,1). This information can be used to evaluate the 1st phase •*OH-Ct* such that:

$$\bullet OH - Ct_{1st\ phase} = \frac{ln\left(\frac{[pCBA]}{[pCBA]_o}\right) evaluated\ at\ Ct_{O_3}=0}{-k_{\bullet OH/pCBA}} \quad (5)$$

1.2 Ceramic membrane overview

1.2.1 Basic definitions

Membranes are defined as a physical barrier that allows permeation of certain species. They are widely used in industry for separation and purification processes. According to their constituents, they can be classified as organics (polymeric and biological), inorganics (metallic and ceramic) and hybrids (organic+inorganic components) (Lu et al., 2007). According to their porosity, they can be divided into non-porous and porous membranes. In non-porous membranes (reverse osmosis), selective separation takes place when molecules 'dissolve' into the matrix of the membrane, then diffuse and finally get desorbed from the structure. For porous membranes (NF, UF, MF), size exclusion (sieving) is the main means in which separation is achieved (Akbarnezhad, Mousavi, & Sarhaddi, 2010). As a consequence, the driving force during a filtration process is either a concentration or a pressure gradient (Lu, et al., 2007). Table 1.2 shows a classification of membranes according to their pore size and filtration capabilities:

Table 1.2: Membrane types and characteristics

Membrane type		**Operating Pressures (atm)**	**Pore diameter (nm) or MWCO (Da)**	**Removal capacity**
Low pressure (<2 atm)	Microfiltration[1]	0.1-1	$10^2 – 10^4$ (macroporous)	Suspended molecules Bacteria
	Ultrafiltration[1]	1-5	$2 - 10^2$ (mesoporous) MWCO 1-100 kDa	The previous, plus: Colloids, macromolecules High turbidity removal High NOM removal Giardia, bacteria and virus
High pressure (>2atm)	Nanofiltration	5-20	0.1-2 MWCO 0.15-1 kDa	The previous, plus: Some dissolved solids (some small organics, some monovalent salts) Multivalent salts
	Reverse osmosis	20-40	50-150 Da	The previous, plus: Dissolved solids

(Gao et al., 2011; Jermann, Pronk, Meylan, & Boller, 2007; Koo, Mohammad, Suja, & Talib, 2013; Larbot, Fabre, Guizard, & Cot, 1989; Pabby, Rizvi, & Sastre, 2009; Van Geluwe, Braeken, & Van der Bruggen, 2011)

[1]UF and MF do not remove dissolved solids at all (Al-Amoudi, 2010), but pre-treatments can be installed to do so (adsorption, coagulation, precipitation) (AWWA, 2005).

In drinking water treatment, the use of membranes (polymeric) is a relatively recent technology that started to gain popularity in the 90s and has not since stopped (AWWA, 2005), so that its demand increases about 8% per year (Van Geluwe, Braeken, et al., 2011). UF in particular has experienced a great boost because it offers the possibility of removing bacteria and viruses at a comparatively lower costs than NF, which consequently minimizes the use of disinfectants and the risk of producing disinfectant by-products as long as NOM has been sufficiently removed (Gao, et al., 2011). The advantage of using membranes is the enhanced purification that is possible to achieve; *i.e*. increase in drinking water quality (better removal of molecules and microorganisms) (Al-Amoudi, 2010; AWWA, 2005), without the need of a physical-chemical pre-treatment and moreover, with a reliable quality on produced water (AWWA, 2005). The drawback is the relatively high energy requirements for this technology (Zhu, Wen.X, & Huang, 2012) and the inability of low pressure membranes to remove dissolved contaminants such as NOM or trace micro-pollutants.

Polymers are the most widely used material for filtration membranes due to their relative low cost and commercial availability. The most popular module is the hollow fiber, a versatile system that allows for compact design, easy installation (Madireddi, Babcock, Levine, Kim, & Stenstrom, 1999), and filtration of high quantities of water using a variety of membrane materials and configurations. Besides, it facilitates the washing process as it can be operated in 2 directions (in-out, out-in). Furthermore, membrane's integrity can be verified under this module, which is a valuable tool to evaluate the performance of the filtration process and assess the need of repairing the membranes when necessary (AWWA, 2005). It can be operated in two modes: dead-end and cross-flow. Dead-end mode is more economic, in terms of capital and energy costs, than cross-flow applications (Blankert, Betlem, & Roffel, 2006).

Basic definitions of membrane technology include (AWWA, 2005):

1) **Water flux (*J*)**, which is defined mathematically by a modification of Darcy's law:

$$J = \frac{Q_{total}}{A} = \frac{\Delta P}{\mu R_m} \qquad (6)$$

where J is the permeate flux[a] ($m \cdot s^{-1}$), Q_{total} is volumetric flow rate of pure water, A is the effective filtration area, ΔP is the transmembrane pressure (Pa), μ is the dynamic viscosity[b] of the permeate (Pa.s), and R_m[c] is the intrinsic membrane resistance to the passage of water (m^{-1}).

[a]Flux is usually expressed in liters per square meter of membrane per hour (LMH) or gallons per square foot of membrane per day (gfd), where gfd=1.7 LMH.

[b]Viscosity depends on temperature. The following formula is applied to find the viscosity of water (in centipoise) at a temperature in the range 0-35ºC and a pressure of 1 atm:

$$\mu_T = 1.777 - 0.052T + 6.25 * 10^{-4}T^2 \quad (7)$$

Thus, to report flux values, they should be standardized for 20ºC to allow for comparisons. The correction is made by multiplying the flux calculated at ambient temperature by a correction factor defined as: $\mu_T/\mu_{20ºC}$.

[c]The R_m is mathematically derived from Equation 5 and Pouseuille's law:

$$Q_{1pore} = \frac{\pi r^4}{8\mu}\frac{\Delta P}{\Delta z} \quad (8)$$

where Q_{1pore} is the flow through one pore, r is the pipe's radius, μ is the viscosity and $\Delta P/\Delta z$ is the pressure gradient through the pipe.

Then, the total flux Q_{total} will be:

$$Q_{total} = \frac{\pi r^4}{8\mu\tau}\frac{\Delta P}{\Delta z} A\rho_{pore} \quad (9)$$

where Q_{1pore} has been corrected for the tortuosity (τ) and the number of pores available on the membrane ($A\rho_{pore}$).

Finally, replacing Equation 7 in Equation 5:

$$R_m = \frac{8\tau\Delta z}{\pi r^4 \rho_{pore}} \quad (10)$$

from where it is observed that the radius of the membrane pore is highly important for the fluid transportation (the bigger the pore, the lower the membrane resistance and the higher the flux). R_m also depends on tortuosity and the number of pores of the membrane (AWWA, 2005)).

2) **Permeability** or specific flux (J_s), which is the flux per unit pressure applied on the membrane:

$$J_s = J/\Delta P \quad (11)$$

where ΔP can be expressed as:

$$\Delta P = \frac{P_{in} + P_{out}}{2} - P_p \quad (12)$$

where P_{in} is inlet P, P_{out} is outlet pressure and P_p is pressure of the permeate (AWWA, 2005). Note that in the case of a dead-end application, P_{out} is considered equals to P_{in}.

3) **Rejection** (R_i) is the amount of substance that was removed from the original water. *Ri* tends to vary with time (Schäfer, 2001).

Ceramic membranes

Ceramic constitutes an alternative material to polymers. Ceramic membranes were first introduced for industrial liquid separation in the early 80's at the microfiltration level; afterwards, ultrafiltration was developed by the end of the same decade (Sondhi, et al., 2003). In drinking water, their use is still at the pilot or small scale level due to cost constraints; but ceramic membranes offer unique advantages over polymeric ones, such as the possibilities of applying high feed hydraulic and high backwashing pressures (Zhu, et al., 2012). Japan is undoubtedly, the leading country in drinking water ceramic membrane applications, with approximately 100 installations throughout the territory (Freeman & Shorney-Darby, 2011; Gaulinger, 2007; Metawater Co., 2014). Production capacities are generally below 3 800 m^3/d (1 mgd) (Freeman & Shomey-Darby, 2011), with the highest plant capacity at 39 000 m^3/d (9.8 mgd) by 2007 (Gaulinger, 2007). Currently, an installation of 171 000 m^3/d (45 mgd) is planned to start operations in 2015 (Metawater Co., 2014). The biggest ceramic application outside this country is found at Netherlands. With a capacity of 120 000 m^3/d (32 mgd), the Andijk III water treatment plant started operations this year (Freyberg, 2014) using a hybrid ion-exchange resin+ceramic membrane+ozonation process (BV, 2012-2013).

1.2.2 Ceramic membrane modules

These are hard cases, generally made of stainless-steel, that house one or many ceramic elements. A critical feature related to modules is their sealing. The sealing should be optimal enough to withstand the potential harsh conditions the membranes will be subjected to, so that each manufacturing company has its own technology (Pabby, et al., 2009). Modules can be arranged in 'cascade' mode so to achieve the required final water quality (Pabby, et al., 2009).

The elements inside the modules can be flat sheets, but it is more common to find channeled monoliths of cylindrical shape, as the latter provide better mechanical properties and easiness for sealing. The channels are shaped in different geometries, which have evolved in time. The first elements consisted of only one channel that provided a limited surface filtration area. Then multichannel elements appeared in the market, with channels in different arrangements (ex. flower-like), and shapes: circular, triangular, rectangular, oval, and finally

honeycomb (see figure 1-2). This latter shape grants superior surface filtration area and high turbulence inside the channels. It also requires low pressures (less energy) to make the fluid flow (Pabby, et al., 2009).

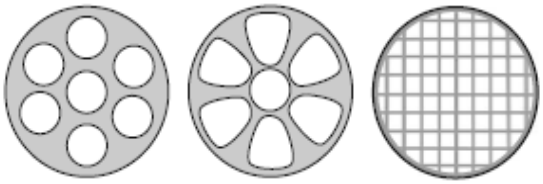

Figure 1-2: Evolution of channel geometries & arrangements: circular, floral, honeycomb
Adapted from (Pabby, et al., 2009)

The latest advancements in ceramic membrane modules include the hollow fiber and capillary ceramic membranes (see figure 1-3) (Pabby, et al., 2009).

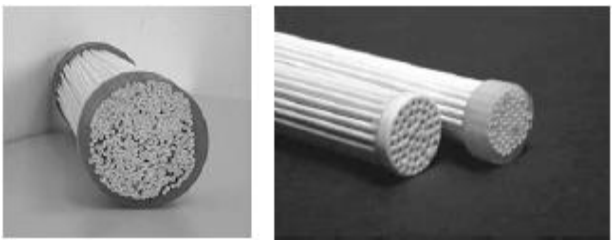

Figure 1-3: Images of a hollow fiber (left) and a capillary (right) ceramic membrane
Adapted from (Pabby, et al., 2009)

1.2.3 Physical structure

Figure 1-4 shows the typical asymmetrical structure of the element of a ceramic membrane, which comprehends various layers of increasing pore size and layer thickness from top to bottom. This design strategy provides for mechanical support to the upper and finer layers and prevents a premature clogging of the membrane during its operation (Kim & Van der Bruggen, 2010; Szymczyk, Fievet, Reggiani, & Pagetti, 1998a).

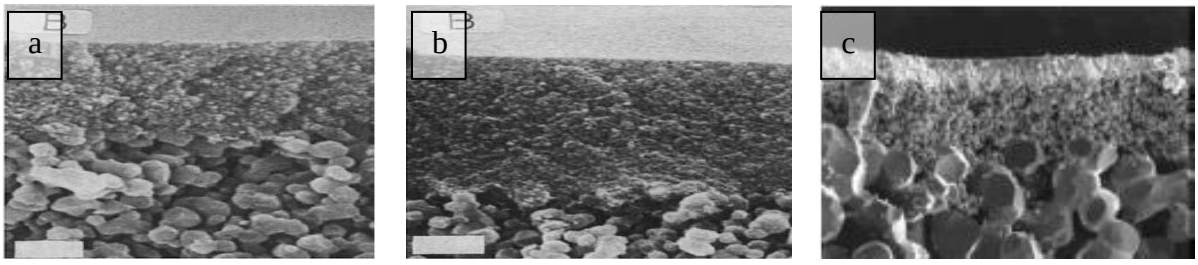

Figure 1-4 : Assymetric structure : a) titania; b) zirconia; c) alumina ceramic membranes
Extracted from (Larbot, et al., 1989; Pabby, et al., 2009)

1.2.4 Preparation

The preparation method of ceramic membranes greatly influences their properties. Different methods are used: ceramic paste extrusion for supports, slip cast for MF layers, sol-gel for UF and NF layers (Pabby, et al., 2009). To prepare the supports, metal oxides, binders and plasticizers are mixed and then pressed, extruded or slip cast (Kim & Van der Bruggen, 2010).

The top layer can be prepared through various methods: slip cast, state-molecule-sintering, sol-gel, anodic oxidation, chemical vapor deposition and the reversed micelle method, but the most widely used is the sol-gel process because it allows for reaching outstanding homogeneity and purity, well-defined pore size distribution and good control of the micro-properties of the metallic compounds used (Akbarnezhad, et al., 2010; Alem, Sarpoolaky, & Keshmiri, 2009; Shi, Tin, & Wong, 1999). Moreover, sol-gel is considered to be the only method to be used for UF membrane preparation because of the compromise between achieving fine pores and high permeability with thin layers (Larbot, et al., 1989). In the sol-gel method, hydroxides or hydrous metal oxides are dispersed in water to prepare the sols. The particles size and distribution, which are a function of pH and concentration of the oxides dispersions, have an influence on the final pore size and membrane surface properties (Kim & Van der Bruggen, 2010; Larbot, et al., 1989). The particles shape influence the shape of the membrane pores. For example, spherical molecules (titania, zirconia, α-alumina) give bottle-neck shapes, plat forms (clay, γ-alumina) give slit pores, lyotropic liquid crystals give cylindrical pores (see figure 1-5) (Pabby, et al., 2009).

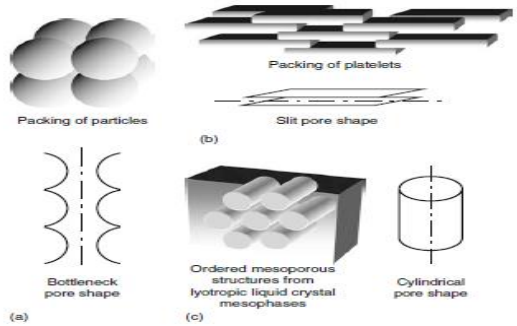

Figure 1-5: Ceramic membranes pore shapes: a) bottleneck, b) slit shape, c) cylindrical shape
Adapted from (Pabby, et al., 2009)

Next, the sol is transformed into a gel (polymerized) in acidic media; and finally, selected additives (organic binders) are added to adjust for viscosity (Larbot, et al., 1989) and to prevent the cracking of the top layer during the drying process (Larbot, Alary, Guizard, & Cot, 1987).

In order to join both layers, the support is submerged many times in the sol-gel solution in controlled time periods. The number and duration of these periods depend on the desired top layer thickness (Alem, et al., 2009), which is recommended to be between 1-10 μm to achieve high permeability (Larbot, et al., 1987). The embedded support is dried and then calcined at high temperatures (sintering process). Sintering grants mechanical properties to the ceramic and makes possible the binding of the thin layer to the support, as traces of water and organics will be eliminated by heat (Akbarnezhad, et al., 2010; Shojai & Mäntilä, 2001). Sintering temperatures also determined membrane surface properties and membrane pore sizes (higher temperatures produce bigger pores, and vice versa) (Kim & Van der Bruggen, 2010; Larbot, et al., 1989).

1.2.5 Chemical composition

Common materials used in the preparation of ceramic membranes are Al_2O_3 (alumina), TiO_2 (titania), ZrO_2 (zirconia), SiO_2 (silica) or a combination of them (Akbarnezhad, et al., 2010; Alem, et al., 2009). All of these materials show an amphoteric character (negative or positive charge according to the pH of the feed solution) and electrokinetic properties (zeta potential) that are important for the transport of electrolytes through the membranes (Szymczyk, et al., 1998b). The amphoteric behaviour comes from the hydroxyl groups associated with the hydrated metal oxides (Chevereau et al., 2010).

TiO_2 membranes: titania is one of the favorite materials used among ceramic membranes as it grants advantageous properties to the units prepared: high hydrophilicity, high water flux, high chemical resistance and photocatalytic activity. The latter allows for the decomposition of toxic compounds in water (Alem, et al., 2009). Sintering is done above 400ºC. Between 550-600ºC the anatase phase is transformed irreversibly to the rutile phase; although the change can generate cracks on the surface (Alem, et al., 2009; Larbot, et al., 1989). Pore sizes can vary between 3-180 nm (Larbot, et al., 1989). The thickness of titania layers have been reported to be between 1-5 μm (Alem, et al., 2009; Chevereau, et al., 2010). Too thin or too thick of a layer can lead to

cracks formation. The photocatalytic properties depend on the size of the titania particlle, its phase (anatase) and the specific surface area of the membrane (the highest possible) (Alem, et al., 2009). Isoelectric point has been referenced between 4 and 7.3 (Szymczyk, et al., 1998a); Changwo, 2013); varying according to the crystalline form of TiO_2 (Chevereau, et al., 2010). Contact angle has been reported at ±40º (Kujawa et al, 2014). In addition, TiO_2 has a strong affinity for Mg^{2+} ions, so that its adsorption importantly modifies the surface charge; for example: zeta potentials will be more positive when pH increases if Mg^{2+} ions are present compared to the presence of monovalent salts (NaCl) (Chevereau, et al., 2010). These authors also showed that hydration of the TiO_2 surface is a very slow process. The team obtained decreasing permeability values for pure water in a period of 500 h during the conditioning phase. Hydroxyl group formation and adsorption (physical and chemical) of water molecules took place during this period.

ZrO_2 membranes : these membranes have a higher chemical resistance than titania or alumina membranes, which make them suitable for filtration in harsh conditions (Shi, et al., 1999). ZrO_2 uniquely exhibits four chemical properties: being an acid and a base, as well as a reduction and oxidation agent. It possesses three crystallization phases: cubic, tetragonal and monoclinic (Shojai & Mäntilä, 2001). Sintering is performed above 470ºC. When reaching 720ºC, zirconia changes the tetragonal crystalline structure (8 O atoms surrounding Zr) to a monoclinic one (7 O atoms surrounding Zr), which causes cracks in the layer formed (Medvedkova & Nazarov, 1995; Shi, et al., 1999). Yttria could be added to avoid the cracks (Shi, et al., 1999), as well as to increase the mechanical resistance of ZrO_2 (Shojai & Mäntilä, 2001). Sol-gel ZrO_2 membranes are normally in the tetragonal phase (Shi, et al., 1999); whereas slip cast ones in the monoclinic phase (Shojai & Mäntilä, 2001). Pore diameters vary in the range of 3-80 nm (Larbot, et al., 1989). The isoelectric point has been reported to be around 4.5-6 (Changwon, 2013; Moritz, Benfer, Árki, & Tomandl, 2001; Szymczyk, et al., 1998a), whereas the value of contact angle has been referenced at ±40º (Changwon, 2013).

Al_2O_3 membranes: for UF applications, alumina membranes are prepared via the sol-gel technique. Sintering temperatures allow for three types of structure and pore size ranges: γ-alumina between 400-900 ºC with pore sizes 2.5-5 nm, θ-alumina between 900-1100 ºC with

pore sizes of ±5 nm, and α-alumina above 1100 ºC with pore sizes 5-55 nm (Larbot, et al., 1987). α-alumina has a good chemical stability in acidic and basic conditions (Alem, et al., 2009). Depending on the type of alumina used, different isoelectric points are reported: 8-9 for fused alumina, 5-6 for calcined alumina (Chiu, 2011). Alumina is commonly used as the support's material of a ceramic membrane. Permeability of alumina membranes is poor compare to zirconia or titania ones (see table 1.3) (Larbot, et al., 1989).

Table 1.3 : Water flux (LMH, P : ±10atm) through γ-alumina, zirconia and titania membranes

Pore diameter (nm)	γ-alumina	zirconia	Titania
6	100	1750	4400
8	200	1900	4700
10	450	2100	5000

Adapted from (Larbot, et al., 1989)

SiO_2 membranes: this material has low stability with hot water and also has low chemical resistance. To improve these properties, titania or especially, zirconia is doped in its structure. Pore sizes, however, are well-controlled with silica membranes (Araki, Kiyohara, Imasaka, Tanaka, & Miyake, 2011). Contact angle has been reported at ±111º (Jeens et al, 2005), and isoelectric point between 2-2.5 (Changwon, 2013).

1.2.6 Operation mode

Ceramic membranes generally operate in cross-flow filtration mode, but some dead-end applications can be found, especially for low suspended solids application such as the treatment of surface waters. In monolith multichannel ceramic membranes (the most common configuration), the direction of the feed flow is inside-out (Pabby, et al., 2009).

1.2.7 Comparison of ceramic vs polymeric membranes

Table 1.4 condenses the advantages and disadvantages of each of these materials used in membrane filtration technology.

Table 1.4: Comparison of ceramic versus polymeric membranes

Membrane	Advantages	Disadvantages	Current status
Ceramic	• Long lifespan[2] • High thermal, chemical and mechanical resistance[2] • Less prone to fouling[3] • Composition is better defined[4] • More uniform pore distribution[4] • Less prone to bacterial colonization[1] • Requires less feed pre-treatment[5] • Allows for harsher and more effective cleaning[5]	• Expensive[2] • Brittle[2] • Lower permeability	• Small scale applications[2] • Surface modifications (with nanomolecules) to improve permeability and fouling resistance[4]
Polymeric	• Cheap[2] • Produced in large scale[2] • Good quality control[2]	• Structurally weak[2] • Limited thermal resistance[2] • Short life due to denaturation and contamination[2] • Low resistance to O_3	• Widespread and large applications in drinking water[2]

[1]Larbot, et al., 1989; [2]Lu, et al., 2007; [3]Alem, el al., 2009; [4]Kim & Van der Bruggen, 2010; [5]Pabby, et al., 2009

Other precisions:

- Mg^{2+}: It has been reported that adsorption of ionic species such as Mg^{2+} on polymeric surfaces does not influence the selectivity of the membranes, contrary to the ceramic ones (Chevereau, et al., 2010).

1.3 Principles of membrane fouling

1.3.1 Basic concepts

Fouling is defined as the loss of performance (throughput) of a membrane due to undesirable deposition of suspended (colloids and/or solids) or dissolved substance on/inside the pores. Fouling may affect water quality, although more research needs to be done in that sense (Gao, et al., 2011). Fouling of membranes causes increase in costs of energy, frequent chemical cleaning cycles, early membrane replacement (lower lifetime), and additional labour for maintenance (Al-Amoudi, 2010).

The fouling event is determined by biological, physical, chemical and/or electrical interactions among the solutes and/or between the solutes and the membrane's surface (Gao, et al., 2011; Jermann, et al., 2007). At the beginning, the process is driven by solute-membrane interactions, but later on, it is controlled by foulant-foulant relations (Jermann, et al., 2007). The evolution of fouling behaviour during surface water filtration involves a cake formation over the membrane that can be preceded or not by pore blocking or pore adsorption events (Jermann, et al., 2007). It has also been reported that fouling mechanisms of interacting foulants are different and often more severe than independent foulants (Gao, et al., 2011; Jermann, et al., 2007).

Recognized membrane foulants are (Al-Amoudi, 2010; Gao, et al., 2011; Koo, et al., 2013):

- Particles: this classification obeys a size criterion. Larger molecules than the membrane pore size are rejected and deposit over the membrane surface; whereas small molecules tend to block or adsorb inside the membrane pores.
- Organics: in drinking water, the major foulant is natural organic matter (NOM). The first investigations pointed at the hydrophobic fraction (derivatives of humic substances: the humic acids) as the main fouling agents, as long as they adsorb onto the membranes surface (Combe, Molis, Lucas, Riley, & Clark, 1999; Nilson & DiGiano, 1996; Yuan & Zydney, 1999; Zularisam, et al., 2006); but later studies remarked the role of the hydrophilic fraction (biopolymers) on this process as these huge molecules block membrane pores and adhere to membrane surfaces by hydrogen bonds (Katsoufidou, Yiantsios, & Karabelas, 2005; Kennedy, Chun, Quintanilla, Heijman, & Schippers, 2005; Kimura, Tanaka, & Yoshimasa, 2014; N. Lee, Amy, & Croué, 2006; Yamamura, Okimoto, Kimura, & Watanabe, 2014). Currently, increasing focus is given to the role of biopolymers on membrane fouling.

- Inorganics: dissolved inorganics ($BaSO_4$, $CaSO_4$, $CaCO_3$) and/or slightly soluble compounds (inorganic salts, minerals and/or colloidal matter) may form a scale on the membrane surface. However, this is expected to be of significance only if the solubility products are exceeded.
- Biological: microorganisms attach to the membrane surface, and subsequently grow and reproduce in the presence of enough nutrients.

Fouling mechanisms: AWWA (2005) describes two types of fouling: cake (gel-layer) on the feed-side of the membrane and pore blocking. For a dead-end filtration, the latter is divided in: complete pore blocking, incomplete pore blocking, and standard pore blocking (see figure 1-6).

- Complete pore blocking: a monolayer of molecules blocks all the pores of the membrane surface; no superimposition is allowed. It occurs when molecules are bigger or of comparable size than the membrane pores (AWWA, 2005; Chellam & Cogan, 2011; Hlavacek & Bouchet, 1993). It is commonly observed in NF membranes filtration (Al-Amoudi, 2010).
- Intermediate blocking: molecules can deposit, either over the membrane's surface, or over another layer of molecules that is already deposited on the membrane's surface (Z. Ho, 1999). Any deposition site has equal chances of being occupied (Koo, et al., 2013). A pore is always completely blocked when reached by a bigger molecule (Chellam & Cogan, 2011; Hlavacek & Bouchet, 1993).
- Standard pore blocking or pore adsorption: it occurs when all the molecules are smaller than the pore size of the membrane and thus deposit inside the pores, reducing their diameter in a uniform way (AWWA, 2005; Chellam & Cogan, 2011; Koo, et al., 2013). It commonly leads to irreversible fouling, and may only be partly removed by chemical cleaning (Jermann, et al., 2007).
- Cake filtration: a ubiquitous mechanism (Huang, Young, & Jacangelo, 2008) where molecules that are larger than the membrane pore size deposit on the membrane surface (blocking of pores is not considered in ideal cake filtration). It can also be induced by concentration polarization (AWWA, 2005; Chellam & Cogan, 2011). The resistance of the cake increases proportionally to the depth of the cake (Koo et al, 2012). To eliminate a cake layer, a backwash or an important shear stress should be applied to the surface (Jermann et al, 2007). Filtration cakes can be classified as incompressible (cake structure does not change even if increasing the TMP or the rate of deposition of materials; example: silica), and

compressible (cake becomes denser and with higher resistance when increasing the TMP or the flow rate across the cake) (Al-Amoudi, 2010). Compressibility depends on the type and shape of the molecules, and is crucial for fouling behaviour. In water and wastewater treatment, it is very common to deal with compressible molecules (organic material, bacteria, clays, etc.) (Chelam et al, 2006; Kim & DiGiano, 2009).

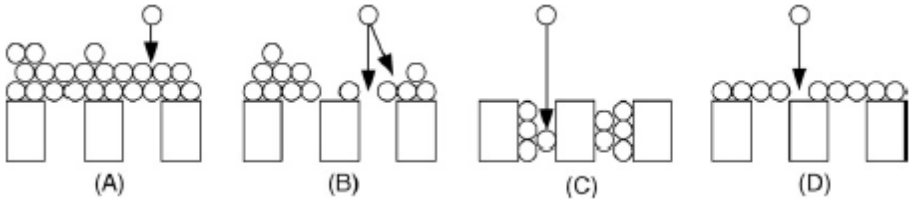

Figure 1-6 : Filtration laws for dead-end mode : a) cake filtration, b) intermediate blocking, c) standard blocking, d) complete blocking
(Extracted from Blankert et al, 2006)

- **Concentration polarisation** (CP) is not considered a fouling mechanism, but a condition that can lead to its establishment. It is defined as the accumulation of rejected material (dissolved, colloidal and/or microbial) in the proximity of the membrane surface, yielding higher concentrations than the bulk itself (AWWA, 2005; Koo et al, 2012). CP aggravates fouling and can deteriorate filtrate quality if TMP is increased (Madireddi et al., 1999; Koo et al., 2012). This mechanism is reduced if a tangential flow is applied, or if the pressure exerted is decreased (Jermann et al, 2007). Concentration polarisation takes place when convective forces balance back-diffusion ones. The mass balance becomes:

$$JC - D\frac{dC}{dx} = JC_p \qquad (13)$$

where J is flux, C is concentration of material, Cp is concentration of material in filtrate. With boundary conditions $C_{x=0} = C_m$ and $C_{x=\delta} = C_b$, Equation 8 becomes:

$$\exp\frac{J\delta}{D} = \frac{C_m - C_p}{C_b - C_p} \qquad (14)$$

where $J\delta/D$ is the Peclet number (dimensionless), C_m concentration at the membrane, C_b concentration of the feed (AWWA, 2005).

Reversibility: reversibility describes the ability of a membrane to recover from a given fouling condition.

- Reversible fouling: fouling that is eliminated by physical cleaning (air, water) such as external fouling or cake formation (Gao et al, 2011; Zhu, 2012); or chemical cleaning.
- Irreversible fouling: fouling that cannot be eliminated by any means. It is the reason for the loss of permeability of the membrane in the long term use (Gao et al, 2011).

1.3.2 Factors influencing the fouling of membranes

The fouling of porous membranes implies many complex physical and chemical related interactions. Factors that affect membrane fouling in the presence of NOM are (Schäfer, 2001; Al-Amoudi, 2010):

1. Membrane characteristics: surface morphology, structure, pore size, pore size distribution, shape, surface chemical properties.
2. Chemistry of the feed solution: ionic strength, pH, concentration of monovalent and divalent ions, molecules, colloids, NOM, inorganic components, and their properties such as nature, morphology, size, size distribution, surface potential.
3. Hydrodynamic and operation conditions: permeate flux, pressure, concentration polarization and the mass transfer properties of the fluid boundary layer.

Membrane characteristics

Surface morphology.- The rougher the surface of the membrane, the more clogging will be produced as colloidal molecules accumulate in the valleys of rough membranes (Van Geluwe, 2011).

Pore size and distribution.- A homogeneous distribution of pores size allows for higher selectivity of the membrane (Larbot, et al., 1987) and higher pore diameters grant higher permeability to the membrane (Larbot, et al., 1989). But it may happen that for larger pore-size membranes fouling is faster and more important due to the fact that bigger molecules are allowed into its structure and facilitate pore blocking or adsorption (Al-Amoudi, 2010).

Membrane structure.- Membranes that have high interconnectivity between the pores tend to foul slower than non-connected membrane pores because they provide for alternative pathways for fluid flow (Ho & Zydney, 1999; Koo et al, 2012).

Surface chemical properties.- They are related to the membrane material. For ceramic membranes, the surface properties depend on the metal oxide used, as this defines the grade of

sorption and desorption of protons on the surface when interacting with aqueous solutions (Chevereau, et al., 2010). This is related to the isoelectric point and the zeta potential of the membrane (Pabby, et al., 2009), factors that have an influence on the rejection patterns and consequently, the fouling behaviour. For example, it has been observed that permeate flux decreases when a membrane has a high zeta potential (Chevereau, et al., 2010).

Chemistry of the feed solution

The chemistry of the feed solution simultaneously affects the membrane surface and NOM properties, as follows:

Ionic strength.- membrane surface charge is affected by the ionic strength, pH and presence of multivalent ions in the feed solution (Costa & de Pinho, 2005). Lee & Kim (2014), indicates that at high ionic strength, the repulsions between membrane and fouling agents decrease due to compression of electrical double layer; consequently, fouling agents deposit on the membrane. The same mechanism would lead to the aggregation of molecules in the aqueous solutions causing the formation of a dense cake. As a consequence, permeability decreases. Similarly, AWWA, 2005 indicates that the permeability of the cake formed on the membrane surface has been modelled by various authors who took into account drag forces, electrical double-layer repulsion forces and van der Waals attraction forces. These models predict an increase in fouling with higher ionic strength and lower zeta potential. Scymyzyk, et al. (1998) found that at low ionic strengths, double layers in the pores are overlapped and diffusion of ionic species decreases due to the influence of surface charges.

The primary, secondary and tertiary structures of NOM depend on ionic strength. At low salt concentrations, low ionic strength and neutral pH, internal electrostatic repulsions are higher and molecular chains are larger (flatter). Likewise, at high salt concentrations, high ionic strength and low pH, NOM molecules shrink in a compact colloidal sphere because functional groups are neutralized by intramolecular charges (internal shielding) (Al-Amoudi, 2010).

pH.- the membrane surface charge can be modified according to the presence of ions in the feed solution, due to adsorption of these ions/molecules or dissociation of functional groups (Chevereau, et al., 2010). Surface charges may become less positive or less negative if submerged in high or low pH^1, respectively (Costa & de Pinho, 2005). Regarding permeability, it

has been reported it tends to decrease, when pH is low and ionic strength is high (Costa & de Pinho, 2005).

[1]Interestingly, it was observed and increase in negative membrane charge at pH 4, which was explained by greater adsorption of humic acid (Al-Amoudi, 2010).

NOM is negatively charged in the pH range of natural waters (Costa & de Pinho, 2005). The pH has a major effect on the fouling behaviour of humic acids. For example, at low pH, humic acids are smaller due to lower internal electrostatic repulsion and therefore, they permeate through the membranes pores (Al-Amoudi, 2010).

Concentration of multivalent ions.- For TiO_2 membranes, divalent ions such as Ca^{2+}, Mg^{2+} and SO_4^{2-}, adsorb on to the membrane's surface and importantly affect its zeta potential and reduce the effective pore size, influencing its selectivity and permeability (Chevereau, et al., 2010). For example, in the presence of increasing amounts of Ca^{2+}, the membrane surface becomes less negative (Al-Amoudi, 2010). Multivalent ions can also link solutes, such as humic acids, to the membrane and induce stronger fouling (Jermann, et al., 2007). Likewise, complexation of these ions with organic matter aggravates fouling (Al-Amoudi, 2010). It was observed that in the presence of EDTA, divalent cations are complexed (those free and those associated to NOM), and the fouling is reduced (Al-Amoudi, 2010).

Molecules.- AWWA, 2005 indicates that molecules reaching the surface of the membrane will not all be deposited on its surface, as many forces play a role in that interaction. They reported that the electrical double-layer repulsion energy increases proportionally with molecule size, as depicted by the Hogg, et al. (1966) equation (AWWA, 2005):

$$\Phi_{EDL} = \pi\varepsilon_0\varepsilon_r\alpha_p\left\{2\psi_p\psi_s ln\frac{1+\exp(-\kappa y)}{1-\exp(-\kappa y)} + \left(\psi_p^2+\psi_s^2\right)ln[1-\exp(-2\kappa y)]\right\} \qquad (15)$$

where Φ_{EDL} is electrical double-layer repulsion energy, ε_0 permittivity under vacuum, ε_r relative dielectric permittivity of water, ψ_p surface potential of the molecules, ψ_s surface potential of the solid surface, and κ is the reciprocal of the Debye length. In addition, under conditions of low shear forces and rates (such as dead-end filtration), the back-transport of molecules is dominated by Brownian motion, so that larger molecules tend to stay close to the membrane (Kim & DiGiano, 2009).

Smaller molecules tend to produce higher fouling due to membrane porosity reduction and denser cake conformation than larger molecules (Kim & DiGiano, 2009). However, it was observed that poly-dispersed solutions (small and big molecules together) tend to produce more fouling than mono-dispersed ones. This would be because bigger molecules thicken the cake layer while smaller ones filled up the void space increasing its density (Koo et al, 2012).

Colloids.- Defined as fine suspended molecules in the size range of a few nanometers to a one micrometer, are an important cause of membrane fouling due to their accumulation on or close to the membrane surface (Koo et al, 2012). Colloids are formed by inorganics (clays, silica salt, metal oxides), organic (natural and synthetic organic), and biological (bacteria and other microorganisms) molecules. They are identified as a main fouling agent in UF filtration (Koo et al, 2012). For example, Kim & DiGiano, 2009 reported that molecules smaller than 0.1 µm produce higher fouling in constant flux than in constant pressure operation. No difference was reported, however, if the molecules were over 0.1 µm. Regarding NOM, the colloidal and dissolved fractions are identified as main fouling agents; more specifically, when molecular weights are in the range of 2-100 kDa, with peaks at 3, 6, and 50 KDa (Al-Amoudi, 2010). Biopolymers can be considered as colloidal matter.

NOM.- NOM is recognized as a the main fouling agent for surface water filtration, even though dissolved NOM passes through the membranes due to its small size (AWWA, 2005). Humic substance is the major fraction of NOM. They are refractory anionic macromolecules in the pH range of surface waters, of low to moderate molecular weight. Their spatial conformation depends on the chemistry of the solution, say pH and ionic strength, in which they are immersed. They contain aromatic and aliphatic components. The main functional groups are carboxylic (60-90%) and phenolic (Costa & de Pinho, 2005; Al-Amoudi, 2010). Biopolymers (carbohydrates and proteins) are also an important NOM fraction related to membrane fouling. These macromolecules are mainly composed of aliphatic carbons and hydroxyl groups (Yamamura, Okimoto, Kimura, & Watanabe, 2014).

NOM fouling is attributed to: a) accumulation of molecules retained on the membrane surface, forming a cake or gel layer; b) the adsorption of non-retained molecules in the inner pores of the membrane, leading to constriction and blocking of the pores (Van Geluwe, 2011).

The fouling potential of NOM is defined by physical and chemical interactions between fouling agents and membranes (Van Geluwe, 2011). The interactions are described below:

- The Van der Waals forces: between molecules and surface follows the following model (AWWA, 2005):

$$\Phi_{vdW} = -\frac{A\alpha_p}{6d(1+\frac{14d}{\lambda})} \quad (16)$$

  where Φ_{vdW} van der Waals attraction energy, A is Hamaker constant of the interacting media, α_p is molecule radius, d is surface-to-surface separation distance of molecules-surface, and λ is characteristic wavelength of the interaction (100 nm by convention) (AWWA, 2005).
- Electrostatic interactions NOM-membrane (electrical double-layer interactions): depending on the pH of the medium, the functional groups of the membrane can be electrically charged (for polymeric membranes the charge is generally, negative at neutral pH, and neutral at pH 3-4) (Van Geluwe, 2011).
- Hydrophobic interactions: they are attractive forces between hydrophobic moieties (AWWA, 2005). Under these forces non-polar material tends to aggregate in aqueous media, therefore, in order to compensate for the electrical poles formed, they adsorb onto the membrane surface (Van der Waals stabilization) forming a cake layer. Fouling is more common and severe with hydrophobic surfaces (Van Geluwe, 2011). This is an advantage of ceramic membranes which are generally more hydrophilic than polymeric membranes.
- Other forces in the interaction molecules-membrane surface include: hydrogen bridges (hydrogen bonds), the hydration force (considered a repulsive force as it demands the input of energy to dehydrate surfaces and allow the binding of molecules), and steric interaction (a repulsive force that arises when molecules approach a surface) (AWWA, 2005).

The hydrophobic fraction of NOM (humic substances) has been related to concentration polarization; but it also has been found to be responsible of severe irreversible fouling. The hydrophilic, non-humic, dissolved or colloidal NOM (polysaccharides and proteins) has been related to adsorptive and irreversible fouling, especially in polymer membranes (Jermann et al, 2007; Al-Amoudi, 2010); although Van Geluwe, 2011 reported that their effect is milder than the hydrophobic fraction. Finally, the transphilic fraction has been associated with cake layer deposition (Gao et al, 2011).

Inorganics.- They form a scale (inorganic fouling) if their salt concentrations surpass the solubility limit. Typical precipitates come from iron, silica, aluminum, calcium, phosphorus and sulphates (Koo et al, 2012).

Hydrodynamic and operation conditions

- Advective and diffusion forces are important in the onset of fouling, so that this will occur anyway at high permeation rates, even if the solution conditions do not promote it (Al-Amoudi, 2010).
- Temperature may also affect fouling as it affects the viscosity of the fluid, the mass transfer in the proximity of the membrane surface, and the water quality of the feed water depending on the sampling season (AWWA, 2005).
- Operation mode, such as dead-end or cross-flow will build up different shear conditions that affect the fouling of the membrane (Hlavacek & Bouchet, 1993).

1.3.3 Filtration blocking laws

Many mathematical equations have been developed throughout the time in order to model fouling behaviour. The objective is to better understand and identify the optimal parameters to minimise fouling (Kim & DiGiano, 2009). There has been, of course, an evolution on the conceptualisation of this phenomenon, according to the deeper understanding of the process and the technological advancements.

The first four forms of the fouling equations were derived by Hermans and Bredée in 1936 and have been used for over 50 years to explain filtration behaviours. This ‘classical model’ is purely mechanical as it considers the fouling is only produced by molecules clogging the pores (Hlavacek & Bouchet, 1993). It was developed on the basis of what is now known as a dead-end, non-stirred, constant pressure operation mode, and it is also based on the assumption that the membrane consists of a series of parallel (non-connected) pores with constant diameter and length (Ho & Zydney, 1999). In 1950, Gonsalves criticized the physical meaning of these equations (Hlavacek & Bouchet, 1993). In 1956 Grace applied these models to predict the performance of a filter. It was not until 1982 that the equations were again revised. This time, Hermia re-formulated the equations considering non-newtonian liquids (Hlavacek & Bouchet, 1993; Cheng et al, 2011). These equations, known as the Hermia models, were and are still often

used to interpret fouling behaviour, even for scenarios that do not correspond to their principles such as cross-flow operation modes. This may be due to the simplicity of the equations (Hlavacek & Bouchet, 1993).

Many improvements have been introduced since Hermia (1982) accounting both for the deeper understanding of the complex filtration process as well as the technological advancements in the field. Hence, in the '90s, the resistance-in-series criteria (based on Darcy's law) started to be applied:

$$J = \frac{\Delta P}{\mu(R_m + R_t)} \quad (17)$$

where J is flux [m.s^{-1}], ΔP is effective or transmembrane pressure [Pa] , μ is dynamic viscosity of the filtrate [Pa.s], R_m is the membrane resistance, and R_t is total fouling resistance [m^{-1}]: $R_t = R_{cp} + R_c + R_a + R_b$, having R_{cp} as resistance due to concentration polarisation, R_c cake resistance, R_a resistance due to pore adsorption and R_b resistance due to pore blocking (AWWA, 2005; Chang et al, 2014; Kim & DiGiano, 2009). Thus, the '90s and later years experienced an intensive period of fouling modeling studies. Factors such as molecule size (Granger et al, 1985), operation mode: cross-flow (Davis, 1992), operation mode: constant flux (Hlavacek & Bouchet, 1993), pores connectivity (Ho & Zydney, 1999), the simultaneity of various fouling mechanisms (Bolton, LaCasse, & Kuriyel, 2006; C. Ho & Zydney, 2000), compressibility of cakes (Chellam & Xu, 2006), change in pores geometry (Cheng, Lee, & Lai, 2011), etc., generated multiple mathematical relations that thicken the knowledge needed to create a unified body of practical equations to predict fouling in real-large scale low-pressure membranes processes. The latter has not yet been possible because of the lack of a standardized experimental protocol to perform fouling tests and the scarce information about the 'scale-up' of the equations to the industrial level (Kim & DiGiano, 2009). Besides the wide variety of factors that affect fouling (Koo, et al., 2012) (water and membrane properties, operation modes, systems configurations, etc.) make it even more difficult for the definition of a universal model. Consequently, in the current development stage, the models proposed are still used to fit data *a posteriori* instead of predicting *a priori* fouling behaviours (Chellam & Cogan, 2011). Thus, the fouling mechanisms are deduced from the best matching of the shape of the experimental filtration curve with the model graph (with adjusted constants). If several mechanisms are suspected from the different graph segments, a model fitting for each segment should be applied (Blankert, et al., 2006; Chellam & Cogan, 2011). Finally, the slopes would indicate the severity of fouling (Blankert, et al., 2006).

In order to illustrate the diversity of the equations developed, and because this work deals with constant flux, dead-end, low-pressure filtration, some of the expressions formulated for this configuration and mode of operation are shown.

Some blocking laws for constant flux operation (tables 1.5 to 1.9):

Table 1.5: Hlavacek & Bouchet (1993) blocking laws

Law/Model	Equation	Linearized form	Fouling Parameter
Complete blocking	$\frac{1}{\Delta P} = \frac{1}{\Delta P_o} - \frac{\sigma V}{R_m \mu Q}$	$\frac{1}{\Delta P} = a + bV$	σ [m^{-1}]
Standard blocking	$\frac{1}{\sqrt{\Delta P}} = \frac{1}{\sqrt{\Delta P_o}} - \frac{cV}{\sqrt{8\pi N \mu L^3 Q}}$	$\frac{1}{\sqrt{\Delta P}} = a' + b'V$	c [-]
Intermediate blocking	$\Delta P = \Delta P_o exp \frac{\sigma V}{\varepsilon A}$	$Ln(\Delta P) = a'' + b''V$	σ [m^{-1}]

where ΔP_o is initial pressure drop $(\Delta P_o = R_m \mu Q/\varepsilon A)[Pa]$, σ is clogging coefficient [m^{-1}], V is volume filtered [m^3], Q is volumetric flow rate [m^3/s], c is volume of deposit per unit filtrate volume, N is number of pores, L is pore length [m], A is membrane area [m^2], and ε is membrane porosity.

Table 1.6: Blankert et al. (2006) fouling laws

Law/Model	Equation	Fouling parameter
Complete Blocking	$R(w) = R_M \left(1 - \frac{w}{w_A}\right)^{-1}$	$\frac{1}{w_A R_M}$
Standard blocking	$R(w) = R_M \left(1 - \frac{w}{w_V}\right)^{-2}$	$\frac{2}{w_V R_M^{1/2}}$
Intermediate blocking	$R(w) = R_M e^{w/w_A}$	$\frac{1}{w_A}$
Cake filtration	$R(w) = R_M \left(1 + \frac{w}{w_R}\right)$	$\frac{R_M}{w_R}$

where $R(w)$ is resistance as a function of the filtration state w, w_A is pore blocking potential, w_V is pore filling potential and w_R is specific cake resistance.

Table 1.7: Kim & DiGiano (2009) fouling laws

Law/Model	Equation	Observation
Incompressible cake	$\Delta P(t) = \frac{\mu\alpha\rho_p\phi_C}{\phi_R - 1}J^2t + \mu J R_m$	α = constant
Compressible cake	same as above	$\alpha = \alpha_o \Delta P^n$

where α is specific cake resistance (mass of cake layer per unit filtration area) [m.kg^{-1}], ρ_p is molecule density [kg.m^{-3}], ϕ_C is solid volume fraction of the cake layer, ϕ_R is ratio of solid volume fraction of cake layer and feed solution, J is filtrate flux, t is time, μ is viscosity of feed solution [kg.m^{-1}s^{-1}], R_m is clean membrane resistance (m^{-1}), α_o and n (compressibility) are constants to be determined experimentally.

The team presented also the typical graph for the variation of pressure in time for a compressible and an incompressible cake (figure 1-7):

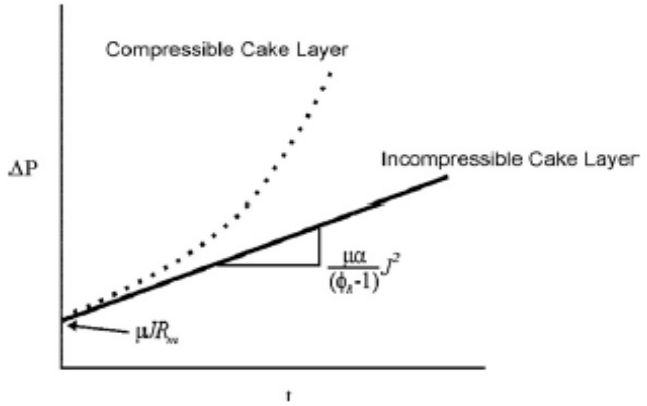

Figure 1-7: Graph for pressure variation in constant flux, dead-end filtration (Adapted from (Kim & DiGiano, 2009))

Table 1.8: Chellam & Cogan (2011) fouling laws

Law/Model	Equation	Observation
Complete blocking	$\Delta P = \frac{Q\mu R}{A_o - \sigma V} = \frac{\Delta P_o}{1 - (\sigma/A_o)V}$	-
Standard blocking	$\Delta P = \frac{\Delta P_o}{(1 - K_s V/2)^2}$	$K_s = \frac{2C}{\pi L N r_o^2} = \frac{2C}{L\varepsilon A_o}$
Intermediate blocking	$\Delta P = \Delta P_o exp\left(\frac{\sigma}{A_o}V\right)$	-
Incompressible cake	$\Delta P = \Delta P_o + \frac{Q\mu\alpha^* c_b}{A_o^2}V$	-
Linear compressible cake	$\Delta P = \frac{\Delta P_o + K_C V}{1 - K_C n_2 V}$	$K_C = \frac{Q\mu c_b \alpha_o^*}{A_o^2}$

where A_o is clean membrane area, σ is clogging coefficient, K_s is standard blocking coefficient, C is volume of deposit per unit filtrate volume, r_o is effective pore radius. The description of the missing constants is not provided by the authors.

Table 1.9: Huang, et al. (2008) fouling laws, applied for constant flux and constant pressure – Equivalent to Hermia (1982) models

Law/Model	Equation	Fouling parameter (k_v or UMFI)
Complete blocking	$J_s' = 1 - k_v V_s$	$C_f \sigma$
Standard blocking	$J_s^{1/2} = 1 + k_v/2V_s$	$2C_f/L\rho$
Intermediate blocking	$Ln\, J_s' = -k_v V_s$	$C_f \sigma$
Cake filtration	$1/J_s' = 1 - k_v V_s$	$C_f \hat{R}_c / R_m$

where J_s' is normalized permeability (permeability/initial permeability), V_s is specific volum [m^{-1} or L/m^2], k_v is fouling parameter, C_f is [kg/m^3], σ is projected area of fouling molecules per unit mass of molecules [m^2/kg], L is pore length [m], ρ is molecules density [kg/m^3], $\hat{R}_c$ is the specific resistance of the cake layer [m/kg], R_m is hydraulic membrane resistance [m^{-1}].

1.3.4 Fouling indices

In filtration practice, the monitoring of TMP or flux decline are the simplest ways to anticipate a fouling phenomenon (Koo et al., 2012). Another way to predict fouling is to analyze the fouling potential of the water. This can be done by analyzing the effect of the presence of the fouling agent in the sample, such in the silt density index (SDI), which evaluates the presence of molecules larger than 0.45µm in the water matrix (Koo et al., 2012). Another tool is the modified fouling index (MFI). The latter analyses the flow rate reduction in a period of time. The graph built from the data (t/V vs V) (figure 1-8*)* has three sections, of which the middle represents cake filtration regime. The slope of this linear segment corresponds to the MFI value (Koo et al., 2012).

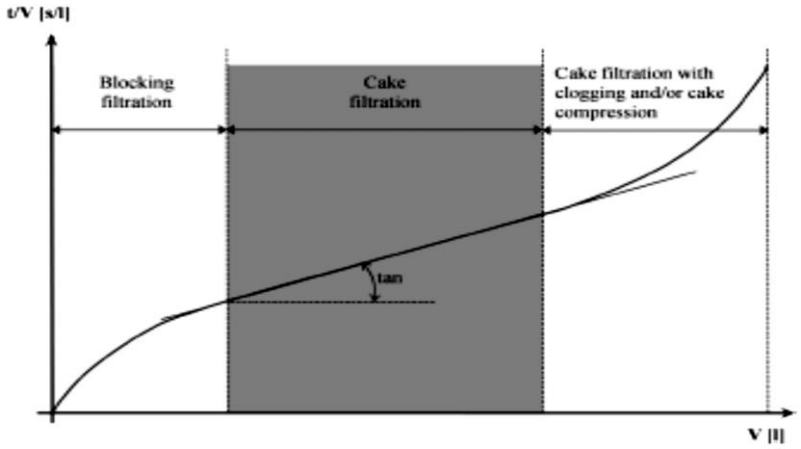

Figure 1- 8: Typical fouling graph for constant pressure filtration
(Adapted from (Boerlage.S et al., 2003))

The SDI is widely used due to its practicability, although it is not related, neither to the concentration of the particulates in the feed (because molecules size can mislead the interpretation), nor to any fouling mechanism. MFI is thus, an improved fouling indicator than SDI, as it addresses SDI drawbacks; but still, to assess the potential fouling of a water sample, an averaging of MFI values obtained from testing on selected membrane types needs to be carried out. In addition, the values of both indices depend on operating conditions (flux, TMP), operation mode (cross-flow or dead-end), and membrane characteristics (pore size, MWCO) (Koo et al., 2012).

In view of these inconveniences, the unified membrane fouling index (UMFI) was formulated by Huang, et al. (2008). This indicator applies for the operation modes of constant pressure or constant flux, and allows for testing the water sample on the membrane of interest (instead of selected surrogates) while keeping the advantage of being able to compare the results with systems with different features and dimensions (Huang, et al., 2008). The equation is presented below:

$$\frac{1}{J_s'} = 1 + (UMFI)\, V_s \qquad (18)$$

where J_s' represents the normalized permeability (J_s/J_o) of the system, and V_s the specific volume of the filtrate (m^{-1} or L/m^2).

1.3.5 Fouling control

Filtration behavior could be improved (less fouling & better filtrate quality) following three known strategies: physical and chemical cleaning of the membrane, modification of operational conditions (flux, pressure, temperature, etc) or pre-treating the feed solution (Gao, et al., 2011). There are also efforts focused on modifying the membranes surface in order to minimise fouling, although the impact of such technology is still considered too weak. These applications involve the incorporation of hydrophilic materials (PVC) or the use of nanomolecules (TiO_2, Al_2O_3, SiO_2, ZrO_2, Ag, zeolite, carbon nanotubes) in the manufacturing of polymeric membranes (hybrid membranes), or the implementation of ceramic nanostructures capable of reducing fouling under the influence of an oxidant in the case of ceramic membranes (Kim & Van der Bruggen, 2010).

Pre-treatment of the feed solution is performed by changing the aggregate characteristics of colloids and flocs, and by influencing the conformation of the organic matter in the feed solution (Schäfer, 2001). These pre-treatments involve adsorption (addition of powdered activated carbon-PAC), ion-exchange resins, coagulation, and oxidation. The first and the second ones help in the elimination of dissolved substances (responsible of odor & taste for example) by adsorption; the third one aggregates NOM; and the last one eliminates metals by precipitation (Fe, Mn) and/or modifies organic matter characteristics (AWWA, 2005; Gao, et al., 2011). The efficiency of the pre-treatments depends on various factors such as type of active agents (coagulants, adsorbents, oxidants, etc), dosing factors (dose, dosing mode, dosing point), mixing dynamics, temperature, chemical properties of the solution molecules, solution chemistry, and of course membrane factors (type, morphology and chemistry) (Gao, et al., 2011).

Coagulation

Coagulation is the most popular pre-treatment as it is operationally easy to handle and involves low costs; besides minimising the formation of disinfection by-products. Inorganic coagulants are generally used (aluminum and ferric salts), which allow for dissolved or colloidal matter to aggregate and consequently, avoid their inner adsorption or blockage of the membrane pores. Coagulation conditions are important, as a defective modification of molecules surface properties can lead to more severe fouling. Thus it has been reported that operating conditions used in classical coagulation treatment need to be adjusted for a UF pre-treatment purpose

because the objectives are different: good flocs settlement properties for the first one, and convenient flocs size, consistency and surface properties for the second. Finally, pre-coagulation can be applied with or without previous sedimentation of the flocs (standard and in-line coagulation, respectively) (Gao, et al., 2011; Zhu, et al., 2012).

Adsorption

PAC is generally the material of choice if used for a UF pre-treatment because of its widely availability and superior adsorption capacity. However, its effectiveness on UF fouling control still needs more research due to the existence of controversial reports. Adsorption conditions need to be better understood and therefore, adjust, in order to remove targeted impurities, and therefore, reduce fouling. PAC and membranes can be used in an integrated or separate process (Gao, et al., 2011).

Ion exchange resins

This pre-treatment has been reported to be effective for the alleviation of UF membranes fouling due to its superior performance in the removal of low molecular weight organic matter, which is considered as an important fouling agent. Its application is more popular in developed countries because of its high cost, and more research is still needed to better understand its impact as a pre-treatment (Gao, et al., 2011).

Oxidation - Ozonation

Pre-oxidation of feed water can be performed with chlorine, permanganate or ozone. These options present inconveniences (such as the generation of disinfection by-products) that discourage their use and further research (Gao, et al., 2011); although the issue may be more controllable with ozonation, so that it has received more attention from the scientific community. In fact, it has been reported that the thickness of the fouling layer decreases if O_3 is applied before filtration (Van Geluwe, Braeken, et al., 2011). The proposed ways in which O_3 may alleviate the fouling of membranes are: a) O_3 reacts selectively with unsaturated bonds, such as aromatic rings, which are well-known fouling agents (in virtue of their hydrophobic nature). O_3 though, renders hydrophobic moieties into hydrophilic ones (carbony, hydroxyl, alkoxyl, amino and carboxyl groups) and decreases fouling severity; b) O_3 decreases molecules size when it

detaches small peripheric fractions of the humic acids (leaving the core of the acid intact), and as consequence, fouling is reduced in most of the cases. Nevertheless, this NOM fragmentation seemed to be less important than the effect of reducing hydrophobicity (Van Geluwe, Braeken, et al., 2011). In addition, it was reported no correlation between the permeability improvement of the membranes and the O_3 doses and no deterioration in filtrate quality due to the generation of smaller NOM fractions. No explanation was given for these observations (Van Geluwe, Braeken, et al., 2011). The drawback of ozonation, however, is the potential production of oxidation by-products, such as bromates, which are considered carcinogens and the formation of assimilable organic carbon that promotes biofilm growth.

CHAPTER 2 MATERIALS AND METHODS

The following pathway was followed in the execution of the experiment (figure 2-1). A natural water sample was collected, then ozonated under various conditions prior to filtering it onto ceramic membranes (8 and 50 kDa). This chapter will describe in details these various steps.

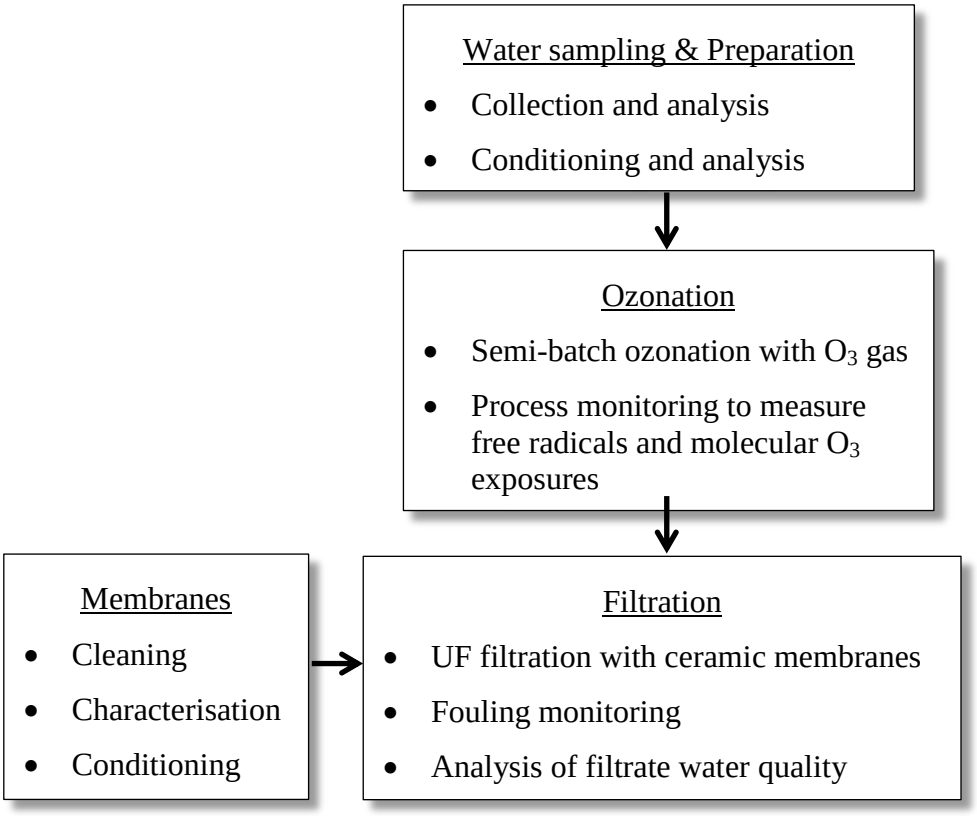

Figure 2-1: Overview of the experimental pathway

The experimental design is presented below:

Type of design:	randomized multifactorial
Number of factors:	3 (membrane MWCO, water pH, ozone dose)
Number of levels:	variable (depending on the factor: 2/membrane, 3/pH, 3/O_3 dose), and deliberately chosen (fixed-effects model)
Number of experiments:	$2*3*3 = 2^1*3^2 = 18$
Nuisance factors:	different membrane units for the filtration step

Number of repetitions: variable, due to constraints in time, materials and analyst's availability. The design was unbalanced.

Details on the assays performed are presented in table 2.1

Table 2.1: Experimental matrix

	Factors			**Number of repetitions**			
	Membrane MWCO	O_3 dose mg O_3/mg C	pH	Ozonation		Filtration 8 KDa	Filtration 50 KDa
				w/o pCBA	w/pCBA*		
Levels	For each, 8 and 50 kDa	0.0	6.5	-	-	1	1
			8.5	-	-	1	1
			8.5+*t*-but	-	-	1	1
		0.5	6.5	1	2	1	2
			8.5	2	2	2	2
			8.5+*t*-but	1	0	1	1
		1.0	6.5	1	2	0	1
			8.5	2	2	1	1
			8.5+*t*-but	1	0	2	2

*Assays done just for analysis purposes: to quantify presence of •OH radicals. These samples were not filtrated as ulterior analysis of filtrate through HPLC-SEC was not recommended.

2.1 Water sampling and preparation

2.1.1 Sample collection and analysis

Raw water was collected from the Thousand Islands River, at the influent of the Sainte Rose's drinking water treatment plant in Laval, QC, Canada, on the morning of October 28th, 2013. The sample was analyzed at 20±1ºC showing the characteristics described in table 2.3.

2.1.2 Sample conditioning and analysis

The sample was first micro-filtered through 0.45 µm polyethersulfone filters (14 cm diameter, Supor 450 No 66553, Pall Corporation). The filters had been previously rinsed with 2 L

of milli-Q water to remove any glycerin residual from the membrane. Next, the sample was conditioned at pH values 6.5 and 8.5 using phosphate and borate buffers, respectively. An additional sample at pH 8.5 was also spiked with 50 mM *t*-butanol to scavenge hydroxyl free radicals.

The procedure followed to adjust the pH, alkalinity and ionic strength of the water sample is described below:

Objective

To simultaneously adjust the pH, alkalinity and ionic strength of the water sample.

Remarks

- Membrane fouling process is strongly influenced by the ionic strength of the sample.
- The ozonation process tends to decrease the pH of the sample solution.
- Ionic strength (IS) equation: IS = 0.5 $\sum C_i Z_i^2$, where C_i=ion molar concentration, Z_i=ion charge.
- Henderson-Hasselbach (HH) equation: $pH = pK_a + log\frac{[base]}{[acid]}$.

Materials, reagents and equipment are shown in table 2.2:

Table 2.2: Materials, reagents and equipment to adjust physical-chemical properties

Materials	Reagents	*Equipment*
Beakers	Buffer borate	*pH meter*
Fioles	Buffer phosphate	*Stirring plate*
Magnetic bars	KH_2PO_4 solution, 0.5 M	
	H_2SO_4 solution, 2 N	
	NaCl solution, 1 M	

Procedure

1. Prepare the buffer using the IS and HH equations. Adjust the pH with NaOH 1M or HCl 1M according to the situation.
2. Calculate the amount of buffer necessary to reach the required pH and ionic strength of the sample (use the IS and HH equations).
3. If the amounts calculated in 2) result in out-of-range characteristics, add the buffer to the sample in a trial & error way, so to reach the required pH, alkalinity and ionic strength. Adjust the parameters using H_2SO_4 2N, KH_2PO_4 0.5M or NaCl 1M when needed.

Sample calculations for this procedure are provided in Appendix A.

The analysis of the characteristics of the conditioned water is shown in table 2.3.

Table 2.3: Characteristics of the water sample: raw, micro-filtrated & pH-conditioned

Parameter	Units	RW	MF 0.45 µm	Buffered pH 6.5	Buffered pH 8.5	Buffered pH 8.5+ *t*-butanol	Instrument or method
pH	-	7.10	7.87	6.59	8.57	8.54	Fisher Scientific AB15 pH meter
Turbidity	UTN	10.7	0.231	0.152	0.200	0.185	Hach 2100N turbidimeter
Conductivity	µS	125	123	590	439	440	EC Testr (0-1999 µS)
Ionic strength	mM	±3	-	±8			Estimated by calculations
Alkalinity	mg $CaCO_3$/L	33	33	58	66	60	Potentiometric-Standard method 2320
UVA 215 nm	cm^{-1}	0.589	0.478	0.473	0.477	0.475	Cary 100 Scan spectrophotometer
UVA 254 nm	cm^{-1}	0.316	0.226	0.223	0.225	0.223	
UVA 285 nm	cm^{-1}	0.232	0.153	0.150	0.152	0.151	
Absorbance at 436 nm	cm^{-1}	0.055	0.012	0.011	0.013	0.012	
DOC	mg C/L	7.54	7.17	7.22	7.15	-	Sievers 5310C TOC analyser
SUVA	L/mg/cm	0.042	0.032	0.031	0.032	-	-
Ca^{2+}	mg/L	8.20	8.10	-	8.30	-	ICP OES iCAP 6000 series
Mg^{2+}	mg/L	1.90	1.90	-	1.90	-	
SEC	-	-	-	See Results section		-	HPLC-SEC. See Note 2 for complete description

Note 1.- See all raw values in Appendix B

Note 2.- HPLC + UVA 254 nm detector system, Waters 600E Multisolvent Delivery System + Waters 486 Tunable Absorbance Detector + Waters 717 Plus Autosampler; DOC detector, Sievers 900 Series Turbo TOC Analyzer (GE Water & Process Technologies, Analytical Instruments); Column TSK HW 50S (Tosoh, Japan), length: 25cm, diameter: 2 cm. Mobile phase: phosphate buffer pH 6.85 (2.5 g KH_2PO_4 + 1.5 g $Na_2HPO_4.2H_2O$ per 1 L). Injection Volume: 1 mL. Flow rate: 1mL/min. The calibration of the column was made with PEG 600, 1500, 3300, 6000; and PSS 15000, 41000.

2.2 Membranes characterization and conditioning

Flat disc-type ultrafiltration composite-ceramic membranes purchased from Sterlitech Corporation (Tami Industries manufacturer) were tested. Membrane characteristics are presented in table 2.4:

Table 2.4: Tami ceramic membranes characteristics

Parameters	**Values**	**Units**
Diameter	47	mm
Filtration area	14.2	cm^2
Support		
Material	Titania (TiO_2)	-
Thickness	2.5	mm
Average pore diameter	3.5	µm
Maximum operating pressure	4 (58)	bars (psi)
Operating temperatures	<350	ºC
Membrane		
Material	Zirconia-Titania	-
MWCO		
Membrane No1	50	kDa
Membrane No2	8	kDa
Operating pH range	0-14	-

(Adapted from Sterlitech Corporation)

The virgin membranes were chemically washed prior to their utilisation (see Appendix I for the description of the procedure followed), and then characterized for their initial permeability. To this purpose, milli-Q water was filtered through the membranes at 5 different fluxes: ± 25, 35, 50, 70, 95 LMH. After reaching stability (15 min for membrane 50 kDa, and 30 min for membrane 8 kDa), the pressures attained were registered, and permeability values were calculated (see Results section for the values obtained). Finally, membranes were stored at ±6ºC in a $Na_2S_2O_3$ (200 ppm) solution until needed. They were also rinsed with milli-Q water (pH 5.5-6.0) for 15 min at 95 LMH prior to their use.

2.3 Ozonation procedure

The conditioned water samples were ozonated with O_3 gas at ambient temperature (20±1ºC), in a bench-scale semi-batch set-up. O_3 gas production (Ozone Solutions TG-10 generator) was measured by means of chemical titration (Standard Methods 2350 E) before injection into the sample. Measurement of the gas production was within 5% variation coefficient (see Appendices C and D).

The O_3 doses applied to the water samples are presented in table 2.5:

Table 2.5: O_3 doses applied to the water samples

Units	Doses		
mg O_3/mg DOC	0	0.5	1.0
mg O3/L	0	3.5	7.0

The lowest ozone dose (3 mg/L or 0.5 mg O_3/mg C) is more realistic of a pre-ozone dose. The upper ozone dose (7.0 mg/L or 1.0 mg O_3/mg C) was selected to make sure that some conditions would yield residual ozone in solution. Repeatability of the gas dosage was within 5% variation coefficient (see Appendix F; see also replicates data in Appendix N).

The procedure used is described below:

Materials, reagents and equipment are shown in table 2.6:

Table 2.6: Materials, reagents and equipment for ozonation

Materials	Reagents	Equipment
Beaker, 1 L	O_2 gas, UHP (Air Liquide)	Ozonator
Burette, 50 mL	KI solution, 2% w/vol	Reactor (5 L)
Magnetic bar	$Na_2S_2O_3$ solution, 0.1 N	KI solution trap
Needles	H_2SO_4 solution, 2 N	Stirring plate
Syringe	Indigo solutions: 3,1,0.2%	UV-Vis Spectrophotometer
	pCBA solution, 25 mg/L	Compressed air chamber

Ozonation schema is shown in figure 2-2:

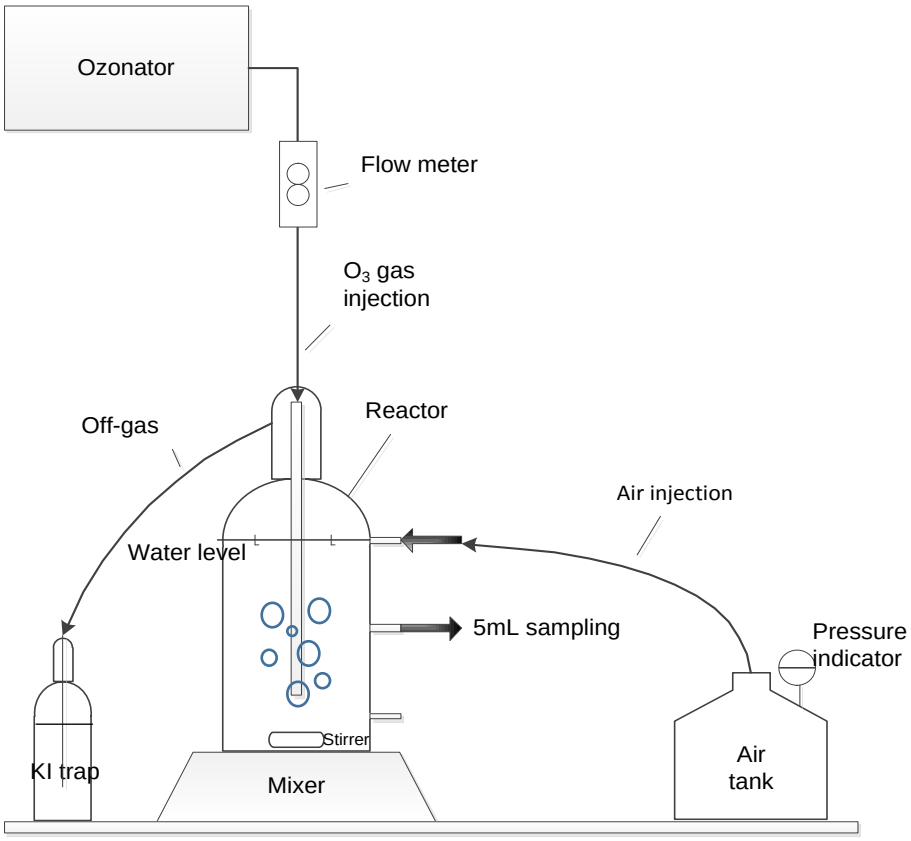

Figure 2-2: Schema for the ozonation set-up

Ozonation set-up is presented in figure 2-3:

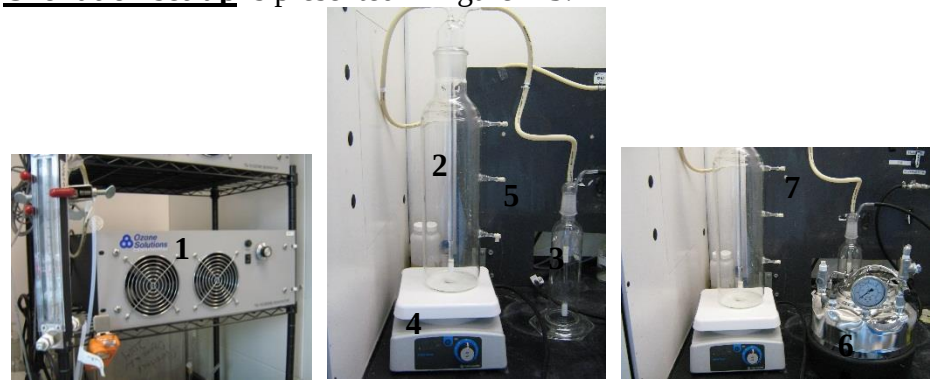

1 Ozonator
2 Reactor (5L)
3 KI trap
4 Stirring plate
5 Sampling port
6 Air tank
7 Air injection port

Figure 2-3: Pictures of the ozonation set-up

Procedure

Apply the O_3 measurement method developed by CREDEAU, 2007 from Standard Methods 2350 E - iodometric method; and Standard Methods 4500-O_3 – colorimetric method; but taking the following precautions:

- Reactor: a 5L glass container provided with several sampling ports to allow for the collection of liquid samples and for off-gas measurements.
- Height of water sample in reactor: 3L (up to the first sampling/injection port)
- Stirring magnet: 6 cm long
- Stirring speed: 7
- Off-gas collection: the off-gas is collected in a KI trap in order to be measured according to Standard Methods 2350 E. Make sure to divert the off-gas residuals trapped in the reactor's headspace to the KI traps by using ±3.5L of air. The latter is injected through a long needle located at the first sampling/injection port (at the water sample's level in the reactor).
- Make sure there is no gas leak in the system (attach KI solution-moistened cloths on the joints). If necessary, use tie-wraps and tape to ensure the set-up is hermetic.
- Sampling: through the middle port, using a long needle that reaches the mid-point between the reactor wall and the gas-injection stem. 5 mL samples are withdrawn in a continuous pace during the injection of O_3 gas, and added to 20 mL flasks containing indigo reagent. The ozonation process was monitored with respect to the presence of molecular O_3 and •OH radicals. The indigo method (Standard Methods 4500-O_3) and the pCBA measurement, as described in Vincent (2009), are respectively used in order to characterize the presence of these species. The water sample is hence spiked with 0.16 mM pCBA in the reactor.

The evolution of the appearance or disappearance of molecular O_3 and pCBA was then plotted on a X-Y graph (see Appendix H for a data manipulation example).

pCBA oxidation is achieved through hydroxyl ($\bullet OH$) radicals formed upon the direct reaction of molecular ozone with NOM or released during a second phase of molecular ozone decay. Therefore, pCBA oxidation rate can be expressed as:

$$ln\left(\frac{[pCBA]}{[pCBA]_o}\right) = -k_{\bullet OH/pCBA}\, x\, \left(Ct_{OH-1st\ phase} + Ct_{OH-2nd\ phase}\right) \qquad (18)$$

Free radical exposure during the first phase ($Ct_{OH\text{-}1st\ phase}$) is observed prior to the formation of measurable ozone residual. It was evaluated using the intercept (*b*) of a graph of $ln(pCBA/pCBA_o)$ vs Ct_{O3} as described in the equation 2:

$$ln\left(\frac{[pCBA]}{[pCBA]_o}\right) = -k_{\bullet OH/pCBA} \times R_{Ct} \times Ct_{O3} + b \qquad (19)$$

Where $b = k_{\bullet OH/pCBA} \times ct_{OH-1st\ phase}$ and $k_{\bullet OH/pCBA}$ is the second order rate constant of pCBA with •OH radicals, posed as 5.2 x 10^9 $M^{-1}s^{-1}$ (Acero & Von Gunten, 2001; Westerhoff, et al., 1999).

Free radical exposure during the second phase ($Ct_{OH\text{-}2nd\ phase}$) can be calculated using the first term of Equation 2 based on the R_{Ct} concept (M. Elovitz, Von Gunten, U, 1999). In that case, the Ct_{OH}-2^{nd} phase is given as:

$$Ct_{OH-2ndphase} = R_{Ct} \times Ct_{O3} \qquad (20)$$

Where Ct_{O3} is the molecular ozone exposure calculated as the area under the residual ozone vs time profile. This approach enables to calculate free radical exposure even when no dissolved ozone residual is detected since $Ct_{OH\text{-}1st\ phase}$ is independent of the persistence of dissolved ozone as opposed to the $Ct_{OH\text{-}2nd\ phase}$.

Finally, the samples were analyzed according to the parameters shown in table 2.3.

2.4 Filtration procedure

Filtration experiments were performed at room temperature (20.5±1ºC) in unstirred dead-end filtration cells (Inside Disram™ disc holder-Tami Industries, supplied by Sterlitech Corporation) at stable flux (38 ± 2 LMH for membrane 8 kDa, and 44 ±2 LMH for membrane 50 kDa) (see figures 2-4 and 2-5).

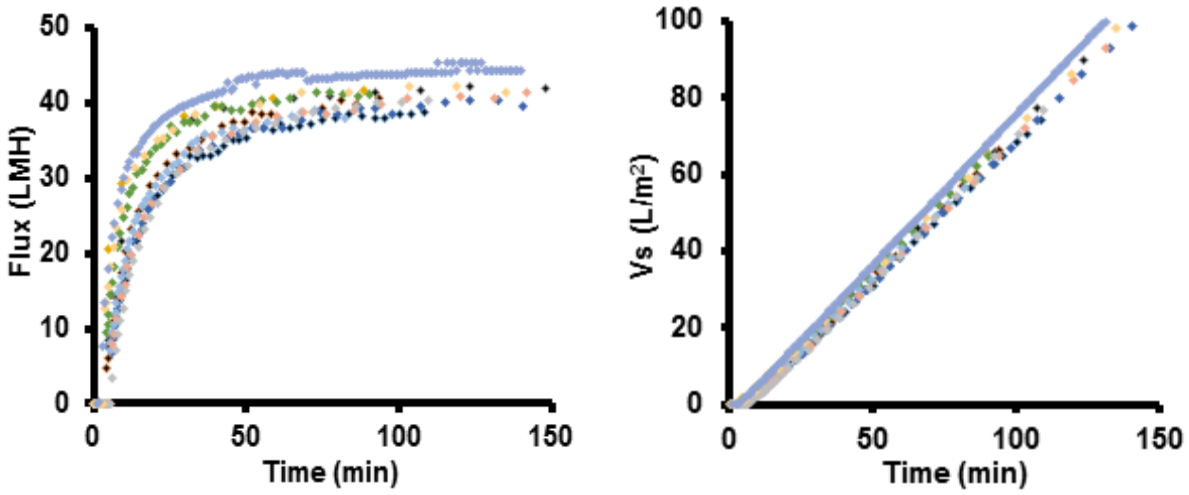

Figure 2- 4: Operating flux (20ºC) for membrane 8 kDa (n=11)

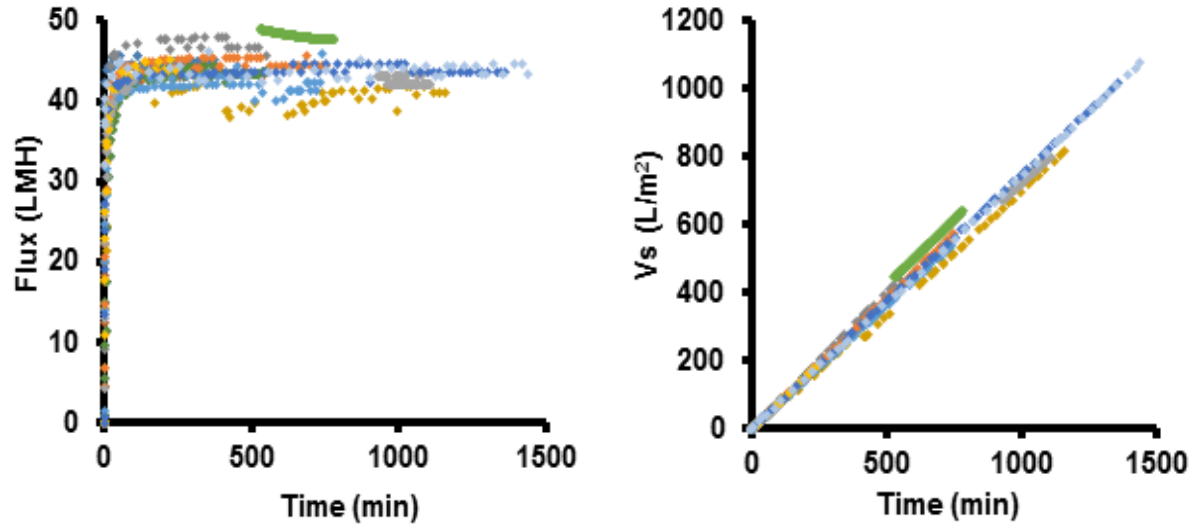

Figure 2-5: Operating flux (20ºC) for membrane 50 kDa (n=12)

Data-acquisition software was used to register temperature and pressure evolution (TRH Central-Omega Engineering Inc) as well as filtrate volume evolution through weight data (Hyperterminal, version 7-Hilgraeve) for filtration through membrane 50 kDa. Manual records were used for the 8 kDa filtration data.

The procedure used is described below:

Materials, reagents and equipment are shown in table 2.7:

Table 2.7: Materials, reagents and equipment for ultrafiltration

Materials	Reagents	Equipment
Beakers	Eau milli-Q	Filtration set-up
pH paper		Electronic balance
Volumetric cylinders		Manometer
		Pressure probe
		Temperature probe

Filtration schema is depicted in figure 2-6:

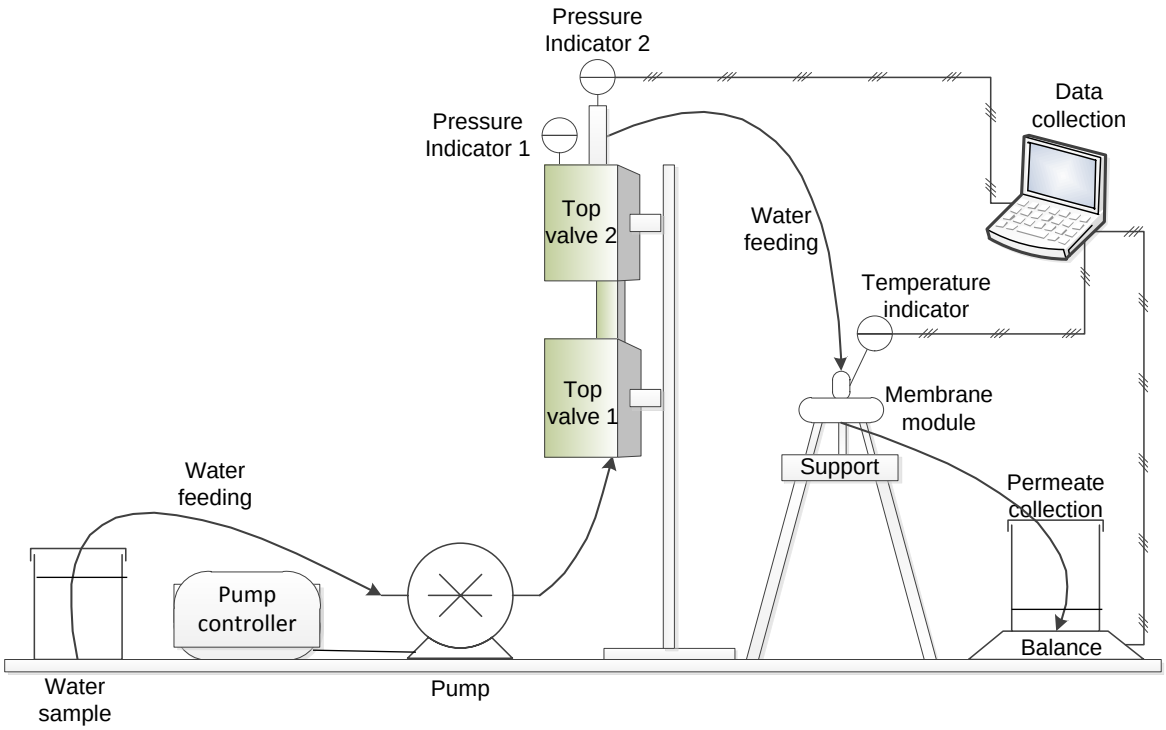

Figure 2-6: Schema for the ultrafiltration process

Filtration set-up is shown in figure 2-7

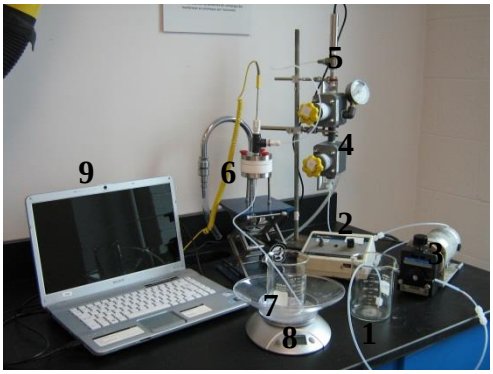

1 Sample
2 Pump controller
3 Pump
4 Valves
5 Manometer
6 Membrane module
7 Permeate
8 Balance
9 Electronic registration

Figure 2-7: Picture of the ultrafiltration set-up

Procedure

- Adjust top valve 1 to reach the desired pressure in order to protect the pump
- Adjust top valve 2 to attain a constant working pressure over the pump
- Adjust the desired flow rate value with the pump controller
- Place the membrane in the respective module
- Record the evolution of pressure, temperature and permeate volume generated during the filtration process

Membranes were used a maximum of two times. Repeatability of the method was evaluated on the basis of the fouling behaviour and the estimated fouling index (see replicates data in Appendix O and also see Appendix L for a sample calculation of fouling index). The concept of Unified Membrane Fouling Index (UMFI) (Huang, et al., 2008) was applied to calculate the degree of fouling of the membranes:

$$1/J_s' = 1 + k_v\, V_s \qquad (21)$$

where J_s' represents the normalized permeability (J_s/J_o) of the system, and V_s the specific volume of the filtrate (L/m^2), and k_v is the fouling index (m^2/L) or UMFI.

The specific permeability (J_s) is defined as:

$$J_s = J/P \qquad (22)$$

where J represents the flux applied to the system (L/m^{2}h), and P the effective transmembrane pressure (bar).

The flux was corrected for temperature variations using the expression (AWWA, 2005):

$$J_{20} = J_T \left(\frac{\mu_T}{\mu_{20}}\right) \qquad (23)$$

where μ_T is the water viscosity at the experimental temperature T (in Celsius), which can be estimated by:

$$\mu_T = 1.784 - 0.0575T + 0.0011T^2 + 10^{-5}T^3 \qquad (24)$$

The precision of the UMFI was calculated as 16% based on the average coefficient of variation of replicate fouling assays.

CHAPTER 3 RESULTS

This chapter presents the results obtained for the two main steps of the experiment. The first section presents the performance of the ozonation process at different conditions in terms of NOM exposure to molecular ozone and/or to hydroxyl radicals. The impact of this oxidation on the quality and quantity of NOM was evaluated through physical-chemical tests and a SEC profile of the treated waters. In the second section, the ultrafiltration process was assessed. It starts with the evaluation of the permeability of several units of virgin ceramic membranes of 8 and 50 kDa. Afterwards, the physical-chemical and SEC analysis of the permeate solutions is presented, followed by the evaluation of the fouling mechanisms and fouling indexes generated. Finally, the relation between the ozone exposure mode and the fouling results was addressed.

3.1 Ozonation process characterization

3.1.1 Molecular ozone vs free radicals

The monitoring of dissolved O_3 was realized during the semi-batch ozonation assays. Figure 3-1 presents the measured data. The vertical dotted lines indicate the duration (2 and 4 minutes) of ozone injection for the targeted doses of 0.5 mg O_3/mg and 1.0 mg O_3/mg C, respectively. Ozonation times for *t*-butanol samples were half of the other two conditions, as *t*-butanol enhances ozone gas transfer to the liquid phase (López, Pic, Benbelkacem, & Debellefontaine, 2007). Actual O_3 doses, expressed in mg O_3/L were 6.8 ± 0.2 (*cv*: 3.4%, n=8) and 3.5 ± 0.1 (*cv*: 3.5%, n=6) giving actual doses of 0.96±0.03 and 0.48±0.07 mg O_3/mg C (DOC was 7.2 mg/L).

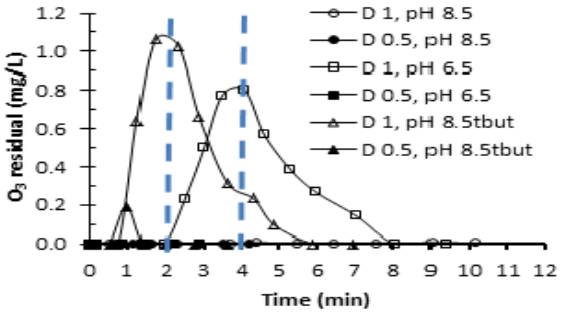

Figure 3-1: Typical profiles of molecular ozone vs time (n=1.0-4.0, doses (D) in mg O_3/mgC)
(replicatas in Appendix N)

For the lowest O_3 dosages of 0.5 mg O_3/mg C (< 2 min O_3 bubbling), ozone residuals were either undetectable or very low (0.2 mg O_3/L in the presence of *t*-butanol). For the highest O_3 dosage of 1.0 mg O_3/mg C (> 2 min O_3 bubbling), significant ozone residual was measured at pH 6.5 (0.8 mg O_3/L). However, at pH 8.5, this was only the case when *t*-butanol was present in solution. Respective molecular ozone Ct exposures (Ct_{O3}) were calculated as the area under the ozone residuals vs time profile (shown in table 3.1; also see Appendix H for a Ct_{O3} calculation example). Globally, these results are consistent with the fact that (i) higher pHs are expected to increase ozone decay (Von Gunten, 2003) and (ii) the addition of *t*-butanol is expected to slow down the ozone decay process (López, et al., 2007; Staehelin & Hoigné, 1985).

Simultaneously, •OH radical exposures (Ct_{OH}) were also indirectly monitored on samples that were not spiked with *t*-butanol, as the latter scavenges these species. pCBA was used as the radical's probe, so figure 3-2 shows its decomposition in time. 70 to 95% of pCBA was oxidised by free radicals depending on the O_3 dose, but no differences ($p = 0.26$) were observed with respect to pH conditions. These results indicate that autocatalysis was not controlling O_3 decomposition.

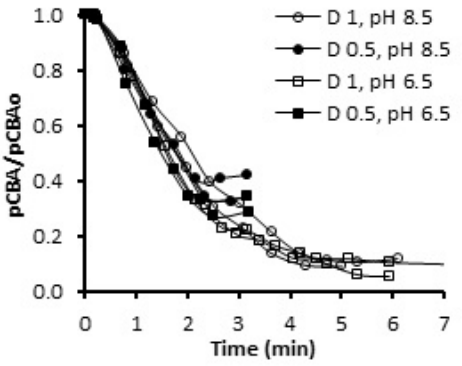

Figure 3-2 : pCBA decomposition graph
(n=2.0, doses in mg O_3/mg C)

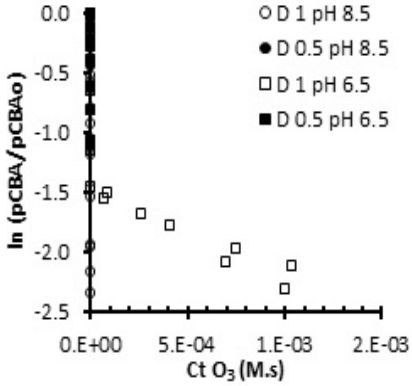

Figure 3-3: Rct graph
(n=2.0, doses in mg O_3/mg C)

Figure 3-3 shows the decomposition of pCBA as a function of Ct_{O3}. Interestingly, three of the four ozonation conditions did not yield measurable O_3 residuals; therefore, all their •OH radical production took place in the first phase of O_3 decomposition ($Ct_{OH\text{-}1st\ phase}$). Only dose 1.0 mg O_3/mg C at pH 6.5 presented both, Ct_{O3} and Ct_{OH} components; i.e., two phases of O_3 decay. The R_{Ct} ratio calculated for this condition was in the order of 10^{-7}, which is typical of an

immediate ozone demand or advanced oxidation regime (R_{ct}>10^{-7} (Von Gunten, 2003), where NOM or hydroxyl radicals control the ozone decomposition.

Table 3.1 shows the Ct_{O3} and Ct_{OH} exposure values calculated for all the ozonation conditions. Overall, Ct_{OH} values doubled from 2.1 to 4.2 x 10^{-10} M.s when the dose of O_3 was also doubled from 0.5 to 1 mgO_3/mg C. pH conditions did not affect global Ct_{OH} levels, again confirming that the ozonation process was driven by an immediate O_3 demand regime, i.e., due to the direct reaction of molecular O_3 on NOM, instead of autocatalysis. Confrontation of figure 3-2 and table 3.1 indicates that pCBA decomposition mainly took place through •OH radicals produced during the 1st phase of O_3 decay; however, those produced in the 2nd phase were also important to complete the oxidation at pH 6.5, dose 1 mgO_3/mg C. In addition, •OH radical concentrations calculated from the Ct_{OH} values of table 3.1, yielded a relatively stable level for all combinations of pH and dose, 1.5±0.15 x 10^{-12} M (*cv* 10%, n=8), which is fairly close to previous findings for advanced oxidation regimes (1.0-1.2 x 10^{-12} M) (Buffle, et al., 2006). This level also agrees with Staehelin & Hoigné (1985) who reported that •OH radicals are difficult to detect over 10^{-12} M concentrations due to their high reactivity.

Ct_{O3} values on the other hand, could only be calculated for t-butanol spiked samples and condition pH 6.5, dose 1mgO_3/mgC. Ct_{O3} values varied in the range of 1.1 to 30 x 10^{-4} M.s (0.8 to 2.4 mg.min.L^{-1})

Table 3.1: Calculated molecular ozone (CtO3) and free hydroxyl radical (CtOH) exposures under various ozonation conditions (n=1.0-2.0, typical or average values, errors: 1 std dev)

Transferred dose (mg O_3/mg C)	**pH**	Ct_{O3} (×10^{-4} M.s)	Ct_{OH} **1st phase** (× 10^{-10} M.s.)	Ct_{OH} **2nd phase** (× 10^{-10} M.s.)	Ct_{OH} **Total** (× 10^{-10} M.s.)
0.50	6.5	0	2.3 ± 0.30	0	2.3 ± 0.30
	8.5	0	1.9 ± 0.20	0	1.9 ± 0.20
	8.5+*t*-but	1.1	N.A.	N.A.	N.A.
1.0	6.5	10 ± 0.20	2.5 ± 0.40	1.6 ± 0.10	4.2 ± 0.30
	8.5	0	4.3 ± 0.25	0	4.3 ± 0.25
	8.5+*t*-but	30	N.A.	N.A.	N.A.

3.1.2 Impact of ozone on NOM characteristics

3.1.2.1 Physical-chemical analysis

As depicted in table 3-2, both O_3 doses produced minimal reductions in the concentrations of DOC (±6-8% for doses 0.5-1.0 mg O_3/mg C, respectively), which converges with previous

literature (Van Geluwe, Braeken, et al., 2011) that explains the O_3 mineralisation power is limited by the oxidative capacity of molecular O_3 and short life-time of •OH radicals. pH did not show to have an impact on this quantitative decrease.

Table 3.2: NOM characteristics before and after ozonation treatment
(n=1.0 to 4.0, typical or average values, errors: 1 std dev)

Transferred dose	**pH**	**DOC**	**UVA 215**	**UVA 254**	**UVA 285**	**436**	**SUVA**	**Proposed O_3 active species**
mgO_3/ mg DOC	**-**	**mg/L**	**nm**	**Nm**	**nm**	**nm**	**cm^{-1}. mg^{-1}.L**	
Original sample (MF)	All	7.2 ±0.13	0.476 ±0.007	0.224 ±0.003	0.152 ±0.002	0.012 ±0.001	0.031 ±0.001	-
% reduction with respect to original sample								
0.5	6.5	6±3	25±3	38±4	42±4	48±10	34±3	Instantaneous O_3 on DOM + •OH
	8.5	5±1	24±1	36±3	40±3	56±4	33±2	
	8.5 *t*-but	-	20	35	41	58	-	
1.0	6.5	8±0.2	38±1	59±2	63±2	80±0.0	56±2	Inst O_3+ •OH+O_3
	8.5	8±2	33±1	52±0.4	56±0.3	77±6	47±1	Inst O_3+•OH
	8.5 *t*-but	-	27	48	57	75	-	Inst O_3+O_3

At dose 0.5 mg O_3/mg C, UVA 215, 254, 285, absorbance 436 nm and SUVA were reduced by ± 23, 36, 41, 54 and 34%, respectively; with no significant differences in performance due to pH or t-butanol addition ($p>0.05$). These results suggest once more that direct oxidation (within an immediate O_3 demand regime) was the main mode of NOM oxidation in the samples at this dose.

At dose of 1.0 mg O_3/mg C, ozonation at pH 6.5 performed better than at pH 8.5 ($p<0.05$). UVA 215, 254, 285 nm, absorbance at 436 nm and SUVA were reduced by 38, 59, 63, 80 and 56%, respectively for pH 6.5, which was ≈ 13% higher than the reduction reached at pH 8.5 (33, 52, 56, 77, 47%, respectively). Condition pH 8.5+*t*-butanol was ≈ 8% less effective than condition pH 8.5 alone (27, 48, 57, 75%, N.A. reductions, respectively). Interestingly, the high difference in Ct_{O3} at these conditions (0 versus 30 x 10^{-4} M.s, table 3.1) was not enough to widen the gap, suggesting once more that the immediate ozone demand regime was mainly responsible for the changes in NOM characteristics.

3.1.2.2 SEC analysis

Figure 3-4 presents the size exclusion chromatograms under variable ozonation regimes. Results confirmed that the lowest ozone dosage (0.5 mg O_3/mg C) provided equivalent UVA_{254} reductions (39%). On the other hand, for the highest dosage of 1.0 mg O_3/mg C, improved UVA_{254} was achieved at pH 6.5 (57% versus 50%).

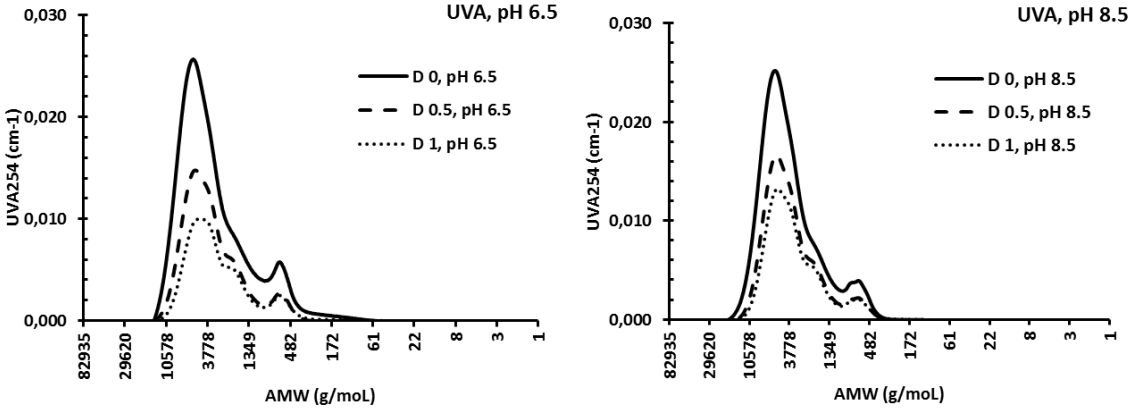

Figure 3-4: Typical reductions in NOM aromaticity for the various conditions (normalized dosages and pH)

3.2 Filtration process characterization

3.2.1 Initial membrane permeability measurements

The permeability values of the virgin membranes were different within the same lot.

Membrane 8 kDa presented an average permeability of 54 LMH/bar with vc of 32%; whereas the 50 kDa showed an average permeability of 176 LMH/bar with 13% vc (see figures 3-5 and 3-6).

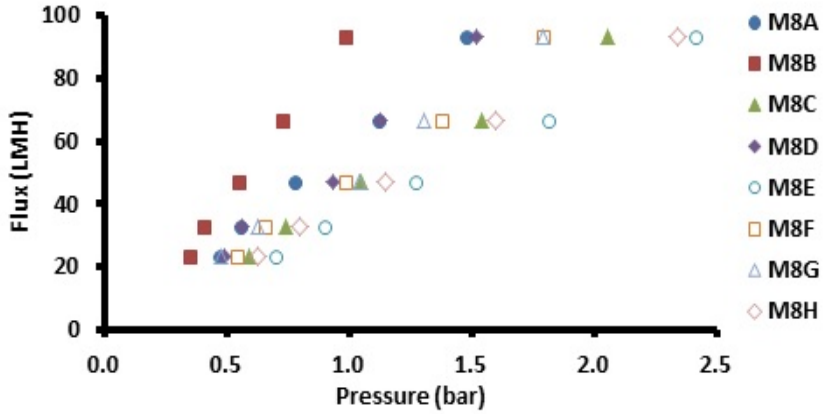

Membrane 8 KDa	A	B	C	D	E	F	G	H	Mean	vc (%)
Permeability (LMH/bar)	61	90	44	58	38	50	50	40	54	32

Figure 3-5: 8 kDa membrane initial permeability (20ºC, milli-Q water)

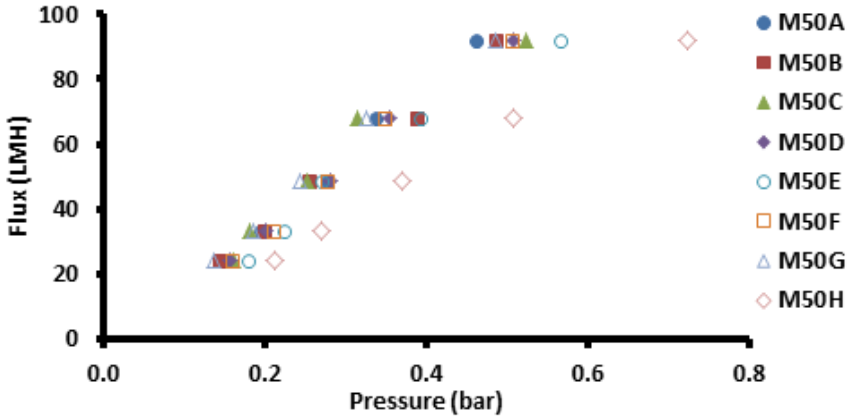

Membrane 50 KDa	A	B	C	D	E	F	G	H	Mean	vc (%)
Permeability (LMH/bar)	193	185	184	182	166	178	196	128	176	13

Figure 3-6: 50 kDa membrane initial permeability (20ºC, milli-Q water)

3.2.2 Pre-ozonation impacts on ceramic membranes performance

3.2.2.1 DOC removal

Most of the DOC measurements were unfortunately lost in this experiment, but the remaining samples (40%) indicated overall (ozonation+filtration) rejections between 10-20% for the 50 kDa membrane, and 20-30% for the 8 kDa membrane (table 3.3). Rejections at dose 0.0 mgO_3/mgC agree with the AWWA (2005) report, which indicates MF/UF DOC removals lower than 20% in the absence of any pre-treatment.

Table 3.3: Typical DOC removal (%) by the hybrid ozonation-filtration treatment

Dose/ Memb-pH	50kDa, pH 6.5	50 kDa, pH 8.5	8 kDa, pH 6.5	8 kDa, pH 8.5
0.0	-	13%	21%	-
0.5	14%	-	-	23%
1.0	18%	18%	-	29%

3.2.2.2 UVA_{254} removal

NOM removal was monitored through UVA_{254} measurements on the filtrate, as humic/fulvic acids were identified as the main potential fouling agents for this experiment. In accordance to COD results, superior rejection of material was obtained for membrane 8 kDa over 50 kDa (10% higher or more). Figure 3-7 shows overall removal (coupled ozonation-filtration treatment) of UVA_{254}-bearing molecules was proportional to ozone doses for all conditions. Most of this effect was caused by the ozone oxidation rather than the filtration step.

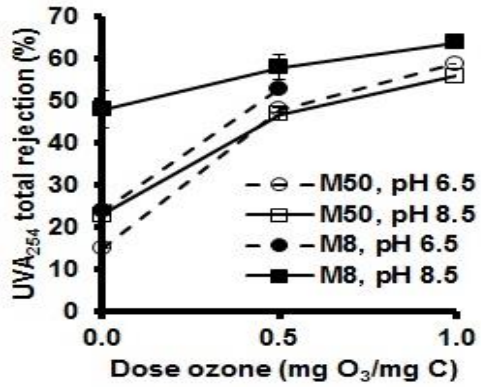

Dose/ Memb-pH	M 50, pH 6.5	M 50, pH 8.5	M 8, pH 6.5	M 8, pH 8.5
0	15	23	24	48±4
0.5	48±0.5	47±2	53	58±3
1	59	56	-	64

Figure 3-7: Total UVA_{254} removals (%) by hybri ozonation-filtration treatments
(n=1.0-2.0, typical or average values, error bars: min-max)

The impact of pH on UVA_{254} rejection by UF alone is presented in figure 3-8. For example, in the absence of pre-ozonation, UVA_{254} rejections increased from 16-24% at pH 6.5 to 23-48% at pH 8.5. This effect was also noticeable in ozonated samples, albeit to lesser extent. The latter may be attributed to the reduction of aromaticity, molecules size, and changes in hydrophilicity of the NOM fractions due to ozone oxidation. In fact, UF UVA_{254} rejection was only higher in 10-20% (normalized dose 0.5) and 3-6% (normalized dose 1.0) with respect to ozonation. These results suggested that increasing O_3 doses reduces molecule size, so that NOM

removal by UF becomes less effective (Kim, Davies, Baumann, Tarabara, & Masten, 2008; S. Lee, Lee, Wan, & Choi, 2005; Lehman & Liu, 2009).

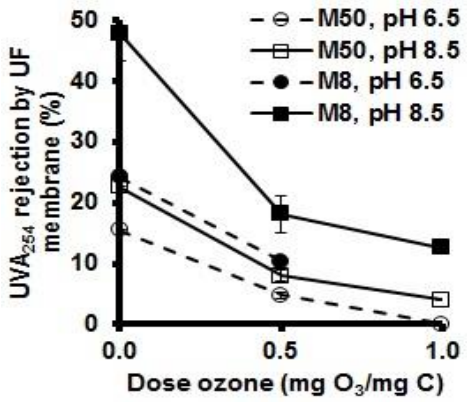

Figure 3-8: UVA_{254} removals by 8 and 50 kDa ceramic membranes for variable pre-ozonation treatment conditions
Note: UVA removals achieved by the UF processes alone;
n=1.0-2.0; typical or average values, error bars=min-max

3.2.2.3 Colour

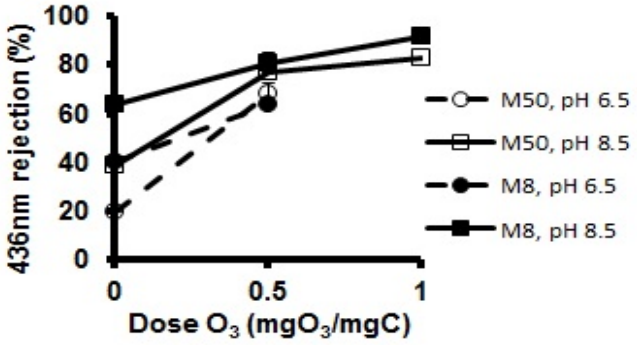

Figure 3-9: Colour (436 nm) removal (%) by hybrid ozonation-filtration treatment
(n=1.0-2.0, typical or average values, error bars: min-max)

UF is not expected to eliminate colour in a water sample as pore sizes are too large to screen dissolved molecules (AWWA, 2005). However, for non-ozonated samples (figure 3-9) colour (absorbance at 436 nm) was removed at 20-40% (50 kDa) and 40-60% (8 kDa) for pH 6.5 and 8.5, respectively. This result is compatible with the percentages found by Thompson & Galloway, 2001, who reported a range of 17-54% colour reduction for surface waters in UF membranes (AWWA, 2005).

3.2.3 Fouling mechanism

Figures 3-10 and 3-11 present the resistance behaviour for the 50 and 8 kDa fouling assays, respectively. Membrane fouling was influenced by both pH and applied ozone dosages. However, the analysis of the two pH conditions reveals a different trend in fouling mechanisms between pH 6.5 and pH 8.5.

The isoelectric point of the membranes used has been measured as ± 6.5 (Sczymick, 1998; Lee, 2014). Therefore, at pH 8.5, the membranes and the NOM were both negatively charged. Besides, earlier data on NOM rejection indicated higher UVA_{254} rejections under this pH condition. Thus, it was proposed that electrical repulsions NOM-membrane and NOM-NOM, favored the accumulation of material (concentration polarization) on the feed side of the membrane and subsequently formed a cake under the influence of hydrophobic and Van-der-Waals forces. This phenomenon was in agreement with the form of the fouling graphs at pH 8.5, which were always shown to be a straight upward line that best fitted the cake filtration unified model from Huang et al (2008) ($R^2 > 0.90$). In the absence of electrical repulsions a classic two segments graph including some type of initial blocking (highly plausible due to the low solute to pore size ratio (Wang, Wang, Liu, & Duan, 2007) and cake formation would have been observed.

At pH 6.5, the membranes were not electrically charged which allowed for a higher probability of material introducing within the membrane matrix. This explains the form of many of the fouling graphs, which exhibited two main segments (figures 3-10 and 3-11): the first one was reasonably associated with an initial blockage of the membrane and indeed, it fitted (R^2>0.90) the intermediate blocking unified model (Huang, et al. 2008) with UMFI values in the order of ±400E-04 and ±18E-04 m^2/L for O_3 doses 0.5 and 1 mg O_3/mg COD); the second segment corresponded to the formation of a cake, which actually fitted the unified model for cake filtration ($R^2 > 0.90$) with UMFI values in the order of ±20E-04 and ±5E-04 m^2/L for O_3 doses 0.5 and 1 mg O_3/mg COD).

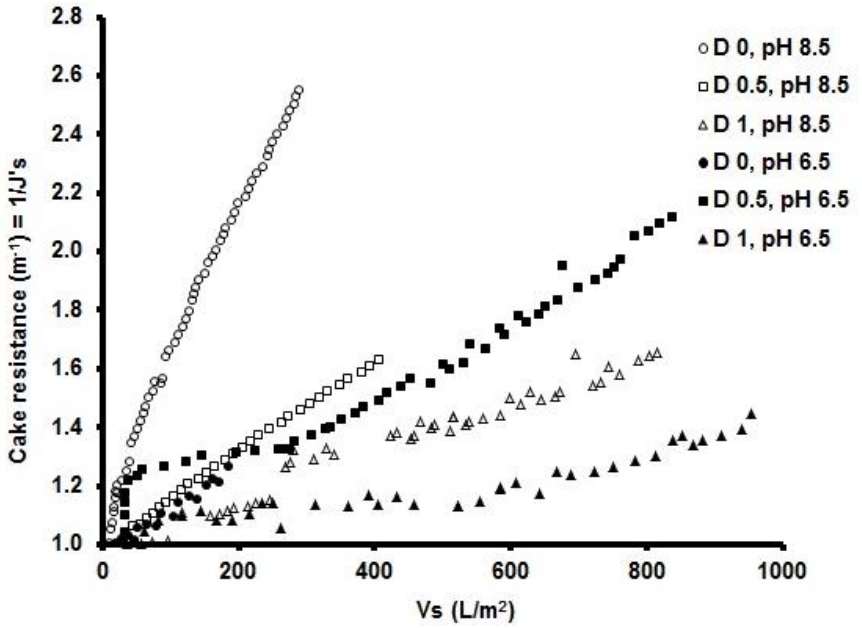

Figure 3-10: Typical fouling behaviour of membrane 50 kDa (n=1.0, duplicatas in Appendix O)

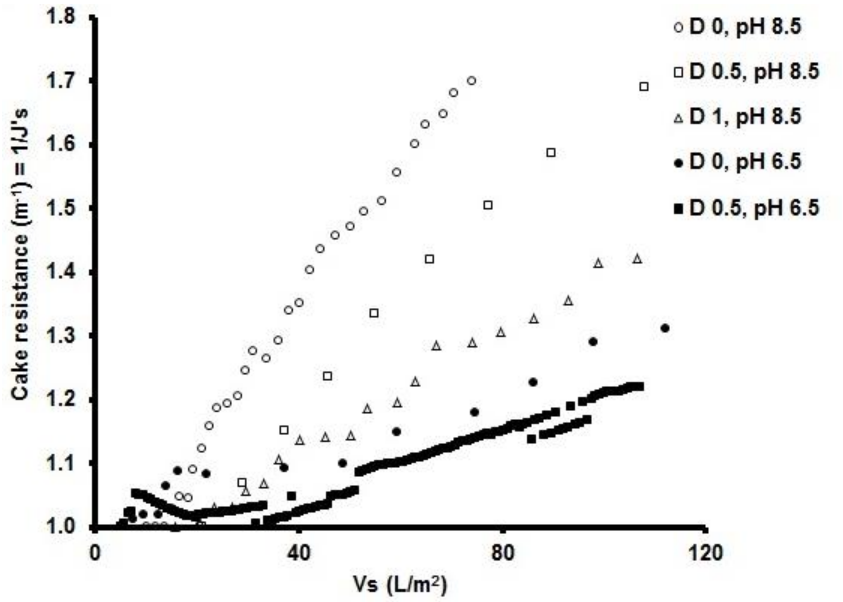

Figure 3-11: Typical fouling behaviour of membrane 8 kDa (n=1.0, duplicatas in Appendix O)

The hypothesis of concentration polarization was confirmed with additional experiments in the laboratory, where clean membranes were soaked at different pH: 5, 6.5 and 10, and fouling experiments were conducted with surface water conditioned at pH 6.5 and 8.5. Figure 3-12 shows higher fouling index at pH 8.5 at all initial membrane conditions.

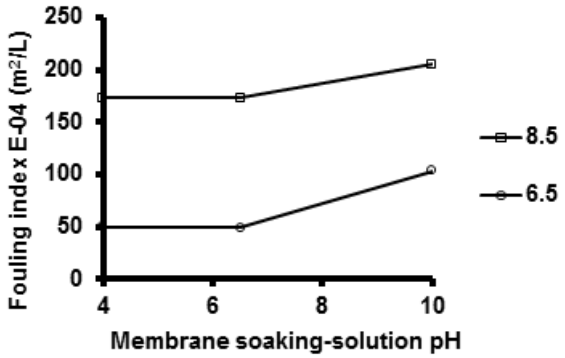

Figure 3-12: Typical fouling index trends according to the initial pH of membranes and feed water (n=1.0)

Figure 3-13 supports the hypothesis of concentration polarization as higher UV and COD rejections at pH 8.5 converge with the higher fouling index presented in figure 3-12, evidencing the prevalence of NOM-NOM over NOM-membrane interactions.

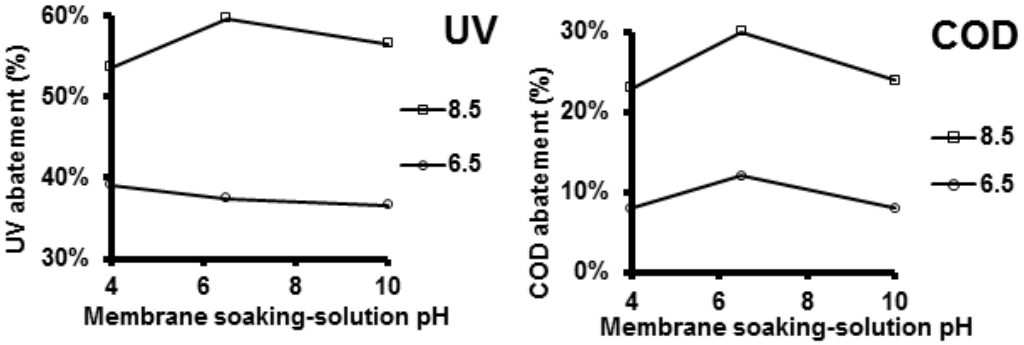

Figure 3-13: Typical UVA_{254} and COD abatements trends wrt the initial pH of membranes and feed water (n=1.0)

The hypothesis of cake formation was also confirmed with additional experiments in the laboratory, where permeability was measured following the filtration process and also after applying two backwashes at ±25 and ±95 LMH (table 3.4).

Table 3.4 : Permeability tests post-filtration process (n=2, error = 1 std dev)

Membrane 8 kDa		
Permeability (LMH/bar)	pH 6.5	pH 8.5
Initial	78±0.0	86±13
After filtration	34±0.0	21±0.7
After backwash ±25LMH	36±4	26±3
After backwash ±95LMH	39±2	27±2

Membrane fouling through cake formation was proposed as permeability was not recovered after performing the two backwashes, as shown in table 3.4. This cake offered more resistance to the passage of pure water at pH 8.5 due to higher accumulation of material on the feed side of the membrane.

3.2.4 Fouling index

The universal membrane fouling index (UMFI) model for cake filtration was used to calculate the degree of fouling on the tested membranes as it was shown in the earlier section to correctly approximate the overall observed fouling behavior. This concept was applied over the portion of the fouling graphs considered to be under a cake layer regime. Figure 3-14 presents the calculated UMFI.

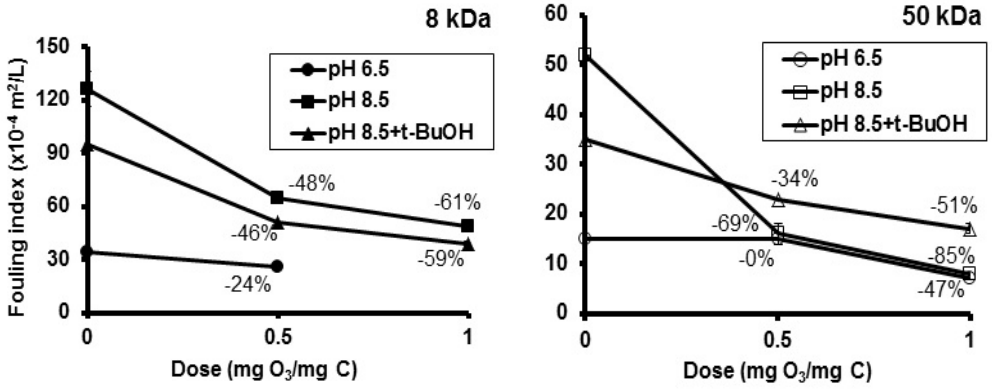

Figure 3-14: UMFI x 10^{-4} [m^2/L] comparison for 8 and 50 kDa membranes
(n=1.0-2.0, typical or average values, error bars: min-max)

Firstly, the 8 kDa membrane underwent higher fouling than 50 kDa membrane (2.7-fold on average). This was expected considering the higher accumulation of organic material in the feed side of the membrane (figure 3-8). As depicted in figure 3-14, ozonation decreases the fouling index of both membranes. The average reduction in fouling was calculated as 48%

although it differed in magnitude according to the ozone dosage and pH. At the normalized dose of 0.5 mg O_3/mg C, UMFI reductions were ≥ 50% for pH 8.5, but less than 25% for pH 6.5. As presented earlier, no significant Ct_{O3} were achieved for the lowest ozone dosage and UVA_{254} removals were equal for both pH. For the dose of 1.0 mg O_3/mg C, UMFI reductions were 60-85% for pH 8.5, and around 50% for pH 6.5. Once again, maintaining ozone residual was not crucial for fouling reduction as illustrated by the identical 50 kDa UMFI at pH 6.5 (Ct_{O3} =10 M.s) and pH 8.5 (Ct_{O3} = 0 M.s). The second phase free radical formation (controllable by t-BuOH) was also observed to be a secondary actor in fouling reduction. This statement is supported by the fact that fouling reduction under the 8.5+*t*-butanol condition was equal or lower than for the pH 8.5 alone. On the other hand, the $Ct_{OH\text{-}1st\ phase}$ was found to be significantly correlated (r = 0.83, p-value < 0.01) with fouling reduction. Consequently, the release of OH radicals during immediate demand and/or the direct ozone oxidation of NOM during this initial stage appear to be the dominant mechanisms to explain fouling mitigation by ozone.

Even though ozone reduced fouling, in this experiment the most efficient strategy for fouling alleviation was observed by controlling the pH of the feed solution. In the absence of the ozonation pre-treatment, the pH 6.5 condition reduced UMFI by ±70% reduction compared to the pH 8.5 condition. Upon ozonation, the impact of pH on membrane fouling was less important (for the 8 kDa membrane) or insignificant (for the 50 kDa membrane).

CHAPTER 4 DISCUSSION

Research conducted on the effect of ozone for alleviating ceramic membrane fouling has been largely focused on the catalytic effect of membrane inorganic material to produce •OH radicals following reaction with molecular ozone reaching its surface. These investigations converge in reporting a sustainable membrane fouling mitigation when the membrane is in contact with a minimal ozone residual (variable values given). The mechanism of fouling reduction would rely on the oxidation of NOM into more hydrophilic low molecular weight compounds (Karnik, et al., 2005; Kim, et al., 2008; Lehman & Liu, 2009; Sartor, Schlichter, Gatjal, & Mavrov, 2008; Schlichter, Mavrov, & Chmiel, 2004; You, Tseng, & Hsu, 2007). In the absence of ozone residual in contact with the membrane, Nguyen & Roddick (2010) observed a 32% decrease in the UMFI value when applying a normalized dose of 0.72 mg O_3/mg C at pH 7.5 prior to a 100 kDa PVDF membrane. Geismar, et al. (2012) measured UMFI reductions on SiC, TiO_2 and PES membranes varying from 40 to 80% for normalized ozone dosages of 0.2 to 1.4 mg O_3/mg C. Distinction between the effect of molecular ozone versus •OH radicals was not assessed in these studies. However, Geismar, et al. (2012) indicated that most of the reduction in fouling occurred for the lowest ozone dose of 1 mg O_3/L (decrease in UMFI of 44, 63, and 41% for the polymeric, the UF ceramic and the MF ceramic membranes, respectively). Such observation is coherent with our conclusions that the immediate demand regime plays an important role in membrane fouling reductions. It was not possible in this study to discriminate if the reduction in fouling observed during the first phase ozonation results mainly from the direct action of molecular O_3 or from the formation of free radicals. This limitation is also an issue for those willing to predict trace contaminants in wastewaters since (i) there is currently no simple method to quench free radicals formed during this ozonation stage and (ii) OH radical formation during this stage is highly correlated with NOM direct oxidation by molecular O_3 (Hübner, Keller, & Jekel, 2013).

Studies evaluating the impact of pH on ceramic membrane report lower fouling at higher pH values (Changwon, 2013; De Angelis & Fidalgo, 2013; Karnik, et al., 2005; S. Lee & Kim, 2014). These results are in apparent contradiction to those found in this experiment. Previous authors have highlighted that pH effects are highly dependent on solute-membrane and solute-solute interactions. Therefore, differences in operating modes, membrane materials and water

characteristics can explain the anticipated role of pH. For example, Karnik, et al. (2005) used a cross-flow, constant flux system, Lee & Kim (2014) worked with dead-end stirred cells at declining flux, and De Angelis & Fidalgo (2013) utilized dead-end at declining flux. Hydrodynamic conditions under declining flux stirred cells are expected to mitigate the concentration polarization phenomenon at basic pH, as opposed to the dead-end, unstirred, constant flux conditions used for our experiments. Changwon (2013) worked with a similar experimental set-up to the one we used (dead-end, unstirred cells at constant pressure). However, the wastewater matrix (DOC ± 6 mg C/L) had a high Ca^{2+} concentration (79 mg/L). Calcium concentration is well known to impact membrane fouling (S. Lee & Kim, 2014). The presence of calcium during ozonation is also known to promote NOM coagulation/flocculation (Jekel, 1994). During this work, calcium/magnesium concentrations were low (8 and 2 mg/L, respectively) and are therefore not expected to have either led to ozone-induced flocculation or reduce the concentration polarization promoted by the NOM-membrane and NOM-NOM repulsions at pH 8.5.

Overall, UVA_{254} measurements in the permeate decreases during a hybrid ozonation-filtration treatment; but it is known that most of the abatement is due to ozone oxidation which reduces the hydrophobicity of NOM and promotes its mineralization (Kim, et al. 2008; Lehman & Liu, 2009). In this study, UVA_{254} reductions by the combined O_3/UF process reached 52 and 59%, from which 36 and 54% were actually achieved by the ozonation process (for the normalized doses 0.5 and 1.0 mg O_3/mg C, respectively). Furthermore, it has also been reported that UVA_{254} retention by membranes can actually be impaired by ozonation, as lower molecular weight molecules are formed upon partial oxidation and may then more readily permeate depending on the membrane MWCO (Kim, et al., 2008; S. Lee, et al., 2005; Lehman & Liu, 2009). This was also observed in the present study as the UF membrane average abatements were observed to steadily decline as ozone dosages increased from 0 to 1.0 mg O_3/mg C.

Based on the test conditions investigated in this work (unstirred, dead-end, constant flux filtration), operating at low pH reduced fouling. Under such scenario, ozonation is a potential fouling mitigation strategy although that high doses (1 mg O_3/mg C) were needed to obtain a high (>50%) fouling reduction. This observation would need further validation at the pilot-scale under conditions where less severe polarisation-concentration is expected (e.g. crossflow or with frequent hydraulic backwash). In all cases, operating the pre-ozonation to fulfill immediate ozone

demand proved to offer the largest benefit in terms of fouling reduction. During the time frame of this experiment, it was not possible to assess the long-term benefits of maintaining ozone residual in contact with the membrane to oxidise accumulated foulants. If proven beneficial, further studies should consider the possibility to achieve this goal using ozonated backwash waters rather than overcoming ozone immediate demand on a continuous basis.

CONCLUSIONS

The impacts of pre-ozonation on the fouling of 8 and 50 kDa ZrO_2/TiO_2 ceramic membranes fed with surface water was investigated under variable ozone dosages and pH. For the test conditions investigated, the following conclusions were drawn:

1. As expected, ozonation reduce NOM aromaticity (UVA_{254nm}) , with reductions of ± 36% and ± 53 % for normalized doses of 0.5 and 1.0 mg O_3/mg C.
2. Direct oxidation of NOM by molecular O_3 during the immediate ozone demand regime was the main mechanism to explain fouling reduction, although it was not possible to discriminate if the free radicals generated during this phase contributed to this performance. Doubling the ozone dose resulted in two-fold increase in free radical exposures (Ct_{OH}).
3. Maintaining ozone residual (Ct_{O3}) was not essential to control fouling. However, achieving detectable ozone residual implied using higher O_3 dosages which led to higher free radical exposures (Ct_{OH}) and consequently lower fouling.
4. The highest fouling indexes were calculated at pH 8.5 due to the suspected NOM-NOM and NOM-membrane electrical repulsions, the phenomenon of concentration polarization and the subsequent cake formation. Ozonation pre-treatment did alleviate the fouling levels with respect to raw waters: up to 60% and 85% for 8 and 50 kDa membranes, respectively. Higher fouling reductions were achieved at pH 8.5 (50-85%) than at pH 6.5 (0-50%).
5. The impact of pH on fouling was generally greater or similar to the effect of pre-ozonation as fouling indexes measured using unozonated waters were 70% lower at pH 6.5 than at pH 8.5.
6. On average, the 8 kDa membrane UMFI were 2.7 times higher than for the 50 kDa membrane. However, equivalent fouling reductions (48% on average) were achieved for both membranes by the use of pre-ozonation.
7. Fouling mechanisms were driven by electrical charge effects, so that solution's pH and the amphoteric property of the ceramic membranes played an important role. Concentration polarization and cake formation are suggested as the dominant mechanisms

at pH 8.5; whereas intermediate pore blocking and cake formation is proposed for the pH 6.5 condition.

Further studies should ascertain the role of pH on concentration-polarisation and its effect on ceramic membrane fouling for various source waters. It would also be of interest to demonstrate the role of immediate ozone demand in fouling reduction and, more specifically, the benefits of maintaining ozone residuals in contact with the membrane as opposed to an operation mode where pre-ozonation would be achieved only to meet immediate ozone demand.

BIBLIOGRAPHY

Acero, J., & Von Gunten, U. (2001). Characterization of Oxidation Processes: Ozonation and the AOP O_3/H_2O_2. *Journal of the American Water Works Association, 93*(10), 90-100.

Akbarnezhad, S., Mousavi, M., & Sarhaddi, R. (2010). Sol-Gel Synthesis of Alumina-Titania Ceramic Membrane: Preparation and Characterization *Indian Journal of Science and Technology, 3*(10), 1048-1051.

Al-Amoudi, A. (2010). Factors Affecting Natural Organic Matter (NOM) and Scaling Fouling in NF Membranes: a Review. *Desalination, 259*, 1-10.

Alem, A., Sarpoolaky, H., & Keshmiri, M. (2009). Titania Ultrafiltration Membrane: Preparation, Characterization and Photocatalytic Activity. *Journal of European Ceramic Society, 29*, 629-635.

Araki, S., Kiyohara, Y., Imasaka, S., Tanaka, S., & Miyake, Y. (2011). Preparation and Pervaporation Properties of Silica-Zirconia Membranes. *Desalination, 266*, 46-50.

AWWA. (2005). Microfiltration and Ultrafiltration Membranes for Drinking Water-Manual of Water Supply Practices. M53. *American Water Works Association*(1st edition).

Beltrán, F. (2004). *Ozone Reaction Kinetics for Water and Wastewater Systems*. U.S.A.: Lewis Publishers.

Blankert, B., Betlem, B., & Roffel, B. (2006). Dynamic Optimization of a Dead-End Filtration Trajectory: Blocking Filtration Laws *Journal of Membrane Science, 285*, 90-95.

Boerlage.S, Kennedy, M., Petros, M., Abogrean, E., Tarawneh, Z., & Schippers, J. (2003). The MFI-UF as a Water Quality Test and Monitor. *Journal of Membrane Science, 211*, 271-289.

Bolton, G., LaCasse, D., & Kuriyel, R. (2006). Combined Models of Membrane Fouling: Development and Application to Microfiltration and Ultrafiltration of Biological Fluids. *Journal of membrane Science, 277*, 75-84.

Buffle, M., Schumacher, J., Meylan, S., Jekel, M., & Von Gunten, U. (2006). Ozonation and Avanced Oxidation of Wastewater: Effect of O_3 Dose, pH, DOM and HO* Scavengers on Ozone Decomposition and HO* Generation. *Ozone: Science & Engineering, 28*(August), 247-259.

BV, C. S. (2012-2013). CeraMac Services-Projects. Retrieved October 23rd, 2014, from www.ceramac-services.com/projects/index.html

Chang, H., Liu, B., Luo, W., & Li, G. (2014). Fouling Mechanisms in the Early Stage of an Enhanced Coagulation-Ultrafiltration Process. *Front. Environ. Sci. Eng.*

Changwon, H. (2013). *Ozonation and/or Coagulation - Ceramic Membrane Hybrid for Filtration of Impaired Quality Source Waters.* King Abdullah University of Science and Technology, Thuwal, Kingdom of Saudi Arabia.

Chellam, S., & Cogan, N. (2011). Colloidal and Bacterial Fouling During Constant Flux Microfiltration: Comparison of Classical Blocking Laws with Unified Model Combining Pore Blocking and EPS Secretion. *Journal of Membrane Science, 382*, 148-157.

Chellam, S., & Xu, W. (2006). Blocking Law Analysis of Dead-End Constant Flux Microfiltration of Compressible Cakes. *Journal of Colloid and Interface Science, 301*, 248-257.

Cheng, Y., Lee, D., & Lai, J. (2011). Filtration Blocking Laws: Revisited. *Journal of the Taiwan Institute of Chemical Engineers, 42*, 506-508.

Chevereau, E., Zouaoui, N., Limousy, L., Dutournié, P., Déon, S., & Bourseau, P. (2010). Surface Properties of Ceramic Ultrafiltration TiO_2 membranes: Effects of Surface Equilibriums on Salt Retention. *Desalination, 255*, 1-8.

Chiu, T. (2011). Effect of Ageing on the Microfiltration Performance of Ceramic Membranes. *Separation and Purification Technology, 83*, 106-113.

Combe, C., Molis, E., Lucas, P., Riley, R., & Clark, M. (1999). The Effect of CA membrane properties on adsorptive fouling by humic acid. *Journal of Membrane Science, 154*, 73-87.

Costa, A., & de Pinho, M. (2005). Effect of Membrane Pore Size and Solution Chemistry on the Ultrafiltration of Humic Substances Solutions. *Journal of Membrane Science, 255*, 49-56.

De Angelis, L., & Fidalgo, M. (2013). Ceramic Membrane Filtration of Organic Compounds: Effect of Concentration, pH, and Mixtures Interactions on Fouling. *Separation and Purification Technology, 118*, 762-775.

Dong, B., Chen, Y., Gao, N., & Fan, J. (2007). Effect of Coagulation Pretreatment on the Fouling of Ultrafiltration Membrane. *Jounal of Environmental Sciences, 19*, 278-283.

Elovitz, M., & Von Gunten, U. (1999). Hydroxyl Radical/Ozone Ratios During Ozonation Processes. I. the Rct Concept. *Ozone: Science & Engineering, 21*(3), 239-260.

Elovitz, M., Von Gunten, U. (1999). Hydroxyl Radical/Ozone Ratios During Ozonation Processes. I. the Rct Concept. *Ozone: Science & Engineering, 21*(3), 239-260.

Fan, X., Tao, Y., Wang, L., Zhang, X., Lei, Y., Wang, Z., et al. (2014). Performance of an Integrated Process Combining Ozonation with Ceramic Membrane Ultra-filtration for Advanced Treatment of Drinking Water. *Desalination, 335*, 47-54.

Freeman, S., & Shorney-Darby, H. (2011). What's the Buzz About Ceramic Membranes? *Journal American Water Works Association*(December).

Freyberg, T. (2014, May 12, 2014). Large Scale Ceramic Membrane Drinking Water Plant Demonstrated in the Netherlands. Retrieved October 23rd, 2014, from http://www.waterworld.com/articles/2014/05/large-scale-ceramic-membrane-drinking-water-plant-demonstrated-in-the-netherlands.html

Gao, W., Liang, H., Ma, J., Han, M., Chen, Z., Han, Z., et al. (2011). Membrane Fouling Control in Ultrafiltration Technology for Drinking Water Production: a Review. *Desalination, 272*, 1-8.

Gaulinger, S. (2007). *Coagulation Pre-Treatment for Microfiltration with Ceramic Membranes*.

Geismar, N., Bérubé, P., & Barbeau, B. (2012). Variability and Limits of the Unified Membrane Fouling Index: Application to the Reduction of Low-Pressure Membrane Fouling by Ozonation and Biofiltration. *Desalination and Water Treatment, 43*(1-3), 91-101.

Gonsalves, V. (1950). A Critical Investigation of the Viscose Filtration Process. *Rec. Trav. Chim., 69*, 873-903.

Gottschalk, C., Libra, J., & Saupe, A. (2010). *Ozonation of Water and Waste Water* (Second ed.): Wiley-VCH Verlag GmbH & Co. KGaA.

Hermans, P., & Bredée, H. (1935). Zur Kenntniss der Filtrationsgesetze. *Rec. Trav. Chim., 54*, 680-700.

Hermia, J. (1982). Constant Pressure Blocking Filtration Laws. Application to Power-Law non-Newtonian Fluids. *Trans. Inst. Chem. E., 60*, 183-187.

Hlavacek, M., & Bouchet, F. (1993). Constant Flowrate Blocking Laws and an Example of their Application to Dead-End Microfiltration of Protein Solutions. *Journal of Membrane Science, 82*, 285-295.

Ho, C., & Zydney, A. (2000). A Combined Pore Blockage and Cake Filtration Model for Protein Fouling during Microfiltration. *Journal of Colloid and Interface Science, 232*, 389-399.

Ho, Z. (1999). Theoretical Analysis of the Effect of Membrane Morphology on Fouling during Microfiltration. *Separation Science and Technology, 4*(13), 2461-2483.

Hogg, R., Healy, T., & Fuerstenau, D. (1966). Mutual Coagulation of Colloidal Dispersions. *Transactions of the Faraday Society, 62*, 1638-1651.

Howe, K., & Clark, M. (2002). Fouling of Microfiltration and Ultrafiltration Membranes by Natural Waters. *Environmental Science and Technology, 36*, 3571-3576.

Huang, H., Young, T., & Jacangelo, J. (2008). Unified Membrane Fouling Index for Low Pressure Membrane Filtration of Natural Waters: Principles and Methodology. *Environmental Science and Technology, 42*, 714-720.

Hübner, U., Keller, S., & Jekel, M. (2013). Evaluation of the Prediction of Trace Organic Compounds Removal during Ozonation of Secondary effluents using Tracer Substances and Second order Rate Kinetics. *Water Research, 47*(17), 6467-6474.

Jekel, M. (1994). Flocculation Effects of Ozone. *Ozone: Science & Engineering, 16*(1), 55-66.

Jermann, D., Pronk, W., Meylan, S., & Boller, M. (2007). Interplay of Different NOM Fouling Mechanisms during Ultrafiltration for Drinking Water Production. *Water Research*(1713-1722).

Kabsch-Korbutowicz, M., & Urbanowska, A. (2010). Water Treatment in Integrated Process Using Ceramic Membranes. *Polish Journal of Environmental Studies, 19*(4), 731-737.

Karnik, B., Davies, S., Chen, K., Jaglowski, D., Baumann, M., & Masten, S. (2005). Effects of Ozonation on the Permeate Flux of Nanocrystalline Ceramic Membranes. *Water Research, 39*(728-734).

Katsoufidou, K., Yiantsios, S., & Karabelas, A. (2005). A Study of Ultrafiltration Membrane Fouling by Humic Acids and Flux Recovery by Backwashing: Experiments and Modeling. *Journal of Membrane Science, 266*, 40-50.

Kennedy, M., Chun, H., Quintanilla, V., Heijman, B., & Schippers, J. (2005). Natural Organic Matter (NOM) Fouling of Ultrafiltration Membranes: Fractionation of NOM in Surface Water and Characterisation by LC-OCD. *Desalination, 178*, 73-83.

Kim, J., Davies, S., Baumann, M., Tarabara, V., & Masten, S. (2008). Effect of Ozone Dosage and Hydrodynamic Conditions on the Permeate Flux in a Hybrid Ozonation-Ceramic Ultrafiltration System Treating Natural Waters. *Journal of Membrane Science, 311*, 165-172.

Kim, J., & DiGiano, F. (2009). Fouling Models for Low-Pressure Membrane Systems. *Separation and Purification Technology, 68*, 293-304.

Kim, J., & Van der Bruggen, B. (2010). The Use of Nanomolecules in Polymeric and Ceramic Membranes Structures: Review of Manufacturing Procedures and Performance Improvement for Water Treatment. *Environmental Pollution, 158*, 2335-2349.

Kimura, K., Hane, Y., Watanabe, Y., Amy, G., & Ohkuma, N. (2004). Irreversible Membrane Fouling During Ultrafiltration of Surface Water. *Water Research, 38*, 3431-3441.

Kimura, K., Tanaka, K., & Yoshimasa, W. (2014). Microfiltration of Different Surface Waters With/Without Coagulation: Clear Correlations between Membrane Fouling and Hydrophilic Biopolymers. *Water Research, 49*, 434-443.

Koo, C., Mohammad, A., Suja, F., & Talib, M. (2013). Use and Development of Fouling Index in Predicting Membrane Fouling. *Separation & Purification Reviews, 42*, 296-339.

Larbot, A., Alary, J., Guizard, C., & Cot, L. (1987). New Inorganic Ultrafiltration Membranes: Preparation and Characterisation. *International Journal High Technology Ceramics, 3*, 143-151.

Larbot, A., Fabre, J., Guizard, C., & Cot, L. (1989). New Inorganic Ultrafiltration Membranes: Titania and Zirconia Membranes. *Journal American Ceramic Society, 72*(2), 257-261.

Lee, N., Amy, G., & Croué, J. (2006). Low-Pressure Membrane (MF/UF) Fouling Associated with Allochthonous versus Autochthonous Natural Organic Matter. *Water Research, 40*, 2357-2368.

Lee, N., Amy, G., Croué, J., & Buisson, H. (2004). Identification and Understanding of Fouling in Low-Pressure Membrane (MF/UF) Filtration by Natural Organic Matter (NOM). *Water Research, 38*, 4511-4523.

Lee, S., & Kim, J. (2014). Differential Natural Organic Matter Fouling of Ceramic versus Polymeric Ultrafiltration Membranes. *Water Research, 48*, 43-51.

Lee, S., Lee, K., Wan, W., & Choi, Y. (2005). Comparison of membrane permeability and a fouling mechanism by pre-ozonation followed by membrane filtration and residual ozone in membrane cells. *Desalination, 178*, 287-294.

Lehman, G., & Liu, L. (2009). Application of ceramic membranes with pre-ozonation for treatment of secondary wastewater effluent. *Water Research, 43*, 2020-2028.

Lin, Y., & Hsien, H. (2011). Characteristics Transformations of Humic Acid during Ozonation and Biofiltration Treatment Processes. *Water Environment Research, 83*(5).

López, A., Pic, J., Benbelkacem, H., & Debellefontaine, H. (2007). Influence of *t*-butanol and of pH on Hydrodynamic and Mass Transfer parameters in an Ozonation Process. *Chemical Engineering and Processing, 46*, 649-655.

Lu, G., Diniz, J., Duke, M., Giessler, S., Socolow, R., Williams, R., et al. (2007). Inorganic Membranes for Hydrogen Production and Purification: A Critical Review and Perspective. *Journal of Colloid and Interface Science, 314*, 589-603.

Madireddi, K., Babcock, R., Levine, B., Kim, J., & Stenstrom, M. (1999). An Unsteady-State Model to Predict Concentration Polarization in Commercial Spiral Wound Membranes. *Journal of Membrane Science, 157*, 13-34.

Medvedkova, N., & Nazarov, V. (1995). Physicochemical Basis of the Sol-Gel Process Giving Selective Layers of Ultrafiltration Ceramic Membranes from Zirconia Hydrosol. *Glass and Ceramics, 52*(11-12), 308-311.

Metawater Co., L. (2014). Ceramic Membrane Filtration System-Installation Record. Retrieved October 23rd, 2014, from

http://www.metawater.co.jp/eng/product/drinking/membrane_clarify/location.html

Mizuno, T., Tsuno,H, Yamada,H. (2007). Development of Ozone Self-Decomposition Model for Engineering Design. *Ozone: Science & Engineering, 29*, 55-63.

Moritz, T., Benfer, S., Árki, P., & Tomandl, G. (2001). Influence of the Surface Charge on the Permeate Flux in the Dead-End Filtration with Ceramic Membranes. *Separation & Purification Technology, 25*, 501-508.

Munla, L. (2012). Reversible and Irreversible Fouling of Ultrafiltration Ceramic Membranes by Model Solutions. *Journal American Water Works Association, 104*(10).

Nguyen, S., & Roddick, F. (2010). Effects of Ozonation and Biological Activated Carbon Filtration on Membrane Fouling in Ultrafiltration of an Activated Sludge Effluent. *Journal of Membrane Science, 363*, 271-277.

Nilson, J., & DiGiano, F. (1996). Influence of NOM Composition on Nanofiltration. *Journal of American Water Works Association, 88*(5, Membrane Processes), 53-66.

Pabby, A., Rizvi, S., & Sastre, A. (2009). *Handbook of Membrane Separations: Chemical, Pharmaceutical, Food and Biotechnological Applications* (Vol. CRC Press - Taylor & Francis Group).

Sartor, M., Schlichter, B., Gatjal, H., & Mavrov, V. (2008). Demonstration of a New Hybrid Process for the Decentralised Drinking and Service Water Production from Surface Water in Thailand. *Desalination, 222*, 528-540.

Schäfer, A. (2001). *Natural Organic Removal Using Membranes: Principles, Performance and Cost*. USA: Technomic Publishing Co, Inc.

Schlichter, B., Mavrov, V., & Chmiel, H. (2004). Study of a Hybrid Process Combining Ozonation and Microfiltration/Ultrafiltration for Drinking Water Production from Surface Water. *Desalination, 168*, 307-317.

Shao, J., Hou, J., & Song, H. (2011). Comparison of Humic Acid Rejection and Flux Decline During Filtration with Negatively Charged and Uncharged Ultrafiltration Membranes. *Water Research, 45*, 473-482.

Shi, L., Tin, K., & Wong, N. (1999). Thermal Stability of Zirconia Membranes. *Journal of Materials Science, 34*, 3367-3374.

Shojai, F., & Mäntilä, T. (2001). Monoclinic Zirconia Microfiltration Membranes: Preparation and Characterization. *Journal of Porous Materials, 8*, 129-142.

Sondhi, R., Bhave, R., & Jung, G. (2003). Applications and benefits of ceramic membranes. *Membrane Technology*(November), 5-8.

Staehelin, J., & Hoigné, J. (1985). Decomposition of Ozone in Water in the Presence of Organic Solutes Acting as Promoters and Inhibitors of Radical Chain Reactions. *Environmental Science and Technology, 19*(12).

Szymczyk, A., Fievet, P., Reggiani, J., & Pagetti, J. (1998a). Characterisation of Surface Properties of Ceramic Membranes by Streaming and Membrane Potentials. *Journal of Membrane Science, 146*, 277-284.

Szymczyk, A., Fievet, P., Reggiani, J., & Pagetti, J. (1998b). Determination of the Filtering Layer Electrokinetic Properties of a Multi-layer Ceramic Membrane. *Desalination, 116*, 81-88.

Thompson, M., & Galloway, M. (2001). *Ozone Micro-flocculation with Ultrafiltration for Color Removal.* Paper presented at the Proceedings of the AWWA Membrane Technology Conference, Denver, Colorado.

Van Geluwe, S., Braeken, L., & Van der Bruggen, B. (2011). Ozone Oxidation for the Alleviation of Membrane Fouling by Natural Organic Matter: a Review. *Water Research, 45*, 3551-3570.

Van Geluwe, S., Vinckier, C., Braeken, L., & Van der Bruggen, B. (2011). Ozone Oxidation of Nanofiltration Concentrates Alleviates Membrane Fouling in Drinking Water Industry. *Journal of Membrane Science, 378*, 128-137.

Vincent,S. Caractérisation de l'activité radicalaire afin de prédire l'abattement des micropolluants dans les eaux ozonées. Département des Génies Civil, Géologique et des Mines. École Polytechnique de Montréal. 2009.

Von Gunten, U. (2003). Ozonation of Drinking Water. Part I. Oxidation Kinetics and Product Formation. *Water Research, 37*, 1443-1467.

Wang, X., Wang, L., Liu, Y., & Duan, W. (2007). Ozonation Pretreatment for Ultrafiltration of the Secondary Effluent. *Journal of Membrane Science, 287*, 187-191.

Westerhoff, P., Aiken, G., Amy, G., & Debroux, J. (1999). Relationships Between the Structure of Natural Organic Matter and Its Reactivity Towards Molecular Ozone and Hydroxyl Radicals. *Water Research, 33*(10), 2265-2276.

Yamamura, H., Okimoto, K., Kimura, K., & Watanabe, Y. (2014). Hydrophilic Fraction of Natural Organic Matter Causing Irreversible Fouling of Microfiltration and Ultrafiltration Membranes. *Water Research, 54*, 123-136.

You, S., Tseng, D., & Hsu, W. (2007). Effect and Mechanism of Ultrafiltration Membrane Fouling Removal by Ozonation. *Desalination, 202*, 224-230.

Yuan, W., & Zydney, A. (1999). Effects of Solution Environment on Humic Acid Fouling During Microfiltration. *Desalination, 122*, 63-76.

Zhu, H., Wen.X, & Huang, X. (2012). Characterization of Membrane Fouling in a Microfiltration Ceramic Membrane System Treating Secondary Effluent. *Desalination, 284*, 324-331.

Zularisam, A., Ismail, A., & Salim, R. (2006). Behaviours of Natural Organic Matter in Membrane Filtration for Surface Water Treatment - a Review. *Desalination, 194*.

APPENDICES

Appendix A: Calculation examples to prepare buffers and adjust pH, alkalinity and ionic strength of the water sample

Preparation of buffer phosphate of IS 0.5 and pH 6

Ionic strength equation

Phosphate buffer: x=[Na_2HPO_4] (142 g/mol) et y=[KH_2PO_4] (136 g/mol)
H_3PO_4: pKa_2= 6.865 (25ºC)
Active species: H_2PO_4 --- $HPO_4^{2-} + H^+$

$0.5 = 0.5 \sum C_i Z_i^2$
$0.5 = 0.5*[2(Na)*1^2 + (HPO_4)*2^2 + (K)*1^2 + (H_2PO_4)*1^2]$
$0.5 = 0.5*(2x*1^2 + x*2^2 + y*1^2 + y*1^2)$
$0.5 = 0.5*(6x + 2y)$
$0.5 = 3x + y$

Henderson-Hasselbach equation

$$pH = pK_{a2} + log\frac{[HPO_4^{2-}]}{[H_2PO_4^-]}$$
$$6 = 6.865 + log\frac{x}{y}$$
$$\frac{x}{y} = 10^{-1.21} = 0.062$$
$x = 0.136y$
$y = 7.33x$

Mixing both equations

$0.5 = 3*(0.136y) + y$
$y = 0.355$ M for [KH_2PO_4]
$y = 0.355$ M * 136 g/mol = 48.3 g/L of KH_2PO_4

And, $x = [Na_2HPO_4] = 0.136y = 0.136*0.355 = 0.048$ M
$x = 0.048$ M * 142 g/mol = 6.88 g/L of Na_2HPO_4

Thus, 48.3 g of KH_2PO_4 and 6.88 g of Na_2HPO_4 are needed to prepare 1 L of buffer.

Amount of buffer phosphate needed to add an IS of 5mM

Do the same calculations, but for the ionic strength desired on the water sample.
Example: for 5mM, we would need 0.483 g of KH_2PO4 and 0.0688 g of Na_2HPO4. Then:

KH_2PO_4: 48.3 g of salt in 1000 mL of buffer
0.483 g of salt in 'v' mL of my water sample
So 'v' = 10 mL

Na_2HPO_4: 6.88 g of salt in 1000 mL of buffer
0.0688 g of salt in 'v' mL of my water sample
So 'v' = 10 mL

Thus, 10 mL of buffer should be added to 1 L of water sample.

Preparation of buffer borate of IS 0.5M and pH 8.5

Ionic strength equation

Borate buffer: x=[$Na_2B_4O_7.10H_2O$] (381.43 g/mol) et y=[H_3BO_3] (61.84 g/mol)
H_3BO_3: pka_1= 9.14
Active species at pH 9: $4H_3BO_3$ --- $B_4O_7^{2-} + 2H^+ + 5H_2O$

$0.5 = 0.5 \sum [C_iZ_i^2$ of borate buffer]
$0.5 = 0.5*[2(Na)*1^2 + (B_4O_7)*2^2 + 0.5(H)*1^2 + 0.25(BO_3)*2^2]$
$0.5 = 0.5*(2x*1^2 + x*2^2 + 0.5y*1^2 + 0.25y*2^2)$ … *Note : $2H^+/4=0.5$ & 1 $B_4O_7^{2-}/4=0.25$*
$0.5 = 0.5*(6x + 1.5y)$
$0.5 = 3x + 0.75y$

Henderson-Hasselbach equation

$$pH = pK_{a1} + log\frac{[B_4O_7^{2-}]}{[H_3BO_3]}$$
$$8.5 = 9.14 + log\frac{x}{y}$$
$$\frac{x}{y} = 10^{-0.64} = 0.229$$
$x = 0.229y$

Mixing both equations

$0.5 = 3*(0.229y) + 0.75y$
$y = 0.348$ M for [H_3BO_3]
$y = 0.348$ M * 61.84 g/mol = 21.5 g/L of H_3BO_3

And, $x = [Na_2B_4O_7] = 0.229y = 0.229*0.348 = 0.0797$ M
$X = 0.0797$ M * 381.43 g/mol = 30.4 g/L of $Na_2B_4O_7$

Amount of buffer borate needed to add an IS of 5mM

Do the same calculations, but for the ionic strength desired on the water sample.
Example: for 5mM, we would need 0.215 g of H_3BO_3 and 0.304 g of $Na_2B_4O_7$. Then:

H_3BO_3: 21.5 g of salt in 1000 mL of buffer
0.215 g of salt in 'v' mL of my water sample
So 'v' = 10 mL

$Na_2B_4O_7$: 30.4 g of salt in 1000 mL of buffer
0.304 g of salt in 'v' mL of my water sample
So 'v' = 10 mL

Thus, 10 mL of buffer should be added to 1 L of water sample.

Bibliography

Gary,C. (1986). Analytical Chemistry (4th ed). Wiley.

Appendix B: Characteristics of the water sample: raw data

Table B.1: Raw data from the water sample

Parameter	RW	MF 0.45 µm	pH 6.5	pH 8.5	pH 8.5+ *t*-butanol	Units
pH	7.10	7.75 7.98	6.53, 6.68 6.62, 6.53	8.60, 8.49 8.60, 8.56, 8.59, 8.60	8.58 8.58 8.47	-
Turbidity	10.7	0.357, 0.267 0.136, 0.163	0.142, 0.163 0.159, 0.142	0.210, 0.193 0.188, 0.200 0.200, 0.210	0.206 0.174 0.174	UTN
Conductivity	125	123 123	588, 590 595, 588	448, 415 447, 432 444, 448	496 412 412	µS
Alcalinity	33	32 33	56, 58 60, 56	68, 61 68, 66 66, 68	61 60 60	mg $CaCO_3$/L
UVA 215 nm	0.589	0.479 0.476	0.465, 0.471 0.490, 0.465	0.474, 0.480 0.486, 0.479 0.467, 0.474	0.475 0.475 0.475	-
UVA 254 nm	0.316	0.226 0.226	0.219, 0.222 0.231, 0.219	0.225, 0.224 0.226, 0.226 0.221, 0.225	0.223 0.223 0.223	-
UVA 285 nm	0.232	0.153 0.152	0.147, 0.149 0.155, 0.147	0.152, 0.152 0.154, 0.153 0.150, 0.152	0.151 0.151 0.151	-
Absorption at 436 nm	0.055	0.012 0.012	0.010, 0.011 0.011, 0.010	0.013, 0.012 0.013, 0.013 0.013, 0.013	0.012 0.012 0.012	-
COD	7.54	7.15, 7.34 7.24, 6.96	7.37, 7.11 7.37, 7.04	7.06, 7.32 7.14, 7.16 7.14, 7.06	- - -	mg/L
SUVA	0.042	0.032 0.031	0.030, 0.031 0.031, 0.031	0.032, 0.031 0.032, 0.032 0.031, 0.032	- - -	L/mg
Ca^{2+}	8.20	8.10	-	8.30	-	ppm
Mg^{2+}	1.90	1.90	-	1.90	-	ppm

Appendix C: Procedure to measure the ozone gas production

Objective

To assure the repeatability of the production and measurement of the ozone gas exiting the ozonator, when using the method adapted by CREDEAU, 2007 from the Standard Methods 2350 E - iodometric method.

Remarks

- To reach a stable production of ozone gas in the ozonator the oxygen-to-ozone conversion is kept to a minimum level, *i.e.*, an excess of pure oxygen is sent to the machine while keeping its power at the lowest level.
- To obtain repeatable measurements of O_3 gas: a) the reactor used should be as thin as possible (to assure homogeneity only with the gas bubbling), b) the level of KI solution in the trap should have a minimum height (to assure enough contact time), and c) a minimal air chamber should be left at the top of the reactor (to minimize loss of ozone gas).
- The KI solution can be buffered or not. A buffer is not used when the mixing process in the reactor is optimal.

Table C.1: Materials, reagents and equipment to measure ozone gas production

Materials	Reagents	Equipment
Beaker, 1 L	O_2 gas, UHP Air liquide	Ozonator
Burette, 50 mL	KI solution, 2% w/vol	Reactor
Magnetic bar	$Na_2S_2O_3$ solution, 0.1 N	KI solution trap
	H_2SO_4 solution, 2 N	Stirring plate

Ozone production and measurement set-up

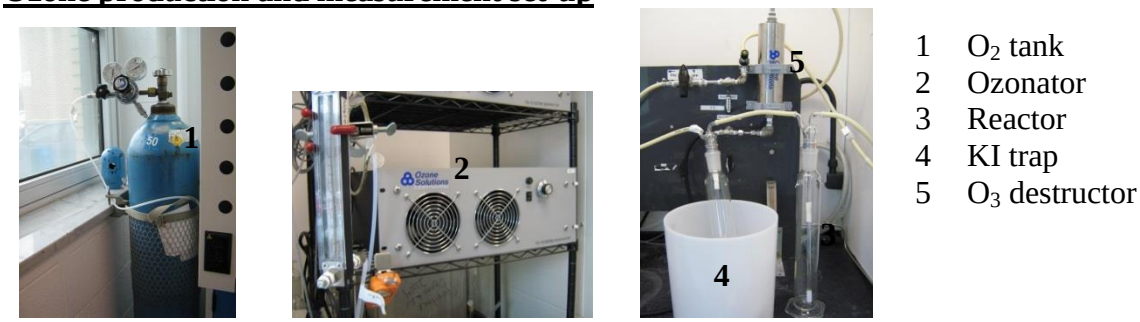

1 O_2 tank
2 Ozonator
3 Reactor
4 KI trap
5 O_3 destructor

Figure C-1: Picture of the ozone production measurement set-up

Procedure

Proceed with the O_3 measurement following the method adapted by CREDEAU, 2007 from the Standard Methods 2350 E - iodometric method, but taking the following precautions:

Parameters for the O_2-to-O_3 conversion process

- O_2 discharge P: 20 psi

- O_2 flow rate (20ºC): 220-265 mL/min (rotameter scale equivalence: 65-76 /150)
  340-400 mL/min (adjusted according to ozonator TG-10 manual)
- Ozonator power: 2

Parameters for the measurement of O_3 production

- If a thin reactor of 500 mL is used, fill it up with 450 mL KI solution. In this way, the KI solution height is >15 cm and the top air chamber is minimised.

Validation

Measurement repeatability: the described parameters led to a ±3-4% w/w conversion of O_2 to O_3; *i.e.*, a measured production of ±11 mg O_3/min (*vc*=5% for n=15). See Appendix D.

O_3 production stability: O_3 gas production slightly varies during the day, and was different each time the ozonator was started. Hence, production measurements were taken for each ozonation experiment, before and after their execution.

Appendix D: Validation of the O_3 gas production measurement

Oxygen gas feed flow measurement

The flow feed of O_2 to the ozonator was measured with a soap film flow meter for a volume of 90 mL of gas, at 20.5±0.5ºC, 20 psi of O_2 pressure discharge, and ozonator power at level 2. The values were associated with the 0-150 scale rotameter connected to the ozonator.

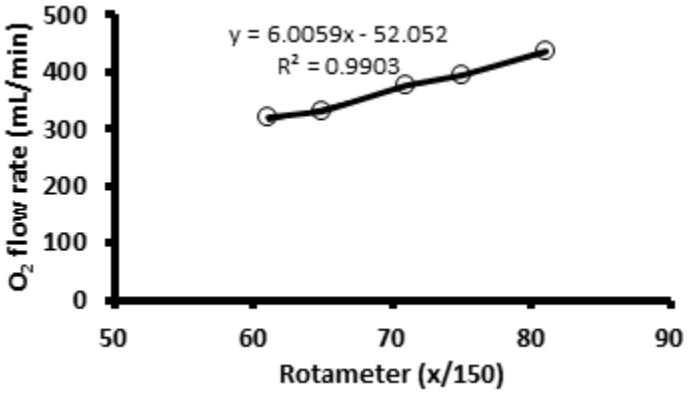

Figure D-1: Calibration of the rotameter scale wrt the O_2 flow rate

Table D.1: Raw data for the rotameter calibration

Rotameter	Time	Flow rate	Mean flow rate	Corrected* flow rate
x/150	s	mL/min	mL/min	mL/min
81	19	284.2	284.2	436.7
	19	284.2		
	19	284.2		
75	21	257.1	257.1	395.1
	21	257.1		
	21	257.1		
71	22	245.5	245.5	377.1
	22	245.5		
	22	245.5		
65	25	216.0	216.0	331.9
	25	216.0		
	25	216.0		
61	26	207.7	207.7	319.1
	26	207.7		
	26	207.7		

*Correction from TG-10 ozonator manual:

$$Corrected\ flow\ rate = flow\ rate_T * \sqrt{(discharge\ P_{psi} + 14.7)/14.7}$$

O_3 gas-production measurement

O_3 gas production was chemically measured through the adapted Standard Method 2350 E, within a specific O_2 flow rate range. Operating conditions were: O_2 pressure discharge: 20 psi, ozonator power: 2, temperature: ambient (±20ºC). *vc* of the measurements at all O_2 flow rate values was 3%; thus any oscillation of the rotameter during the ozonation step that fell within this range was considered acceptable.

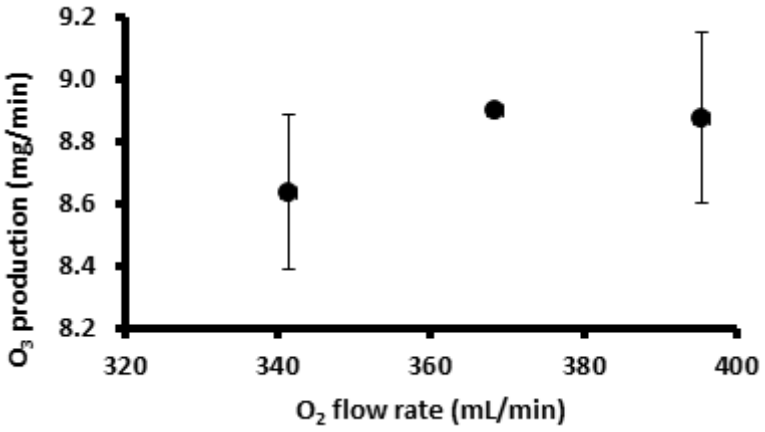

Figure D-2: Calibration for the ozone gas production

Table D.2: Raw data for the calibration of the ozone gas production

Rotameter (x/150)	Corrected O_2 flow rate (mL/min)	n	Avge	Std dev	*vc* (%)
65.5	341	5	8.64	0.25	2.9
70.0	368	1	8.90	0	-
74.5	395	5	8.87	0.27	3.1
Total	-	11	8.77	0.27	**3.0**

O_3 gas production slightly varies during the day, and was different each time the ozonator was started. Hence, production measurements were taken for each ozonation experiment, before and after their execution.

Appendix E: Validation of the procedure to ozonate the water

Objective

To assure the homogeneity and repeatability of the ozone gas dosage in the water sample, when using the methods adapted by CREDEAU, 2007 from: Standard Methods 2350 E - iodometric method and Standard Methods 4500-O_3 – colorimetric method.

Remarks

The ozone injected in the reactor could be found dissolved in the water sample or as off-gas. As for the chemical reactions, O_3 can be consumed in three stages: O_3 instantaneous demand, molecular O_3 and free radicals (•OH).

Validation

1. Reactor homogeneity: performed through indigo 3% solution in the reactor. See Appendix G.
2. Transferred O_3: performed through a mass balance of ozone in pure water (*vc*=5%, n=3). See Appendix F.

Appendix F: Validation of the O_3 gas dosage and monitoring

O_3 gas dosage was estimated through the following formula:

$$O_3 \text{ gas injected} = O_3 \text{ gas residual} + O_3 \text{ dissolved in water}$$

- O_3 gas residual was measured by the adapted Standard Method 2350 E.
- O_3 dissolved in water was measured through the adapted Standard Method 4500-O_3. The *vc* for these measurements was 0.1%, for n=6.

A mass balance with milli-Q water was executed to determine the repeatability of the method, yielding a 5% error (n = 3).

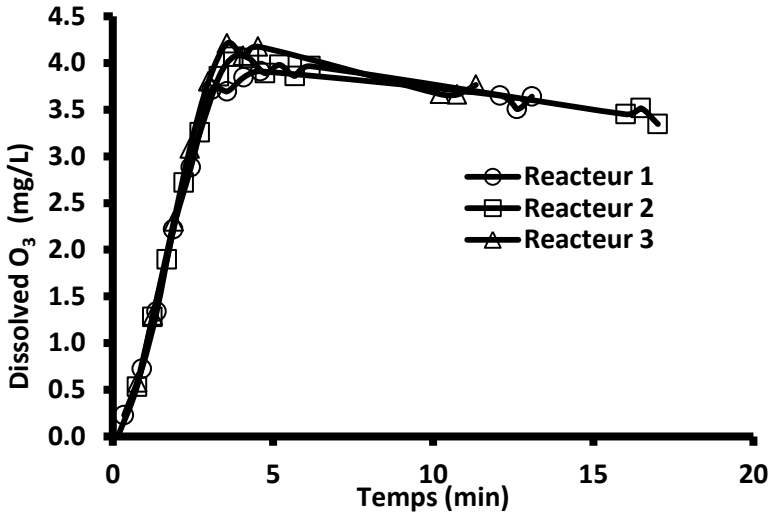

Figure F-1 : Validation of the ozone gas transferred to milli-Q water

Table F.1: Operating conditions and sampling for the validation of the ozone gas transferred

Ozonation operating conditions	
Temperature	ambient (20ºC)
O_2 discharge P	20 psi
Ozonator power	2
Rotameter scale	69-70/150
O_3 gas production	8.91 mg/min
Ozonation time	3 min
Mixing speed	7
Purge air volume	± 3.5 L
Sample	3 L non-buffered milli-Q water, pH 5.5-6

Sampling	
Volume	1 mL
Frequency	as many as possible during 3 min's injection
Indigo sol	3%
Indigo blanks 600 nm absorbance	0.6454, 0.6490, 0.6494 avge: 0.6479

Table F.2: Raw data for ozonation curves in milli-Q water

Reactor 1				Reactor 2				Reactor 3		
Time Min	Abs 600 nm	$[O_3]$ mg/L		Time min	Abs 600 nm	$[O_3]$ mg/L		Time min	Abs 600 nm	$[O_3]$ mg/L
0.35	0.6434	0.23		0.15	0.6480	0.00		0.25	0.6483	0.00
0.90	0.6335	0.72		0.75	0.6373	0.53		0.77	0.6364	0.58
1.37	0.6212	1.34		1.23	0.6224	1.28		1.25	0.6221	1.29
1.88	0.6036	2.22		1.68	0.6100	1.90		1.90	0.6019	2.30
2.43	0.5903	2.88		2.22	0.5936	2.72		2.40	0.5863	3.08
3.08	0.5737	3.71		2.72	0.5828	3.26		2.98	0.5719	3.80
3.57	0.5740	3.70		3.32	0.5708	3.86		**3.57**	**0.5637**	**4.21**
4.08	**0.5710**	**3.85**		3.77	0.5666	4.07		4.07	0.5664	4.08
4.60	*0.5697*	*3.91*		**4.25**	**0.5669**	**4.05**		*4.53*	*0.5644*	*4.18*
12.1	0.5749	3.65		4.75	0.5701	3.89		10.2	0.5746	3.67
12.6	0.5778	3.51		5.20	0.5683	3.98		10.8	0.5747	3.66
13.1	0.5751	3.64		5.68	0.5707	3.86		11.3	0.5726	3.77
-	-	-		*6.17*	*0.5686*	*3.97*		-	-	-
-	-	-		16.0	0.5789	3.45		-	-	-
-	-	-		16.5	0.5776	3.52		-	-	-
-	-	-		17.0	0.5810	3.35		-	-	-

in bold: maximum concentration of dissolved O_3; *in italics*: start of air purge

Table F.3: Mass balance for ozone gas transferred in milli-Q water

		Calculation	Reactor 1	Reactor 2	Reactor 3
A	Amount of O_3 injected (mg O_3)	O_3 production (mg O_3/min) * injection time (min)	8.91*3 = 26.73	8.91*3 = 26.73	8.91*3 = 26.73
B	Amount of O_3 gas residual (mg O_3)	Volume of $Na_2S_2O_3$ used (mL)* normality of $Na_2S_2O_3$ solution (N)*24 – correction’	6.7 * 0.1 * 24 – (3.91-3.65) *3 = 15.30	6.2 * 0.1 * 24 – (3.97-3.45) *3 = 13.34	7.1 * 0.1 * 24 – (4.18-3.67) * 3 = 15.51
C	Amount of O_3 dissolved in water (mg O_3)	O_3 concentration at the end of the injection (mg/L)*volume of water in reactor (L)	3.85 * 3 = 11.54	4.05 * 3 = 12.16	4.21 * 3 = 12.64
	Mass balance	a = (b + c)	b + c = 15.3 + 11.54 = 26.84	13.34 + 12.16 = 25.49	15.51 + 12.64 = 28.15
	Error (%)	[a-(b+c)]/a*100	-0.4	+4.6	-5.3

’ correction = [O_3 dissolved concentration at (the end – the beginning) of air purge]*volume

Appendix G: Homogeneity of the reactor's sample solution

Objective:
To evaluate the homogeneity of the solution placed in the ozonation reactor.

Method:
3 L of a 3% indigo solution was placed in the reactor at ambient temperature (20ºC). Ozonation was started over a short period of time. 5 mL samples were withdrawn simultaneously from each port of the reactor (top, medium & low) before and after stopping the ozonation process. The samples were then read at 600 nm in a spectrophotometer.

Operating conditions:
- O_2 pressure discharge: 20 psi
- Ozonator power: 2
- Rotameter: 65-70/150
- Mixing speed: 7

The data obtained is presented in table G.1:

Table G.1: Raw data for the homogeneity of the reactor's sample solution

Date	Vertical homogeneity	600 nm absorbance of the 3% indigo solution				
15/10/2013	Sampling point	t = 0 s	t = 20 s	t = 30 s	t = 45 s	t > 10 min
	Top	0.625	0.531	Stopped ozonation process	0.201	0.076
	Middle	0.625	0.451		0.127	0.074
	Low	0.628	0.353		0.084	0.072
	Avge top-low	*0.627*	*0.442*	-	*0.142*	*0.074*
21/10/2013	Sampling point	t = 0 s	t = 10 s	t = 18 s	t = 38 s	t > 10 min
	Top	0.651	0.134	Stopped ozonation process	0.095	0.078
	Middle	0.652	0.429		0.096	0.077
	Low	0.652	0.602		0.113	0.077
	Avge top-low	*0.652*	*0.368*	-	*0.101*	*0.077*

Conclusions:
- The reactor is not homogeneous during the ozonation process; but middle-point sampling fairly represents the overall concentration of O_3 in the whole reactor.
- 20 s after stopping the ozonation process, the reactor is practically homogenized; although the oxidation reaction continues.

Additional comment:
The axial homogeneity of the reactor was not evaluated due to the impossibility of withdrawing simultaneous samples. Thus sampling was done at the mid-radius point of the reactor (radius=5.4 cm), and it was assumed to be representative of the overall solution value.

Appendix H: Sample ozonation example: steps, data & calculations

Objective: Ozonation of Ste. Rose water, pH 6.5 and dose 1 mg O_3/mg DOC

Table H.1: Sample conditioning for ozonation

Sample volume	3 L
Buffer volume (pH 6)	18 mL
KH_2PO_4 0.5 M	7.5 mL
NaCl 1 M	0.78 mL
Volume Pcba	24 mL (8 mL/L)
Final pH	6.5 (20ºC)
Initial DOC	7.17 mg/L
Diluted DOC	7.05 mg/L

Table H.2: Ozonation parameters for O_3 production measurement

Temperature	ambient (20±1ºC)
O_2 discharge P	20 psi
Ozonator power	2
Rotameter scale	65-75/150
O_2 flow rate	340-400 mL/min
Ozonation time	6 min
Mixing speed	7
Titration	
Titrant volume (mL) n = 4	Start: 28.1 – 28.7 End: 27.6 – 26.7 Average = 27.8, VC = 3%
O_3 production	11.1 mg O_3/min

Table H.3: Sample ozonation

Temperature	20±0.5ºC
O_2 discharge P	20 psi
Ozonator power	2
Rotameter scale	73
Sample volume	3 L
DOC total	7.05 mgDOC/L * 3L = 21.16 mg DOC
Target dose	1 mg O_3/mg DOC
O_3 needed	1 * 21.16 = 21.16 mg O_3
O_3 transfer estimation	51 % (empirical approx. with previous assay)
Estimated ozonation time	21.16/(11.1*0.51) = 3.65 min
Real ozonation time	3.65 min
Air purge	± 3.5 L

Table H.4: Ozone dosage & molecular ozone monitoring

Indigo blancs					
600 nm absorbance	0.2% solution (n=2)	0.0744, CI: 0.0074-0.0669			
	1% solution (n=2)	0.3710, CI : 0.0371-0.3710			
Sample measurements					
Time (min)	Indigo sol (%)	600 nm absorbance	Residual [O_3] (mg/L)	ct O_3 (mg.min/L)	ct O_3 (M.s)
0.25	0.2	0.0746	0.00	0.00	0.00
0.92	0.2	0.0735	0.00	0.00	0.00
1.57	0.2	0.0732	0.00	0.00	0.00
2.15	0.2	0.0718	0.00	0.00	0.00
2.68	1	0.3486	0.00	0.00	0.00
3.15	1	0.3208	0.30	0.07	8.71E-05
3.72	1	0.2666	0.62	0.33	4.13E-04
4.22	1	0.2918	0.47	0.60	7.54E-04
4.73	1	0.3180	0.32	0.81	1.01E-03
5.33	1	0.3407	-	0.81	1.01E-03
5.93	0.2	0.0659	0.05	1.03	1.28E-03
7.00	0.2	0.0719	0.00	1.05	1.32E-03
8.38	0.2	0.0724	0.00	1.05	1.32E-03
9.50	0.2	0.0721	0.00	1.05	1.32E-03
10.7	0.2	0.0723	0.00	1.05	1.32E-03

Calculation of O_3 concentration (mg/L):

$$\frac{(abs\ blanc - abs\ sample) * total\ volume}{0.42 * cell\ width * sample\ volume} = \frac{(0.3710 - 0.2666) * 25}{0.42 * 2 * 5} = 0.62$$

Calculation of Ct_{O3} (mg.min/L):
By integration of the area under the curve of residual [O_3] vs time using graphical trapezoid method:

$$(3.15 - 2.68) * \frac{(0.3 + 0)}{2} + (3.72 - 3.15) * \frac{(0.62 + 0.3)}{2} = 0.33$$

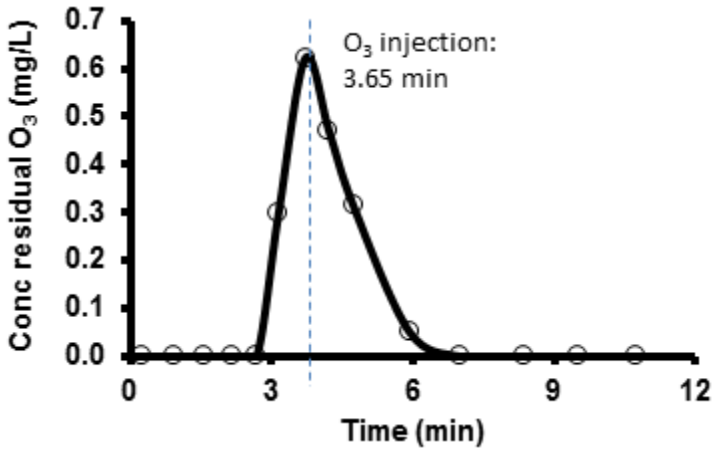

Figure H-1: Molecular ozone curve (example)

Table H.5: Estimation of the dose transferred

	Amount of O_3 …	Calculation	Reactor
a	Injected (mg)	O_3 production (mg O_3/min) * injection time (min)	11.1*3.65 = 40.5
b	Residual gas (mg)	Volume of $Na_2S_2O_3$ used (mL)* normality of $Na_2S_2O_3$ solution (N)*24	9.3 * 0.1 * 24 = 22.3
c	Residual dissolved in water (mg)	O_3 concentration at the end of the injection (mg/L)*residual volume of water in reactor (L)	0.62 * 2.925 = 1.82
d	That reacted (mg)	Injected O_3 – O_3 gas residual	40.5 – 22.3 = 18.2
e	Transferred to water (mg)*	Reacted O_3 + residual dissolved	18.2 + 1.82 = 20.0
f	Estimated real dose (mg O_3/mg DOC)	Transferred O_3 (mg) / DOC amount (mg)	20.0/21.2 = 0.94

*slightly sur-estimated as part of the residual dissolved O_3 is already considered in the ‘reacted O_3 term’

Table H.6: •OH radicals monitoring

pCBA calibration curve		
[pCBA] (ppb)	HPLC area	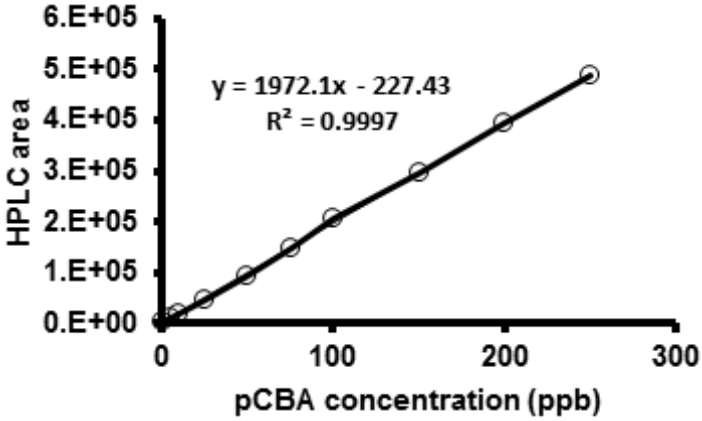
1	1410	
5	9534	
10	18557	
25	47243	
50	94900	
75	148509	
100	204540	
150	296556	
200	395452	
250	488844	

pCBA measurements			
Time (min)	HPLC area	[pCBA] - diluted (ppb)	[pCBA] - real (ppb)
0.00	75889	38.6	193
0.25	74723	38.0	190
0.92	58892	30.0	150
1.57	39657	20.2	101
2.15	24931	12.8	63.8
2.68	17332	8.90	44.5
3.15	16746	8.60	43.0
3.72	12502	6.50	32.3
4.22	10296	5.30	26.7
4.73	7333	3.80	19.2
5.33	4460	2.40	11.9
5.93	4062	2.20	10.9

Calculation of [pCBA] diluted:

$$(HPLC\ area + 227.43)/1972.1$$

Calculation of [pCBA] real:

HPLC diluted * 5

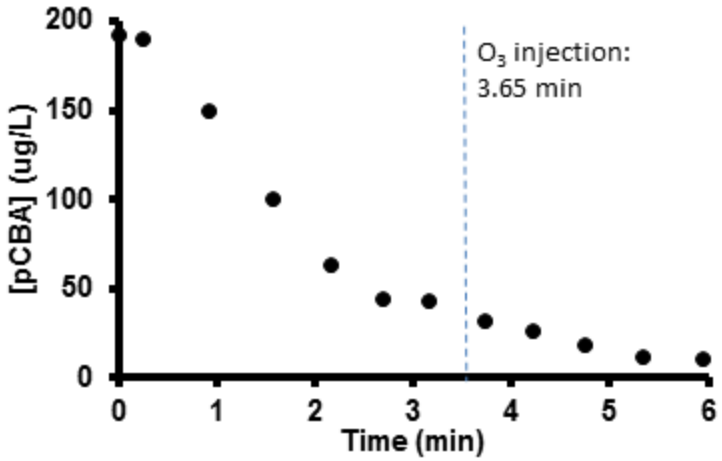

Figure H-2: Evolution of pCBA consumption

Table H.7: Ct and [•OH] calculation

Ct •OH calculation & [•OH]					
Time (min)	Ct O_3 (M.s)	$\frac{[pCBA]}{[pCBA_o]}$	ln $\frac{[pCBA]}{[pCBA_o]}$	Ct •OH (M.s)	[•OH] (M)
0.00	0.00	1	0	-	-
0.25	0.00	0.985	-0.015	2.97E-12	1.98E-13
0.92	0.00	0.777	-0.253	4.86E-11	8.84E-13
1.57	0.00	0.524	-0.646	1.24E-10	1.32E-12
2.15	0.00	0.331	-1.107	2.13E-10	1.65E-12
2.68	0.00	0.231	-1.467	2.82E-10	1.75E-12
3.15	8.71E-05	0.223	-1.501	2.96E-10	1.56E-12
3.72	4.13E-04	0.167	-1.788	3.46E-10	1.55E-12
4.22	7.54E-04	0.138	-1.979	3.99E-10	1.58E-12
4.73	1.01E-03	0.099	-2.309	4.39E-10	1.54E-12
5.33	1.01E-03	0.062	-2.787	4.39E-10	1.37E-12
5.93	1.28E-03	0.056	-2.876	4.81E-10	1.35E-12

Note that pCBAo = 193 ppb

Calculation of Ct •OH in the absence of molecular O_3 residual:

$$\ln\frac{[pCBA]}{[pCBA_o]} = -k_{\bullet OH/pCBA} * ctOH, \text{ where } k_{\bullet OH/pCBA} = 5.2E09\ M^{-1}s^{-1}$$

$Ct_{\bullet OH}$ = -0.015/-5.2E09 = 2.97E-12, for t=0.25 min

Calculation of Ct •OH in the presence of molecular O_3 residual:

in this case, the Rct concept applies, where Rct = Ct•OH/ctO_3

but also, $\ln\frac{[pCBA]}{[pCBA_o]} = -k_{\bullet OH/pCBA} * Rct * CtO_3$ (see literature review)

thus the slope of the ln $\frac{[pCBA]}{[pCBA_o]}$ vs ct O_3 graph is equivalent to $-k_{\bullet OH/pCBA} * Rct$

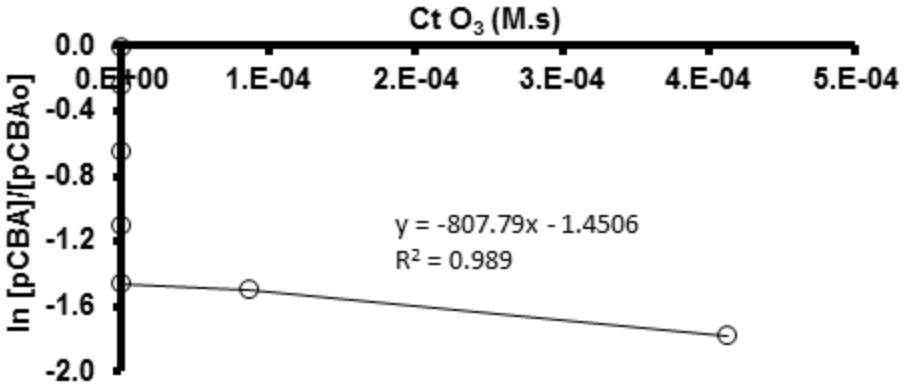

Figure H-3: •OH vs O_3 exposures

as the slope = -807.79, then Rct = -807.79/-5.2E09 = 1.55E-07

and ct •OH = Rct * Ct_{O3}. So for example, at t=3.72 min: 1.55E-07 * 4.13E-04 = 6.41E-11

finally, total Ct •OH for t=3.72min: 2.82E-10 + 6.41E-11 = 3.46E-10

Estimation of •OH concentration

as Ct •OH (M.s) = [•OH] (M) * t (s), [•OH] (M) can be estimated if time (s) is known:

example, for t=3.72 min: [•OH] = 3.46E-10/(3.72*60) = 1.55E-12 M

Appendix I: Procedure for washing ceramic membranes

Objective

To wash new and used ceramic membranes (fouled with organic matter).

Remarks

- New ceramic membranes have to be washed to eliminate any contaminant traces.
- Organic matter is best removed by alkaline solutions, whereas metal traces by acidic ones.

Table I.1: Materials, reagents and equipment for washing ceramic membranes

Materials	Reagents	Equipment
Beaker, 250 mL	NaOH solution, 15 g/L	Heating plate
Aluminum paper	H_3PO_4 75% solution, 5 mL/L	Washing set-up
pH paper	H_3PO_4 75% solution, 1 mL/L	

Washing set-up

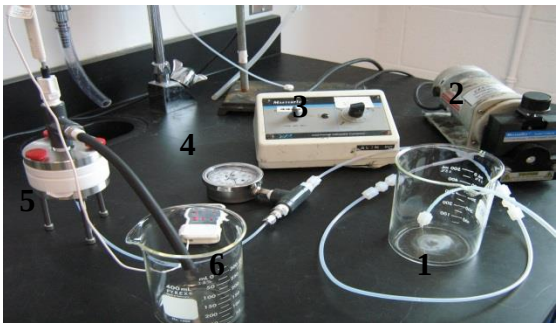

1 Milli-Q water
2 Pump
3 Pump speed controller
4 Manometer
5 Membrane module
6 Residual water

Figure I-1: Picture for washing set-up

Procedure

1. Pour 100 mL of NaOH 15 g/L in a 250 mL beaker. Place the membrane in the solution, and cover the container with aluminum paper. Heat-up the system to 85ºC and for 30 minutes (precaution: always work in a well-ventilated safety hood).

2. Cool down the system. Place the membrane in the washing set-up, and rinse it with milli-Q water in back-wash mode (back-wash flux usually doubles the flux used during the filtration assays; but pay attention to the maximum pressure the membrane can withstand) until the pH of the rinsing water reaches neutrality (pH 7).

3. Pour 100 mL of H_3PO4 5 mL/L solution (50 KDa membrane) or H_3PO4 1 mL/L (8 KDa membrane) in a 250 mL beaker. Place the membrane in the solution, and cover the container with aluminum paper. Heat-up the system to 50ºC and for 15 minutes (precaution: always work in a well-ventilated safety hood).

4. Cool down the system. Place the membrane in the washing set-up, and rinse it with milli-Q water in back-wash mode (back-wash flux usually doubles the flux used during the filtration

assays; but pay attention to the maximum pressure the membrane can withstand) until the pH of the rinsing water reaches neutrality (pH 7).

5. Repeat once more the first four steps.

Cleaning verification

Measure the permeability of the membrane at one or two milli-Q water fluxes. If an irreversible fouling is not expected, then the permeability values should reach the original ones.

Bibliography

Adapted from Sterlitech membrane cleaning guideline (http://www.sterlitech.com/ceramic-membranes-cleaning-guide)

Appendix J : Validation of the procedure to filtrate the water sample

Objective

To filtrate the water sample through UF ceramic membranes.

Validation

1. See Appendix K to confirm the equivalence of the two set-ups used and the stability of the operating conditions.
2. Repetition of filtration assays showed average *vc* of 16%.

Note.- Membranes initial permeability was measured before the filtration experiments, showing *vc* of 13% for the 50 kDa membrane and 32% for the 8 kDa membrane.

Appendix K: Validation of set-ups and filtration operating conditions

Two parallel set-ups were used for the accomplishment of the experiments: one for the 8 kDa membrane and another for the 50 kDa one. Each set-up had its own pumping system and data acquiring systems: manual for the 8 kDa, and digital for the 50 kDa. The reason for this difference was the detection limit of the available pressure probes, which would not support the pressures built by the 8 kDa membranes fouling.

Stability of sample's feed flux

Both set-ups were evaluated for the stability of feed flux during a period of ±5 hours at ±40 min intervals, using milli-Q water, flow rate: ±1.19 mL/min, and membrane effective area: 0.0014186 m^2. Feed flux was considered stable, with *vc* of 0.7 and 1% (see table K.1.a).

Comparison of set-up's pressure measurements

21 flux measurements done over same membranes were compared in order to assess the differences in pressure output for both set-ups (table K.1.b). Absolute differences reached a maximum of 0.8 psi.

Table K.1: Flux stability in time and equivalence of set-ups pressure measurements

(a)

	8 kDa set-up	50 kDa set-up
Time (min)	Flux (LMH)	Flux (LMH)
0	49.76	50.25
40	49.52	49.76
80	49.28	49.76
120	50.25	49.76
160	49.76	50.75
200	49.28	51.27
240	49.28	50.25
280	49.28	49.76
320	49.28	50.25
Mean	49.52	50.20
VC (%)	0.70	1.05

(b)

8 kDa set-up	50 kDa set-up	Abs diff	8 kDa set-up	50 kDa set-up	Abs diff
15.20	15.56	0.36	3.60	3.64	0.04
6.80	6.41	0.39	4.90	4.99	0.09
16.20	15.47	0.73	2.90	2.76	0.14
11.60	11.90	0.30	5.50	5.47	0.03
23.20	22.80	0.40	3.80	3.75	0.05
8.20	8.51	0.31	4.90	4.48	0.42
5.90	5.67	0.23	4.70	4.67	0.03
8.00	7.21	0.79	6.30	6.06	0.24
10.50	10.05	0.45	7.60	7.43	0.17
3.00	3.04	0.04	2 outliers: > 3 std dev		
Min abs diff		0.03	Mean abs diff		0.27
Max abs diff		0.79	Abs diff std dev		0.22

Appendix L: Filtration example: data & calculations

Date: 7/12/2013
Sample: Membrane 8D, O_3 Dose 0, pH 6.5
Feed flow rate: 1.18 mL/min (n=2)

Table L.1: Raw data for UMFI calculation

Time (min)	P (psig)	P (bar)	T (ºC)	Filt vol (mL)	Vs (L/m2)	Flux (LMH)	Flux 20ºC	Permeability (LMH/bar)	Permeability @ 20ºC	Tot resist @20C	Ntot resist Cake resist	Resist P/Po
3.0	7	0.48	20.6	0	0.00	0.00	0.0	0.0	0.0	#DIV/0!		
3.9	8	0.55	20.7	1.2	0.85	13.1	12.8	23.7	23.1	0.043		
4.3	9	0.62	20.7	1.4	0.99	13.9	13.6	22.4	21.8	0.046		
4.8	10	0.69	20.7	1.8	1.27	15.9	15.6	23.0	22.5	0.045		
5.7	11	0.76	20.7	2.5	1.76	18.7	18.4	24.7	24.1	0.042		
6.6	12	0.83	20.7	3.3	2.33	21.3	20.9	25.8	25.1	0.040		
7.6	13	0.90	20.6	4.3	3.03	23.9	23.6	26.7	26.1	0.038		
9.1	14	0.97	20.6	5.7	4.02	26.5	26.1	27.4	26.9	0.037		
11.1	15	1.03	20.6	8.0	5.64	30.4	30.0	29.4	28.8	0.035	1.00	1.00
13.8	16	1.10	20.7	10.5	7.40	32.1	31.5	29.1	28.4	0.035	1.01	1.07
16.9	17	1.17	20.7	13.5	9.52	33.9	33.3	28.9	28.2	0.035	1.02	1.13
20.9	18	1.24	20.7	17.8	12.5	35.9	35.3	28.9	28.3	0.035	1.02	1.20
23.0	19	1.31	20.7	19.8	13.9	36.3	35.7	27.7	27.1	0.037	1.06	1.27
26.0	20	1.38	20.7	23	16.2	37.4	36.8	27.1	26.5	0.038	1.09	1.33
33.3	21	1.45	20.7	31	21.9	39.4	38.7	27.2	26.6	0.038	1.08	1.40
54.2	22	1.52	21.1	53	37.4	41.3	40.2	27.3	26.3	0.038	1.09	1.47
68.4	23	1.59	20.8	69	48.6	42.7	41.8	26.9	26.2	0.038	1.10	1.53
83.4	24	1.65	20.8	84	59.2	42.6	41.7	25.7	25.1	0.040	1.15	1.60
104	25	1.72	20.8	106	74.7	43.3	42.4	25.1	24.4	0.041	1.18	1.67
119	26	1.79	20.9	122	86.0	43.4	42.4	24.2	23.5	0.043	1.23	1.73
135	27	1.86	21.6	139	98.0	43.5	41.8	23.4	22.3	0.045	1.29	1.80
153	28	1.93	21.1	159	112	43.8	42.6	22.7	21.9	0.046	1.31	1.87

Calculation of the specific volume (V_s):

$$V_s = \frac{filtered\ volume}{membrane\ effective\ filtration\ area} = \frac{8 * 10^{-3}\ L}{0.001419\ m^2} = 5.64\ L/m^2$$

Calculation of the flux (J_T):

$$J_T = \frac{V_s}{time} = \frac{5.64}{(11.1/60)} = 30.4 \frac{L}{m^2}.h\ or\ LMH$$

Correction of the flux for temperature (J_{20}):

$$J_{20} = J_T * (1.784 - 0.0575T + 0.0011T^2 - 10^{-5}T^3), \text{ where T is in } ^oC$$

$$J_{20} = 30.4 * (1.784 - 0.0575 * 20.6 + 0.0011 * (20.6)^2 - 10^{-5}(20.6)^3) = 29.8\ LMH$$

Calculation of the permeability (J_s):

$$J_s = \frac{flux}{effective\ pressure} = \frac{29.8}{(1.03 - 0)} = 28.8\ LMH/bar$$

Calculation of the resistance ($1/J_s$):

$$1/J_s = \frac{1}{permeability} = \frac{1}{28.8} = 0.035\ m^{-1}$$

Calculation of the normalized resistance ($1/J_s'$):

$$1/J_s' = \frac{permeability\ value}{initial\ permeability} = \frac{0.035}{0.035} = 1$$

Calculation of the fouling index (FI):
it is the slope of the graph of normalized resistance ($1/J_s'$) vs the specific volume (V_s)

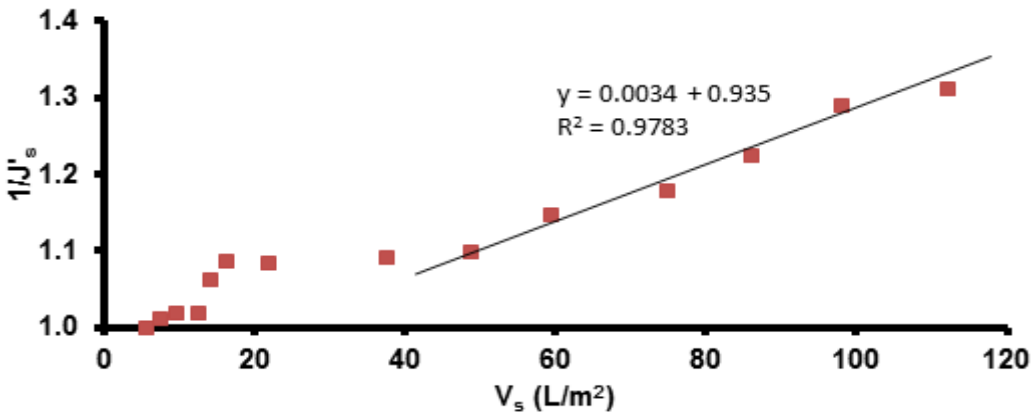

Figure L-1: Fouling graph example

thus, the FI is 34 E-04 m^2/L. The value was taken over the portion of the graph that was presumed to correspond to the cake formation mechanism. The rest of the fouling graph was more likely under pore blocking or pore constriction influences.

Appendix M: Percentage abatement of DOC and UVA after ozonation and filtration (wrt to original sample)

Table M.1: Abatement (%) of DOC and UVA after ozonation and filtration

Membrane	Dose	pH	DOC	UVA 215	UVA 254	UVA 285	436	SUVA	Proposed O_3 active species
-	mgO_3/ mgDOC	-	mg/L	nm	nm	nm	nm	cm^{-1}. mg^{-1}.L	
Non	0.5	6.5	6±3	25±3	38±4	42±4	48±10	34±3	Instantaneous O_3 on DOM + *OH
		8.5	5±1	24±1	36±3	40±3	56±4	33±2	
		8.5 *t*-but	-	20	35	41	58	-	
	1	6.5	8±0.2	38±1	59±2	63±2	80±0.0	56±2	Inst O_3+*OH
		8.5	8±2	33±1	52±0.4	56±0.3	77±6	47±1	Inst O_3+*OH
		8.5 *t*-but	-	27	48	57	75	-	Inst O_3+O_3
50	0	6.5	-	13	16	16	20	-	-
		8.5	13	18	23	24	38	6	
		8.5 *t*-but	-	13	16	18	33	-	
	0.5	6.5	-	37	48	51	68	-	Instantaneous O_3 on DOM + *OH
		8.5	-	34	47	51	77	-	
		8.5 *t*-but	-	27	43	49	75	-	
	1	6.5	18	42	59	61	30	50	Inst O_3+*OH
		8.5	18	39	56	58	83	46	Inst O_3+*OH
		8.5 *t*-but	-	33	53	61	83	-	Inst O_3+O_3
8	0	6.5	20	20	24	26	40	5	-
		8.5	-	40	48	50	64	-	
		8.5 *t*-but	-	34	44	47	58	-	
	0.5	6.5	-	41	53	56	64	-	Instantaneous O_3 on DOM + *OH
		8.5	23	42	58	60	81	49	
		8.5 *t*-but	-	45	59	64	83	-	
	1	6.5	-	-	-	-	-	-	Inst O_3+ *OH
		8.5	29	45	64	67	92	50	Inst O_3+*OH
		8.5 *t*-but	-	39	61	67	83	-	Inst O_3+O_3

Appendix N: Ozonation experiments-raw data

Molecular ozone curves

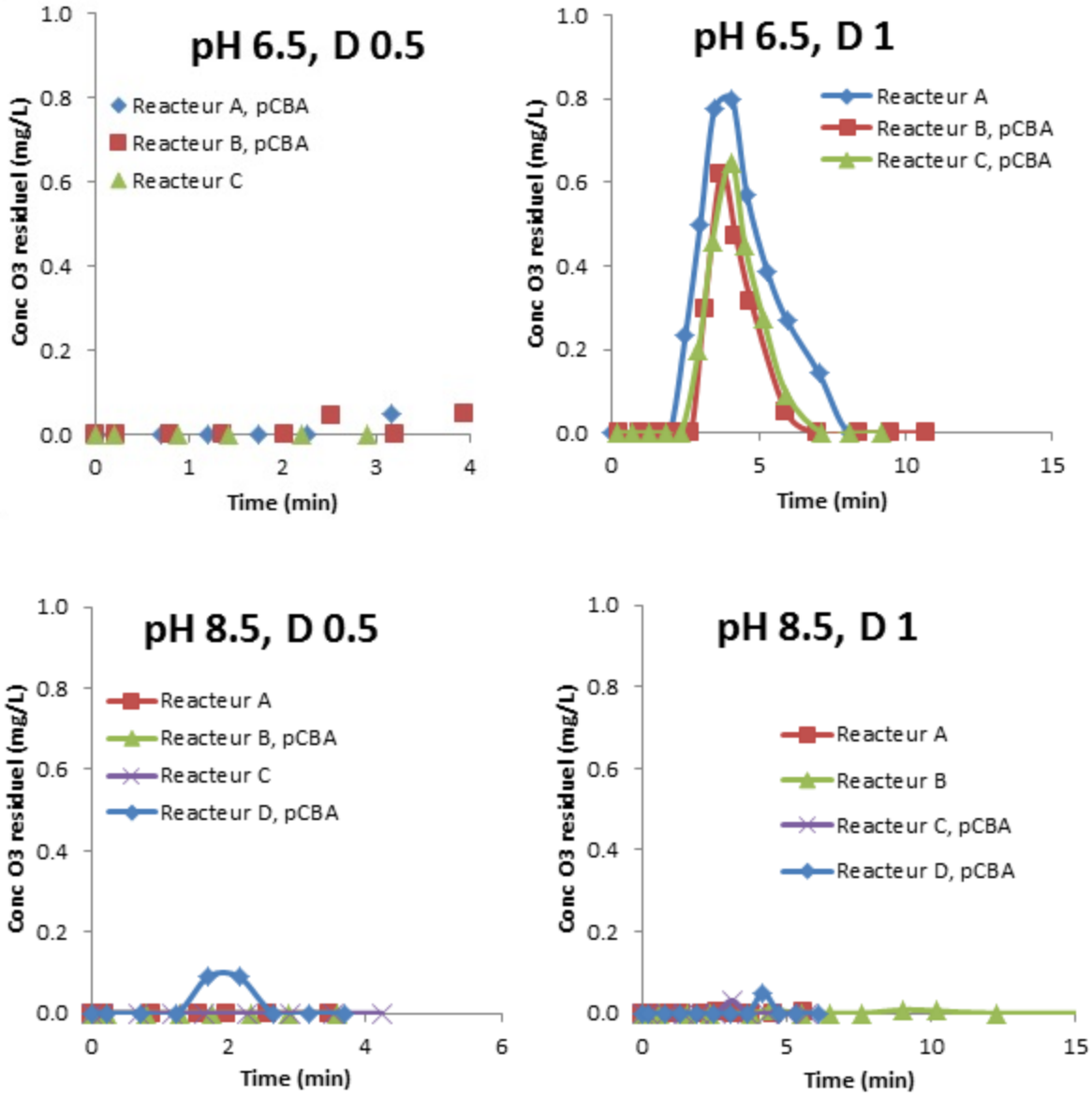

Figure N-1: Molecular ozone curves

•OH curves (pCBA)

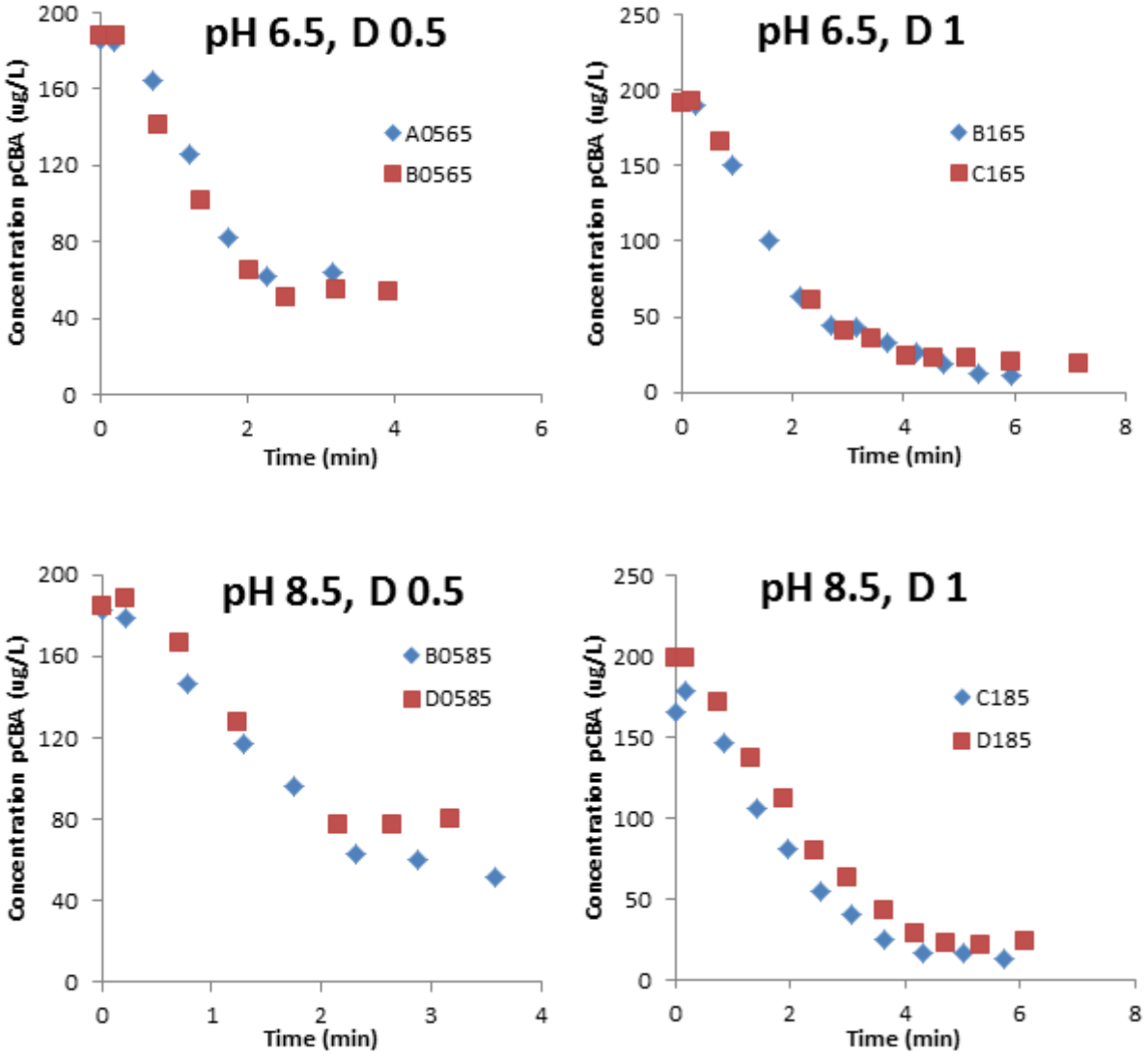

Figure N-2: pCBA consumption curves

Appendix O: Filtration experiments-repetitions

Membrane 8 kDa

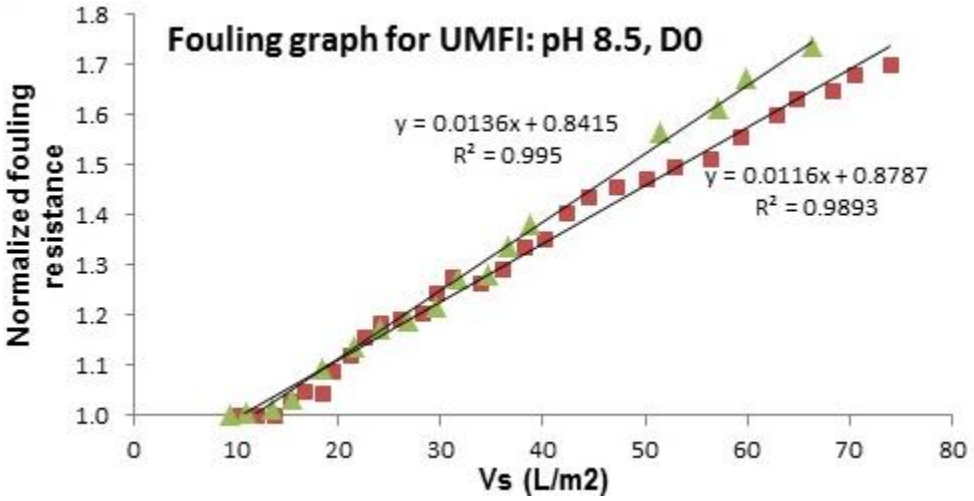

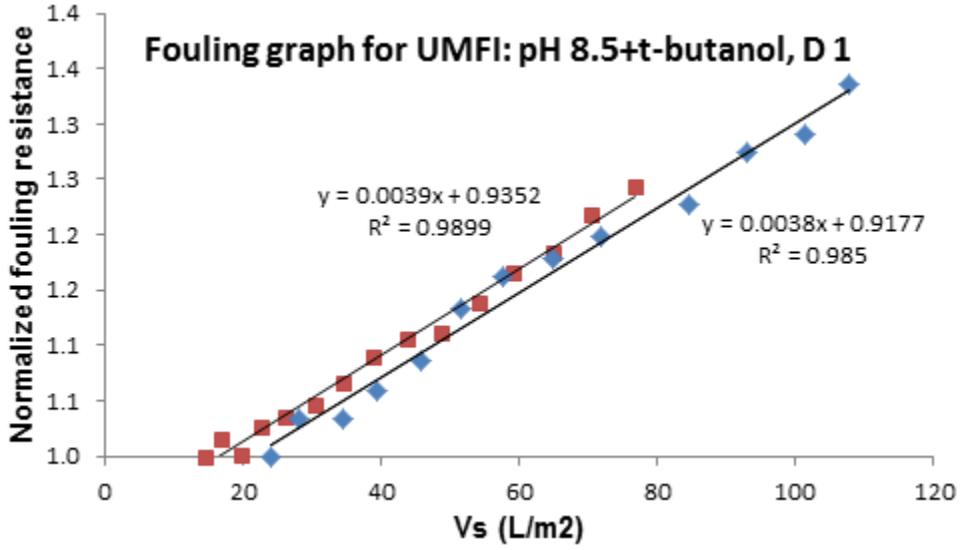

Figure O-1: Membrane 8 kDa fouling graphs-repetitions

Note.- Duplicatas were done in already used membranes, which were previously chemically cleaned.

Membrane 50 kDa

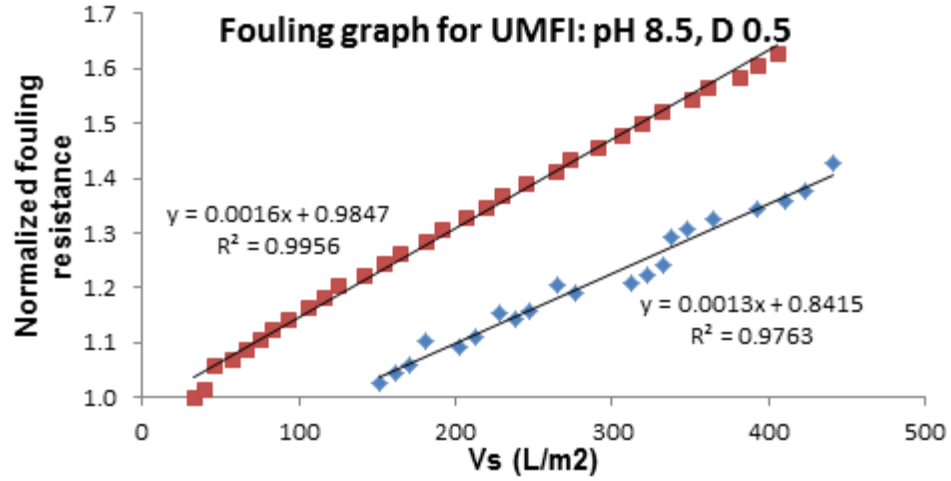

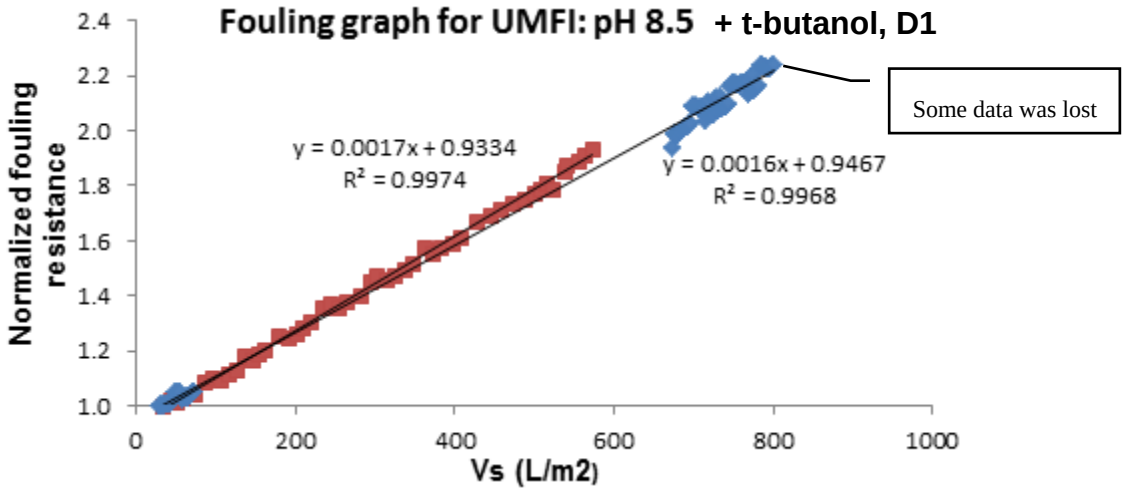

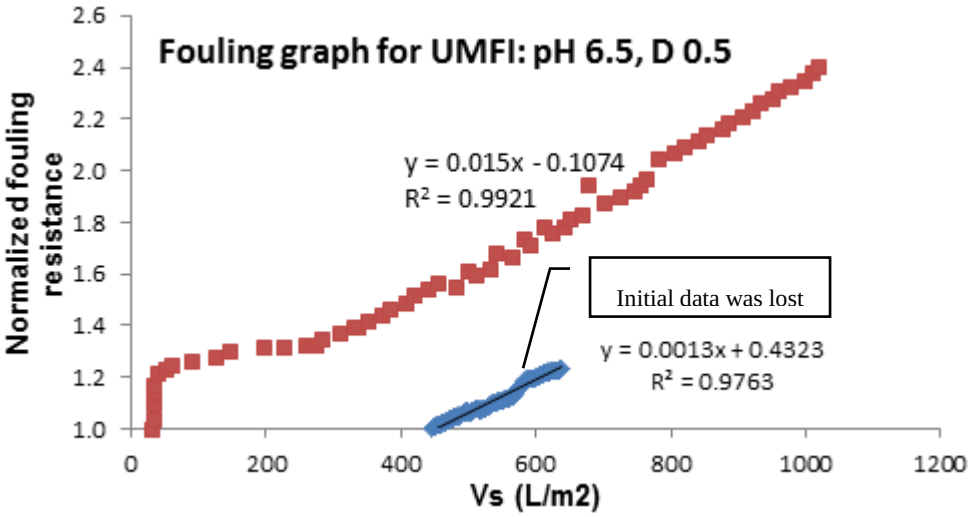

Figure O-2: Membrane 50 kDa fouling graphs-repetitions